Fluorescence microscopy studies of interactions between monomeric α-Synuclein and lipid membranes

Andersson, Alexandra

2023

Document Version:
Peer reviewed version (aka post-print)

Fluorescence microscopy studies of interactions between monomeric α-Synuclein and lipid membranes

ALEXANDRA ANDERSSON | DEPARTMENT OF CHEMISTRY | LUND UNIVERSITY

Fluorescence microscopy studies of interactions between monomeric α-Synuclein and lipid membranes

Fluorescence microscopy studies of interactions between monomeric α-Synuclein and lipid membranes

by Alexandra Andersson

LUND
UNIVERSITY

Thesis for the degree of Doctor of Philosophy
Thesis advisors: Assoc. Prof. Peter Jönsson
Faculty opponent: Prof. Richard Lundmark

To be presented, with the permission of the Faculty of Science of Lund University, for public criticism in lecture hall A at the Department of Chemistry on Friday, the 20th of October 2023 at 09:00.

Organization
LUND UNIVERSITY

Department of Chemistry
Box 124
SE–221 00 LUND
Sweden

Document name
DOCTORAL DISSERTATION

Date of disputation
2023-10-20

Sponsoring organization

Author(s)
Alexandra Andersson

Title and subtitle
Fluorescence microscopy studies of interactions between monomeric α-Synuclein and lipid membranes

Abstract
α-Synuclein (α-Syn), is an intrinsically disordered protein present in the substantia nigra part of the brain. α-Syn is commonly known to associate with lipid membranes containing anionic lipids. Hence, the protein is hypothesized to be involved in the vesicle trafficking at the synapses, but there are yet many unanswered questions regarding the full physiological role of the protein. During the degenerative pathway of Parkinson's disease, α-Syn misfolds and forms fibrillar aggregates. Together with lipids, α-Syn fibrils form Lewy body inclusions, a known hallmark for Parkinson's disease and other synucleopathies. The aim of this thesis has been to study interactions between monomeric α-Syn and lipid membranes, to obtain a better understanding of both the physiological and pathological role of α-Syn.

This thesis has been focused on studying interactions between monomeric α-Syn and different lipid membranes using single vesicle and single protein imaging techniques, to be able to study individual events that otherwise might disappear in a bulk average. The results show that the protein binds cooperatively to both vesicles and supported lipid bilayers in conditions with an excess of lipid membrane. The binding lifetime of α-Syn varies from ms to seconds or longer, depending on the overall protein concentration and the relation between lipids and proteins in the system. Further, a high density of bound α-Syn might deform the membrane and lead to fission of vesicles, depending on the lipid composition of the membrane. However, association only occurs at sufficient membrane charge density, which also limits the number of protein being adsorbed to the membrane.

Key words
Total internal reflection fluorescence microscopy, protein-lipid interactions, α-Synuclein, single molecule imaging, single vesicle imaging

Classification system and/or index terms (if any)

Supplementary bibliographical information

Language
English

ISSN and key title

ISBN
978-91-7422-972-1 (print)
978-91-7422-973-8 (pdf)

Recipient's notes

Number of pages
239

Price

Security classification

Signature

Date 2023-09-04

Fluorescence microscopy studies of interactions between monomeric α-Synuclein and lipid membranes

by Alexandra Andersson

LUND
UNIVERSITY

A doctoral thesis at a university in Sweden takes either the form of a single, cohesive research study (monograph) or a summary of research papers (compilation thesis), which the doctoral student has written alone or together with one or several other author(s).
In the latter case the thesis consists of two parts. An introductory text puts the research work into context and summarizes the main points of the papers. Then, the research publications themselves are reproduced, together with a description of the individual contributions of the authors. The research papers may either have been already published or are manuscripts at various stages (in press, submitted, or in draft).

Cover illustration: Star sky constructed of microscopy images from paper IV. Red stars are protein and blue stars are lipid vesicles. The landscape is constructed in Blender, and merged with the research image.
Credits: Tommy Dam.

Funding information: The thesis work was financially supported by the Knut and Alice Wallenberg Foundation.

Faculty of Science, Department of Chemistry

ISBN: 978-91-7422-972-1 (print)
ISBN: 978-91-7422-973-8 (pdf)

Printed in Sweden by Media-Tryck, Lund University, Lund 2023

Varför ta samma väg som alla andra, när man kan göra sin egen

Contents

Popular summary in English

In a world with an increased life expectancy, neurodegenerative diseases like Alzheimer's and Parkinson's disease becomes more and more abundant. The common factor of neurodegenerative diseases is the death of neurons (nerve cells), in different parts of the brain, resulting in symptoms like tremor and decreased coordination. Most degenerative diseases can be related to proteins that co-aggregates with lipids from the lipid membranes in the body, and form large inclusion bodies. In Parkinson's disease, one of the main components of the inclusion bodies is a protein called α-Synuclein, which normally is present in the area where two nerve cells meet. The function of the protein in the healthy body is not fully understood, but it is commonly known to be monomeric (one and one), and it binds to membranes containing negatively charged lipids. The aim of this thesis has been to study the interaction between monomeric α-Synuclein and lipid membranes, to obtain a better understanding of the function of the healthy and pathological function of α-Synuclein.

The area where two neurons meet is called a synapse, and the region between the neurons is called a synaptic cleft. A signal is passed from one cell to the other by release of neurotransmitters into the synaptic cleft. The neurotransmitters are packed into vesicles, which are small balloons of lipid membrane. The vesicles are merged with the plasma membrane

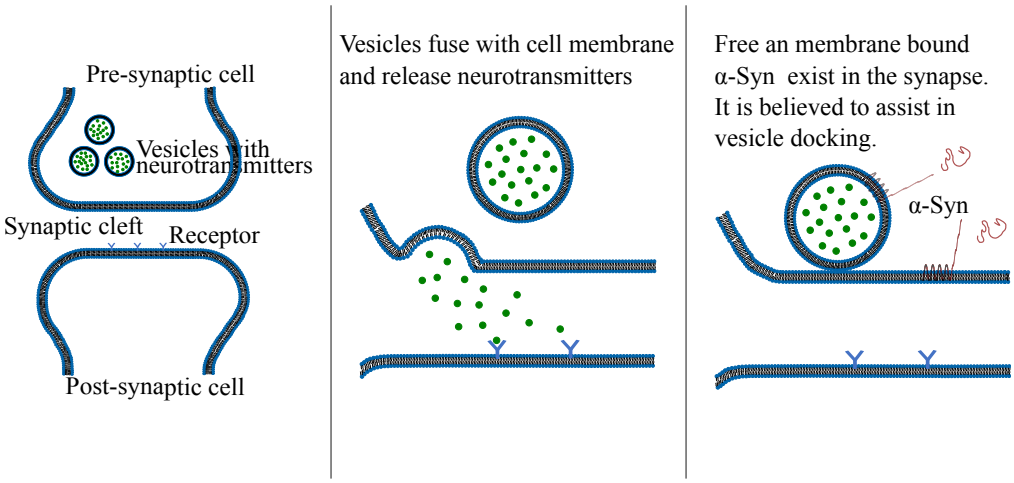

Figure 1: Illustration of the synapse.
Neurotransmitters are released into the synaptic cleft by fusion of vesicles and the cell membrane. α-Synuclein, which can bind to lipid membranes, is likely to take part during this process.

of the cell in order to release the neurotransmitters to the synaptic cleft (Figure 1). The neurotransmitters then bind to receptors on the second cell, which stimulates an electric signal to be passed through the cell. This process is regulated by several proteins and protein containing complexes that bind to the lipid membranes. Since it is known that α-Synuclein binds to negatively charged lipid membranes, the protein is hypothesized to be involved in the regulation of vesicle trafficking across the synapse. Several other proteins in the body binds cooperatively, which means that the proteins prefer to bind next to an already bound protein instead of binding in an area with no other proteins bound. Further, binding of proteins often changes the shape of the lipid membrane.

This thesis has studied the interaction between monomeric α-Synuclein and lipid membranes, mainly using fluorescence microscopy techniques. In this work, synthetic lipid membranes, either vesicles or flat membranes, doped with a fluorescent marker, were deposited to a glass substrate. By adding α-Synuclein labelled with a different fluorescent marker, interactions between the membranes and the protein can be studied. When illuminating the markers with light, they emit light of a different wavelength (color) (Figure 2). If the intensity emitted from one α-Synuclein is known, it is possible to calculate the number of α-Synuclein adsorbed to a certain area of a membrane by comparing the total intensity of that area with the intensity emitted by one protein. Using this principle, this project has shown that α-Synuclein binds cooperatively on both

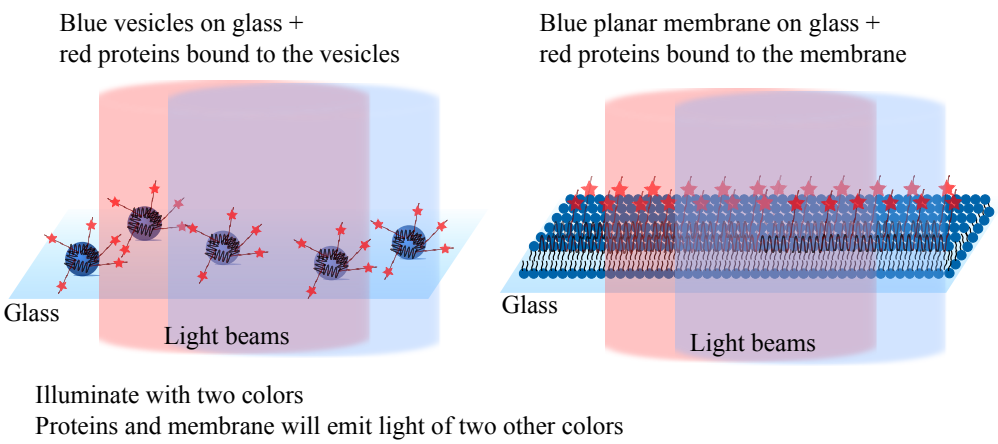

Figure 2: Illustration of the two main systems used in the thesis.
Blue labelled vesicles or blue labelled planar lipid membranes are docked or deposited on a glass surface. Red labelled protein interact with the lipid membranes. The proteins and lipid membranes are visualized by illuminating the system with light with two different colors.

vesicles and flat membranes (Figure 3A). Further, it was shown that, in systems with an excess of lipid membrane, the proteins bind to the membrane for a fairly long time when several proteins binds in the same location, but the lifetime of the binding is very short when the proteins bind sporadically one and one (Figure 3B). However, free and membrane-bound proteins co-exist, and even though the proteins generally remains bound to the membrane, free and bound proteins exchange places.

Another questions investigated in this thesis is the effect of changing the amount of negatively charged lipids in the membrane. The results showed that the membrane needs to contain a certain amount of negatively charged lipids before binding of α-Synuclein occurred (Figure 3C). Increasing the amount of negatively charged lipids in the membrane resulted in more bound α-Synuclein, until the membrane was saturated with proteins. Finally, it was shown that α-Synuclein alone cannot induce fusion of vesicles, but can lead to deformation of the membrane or even

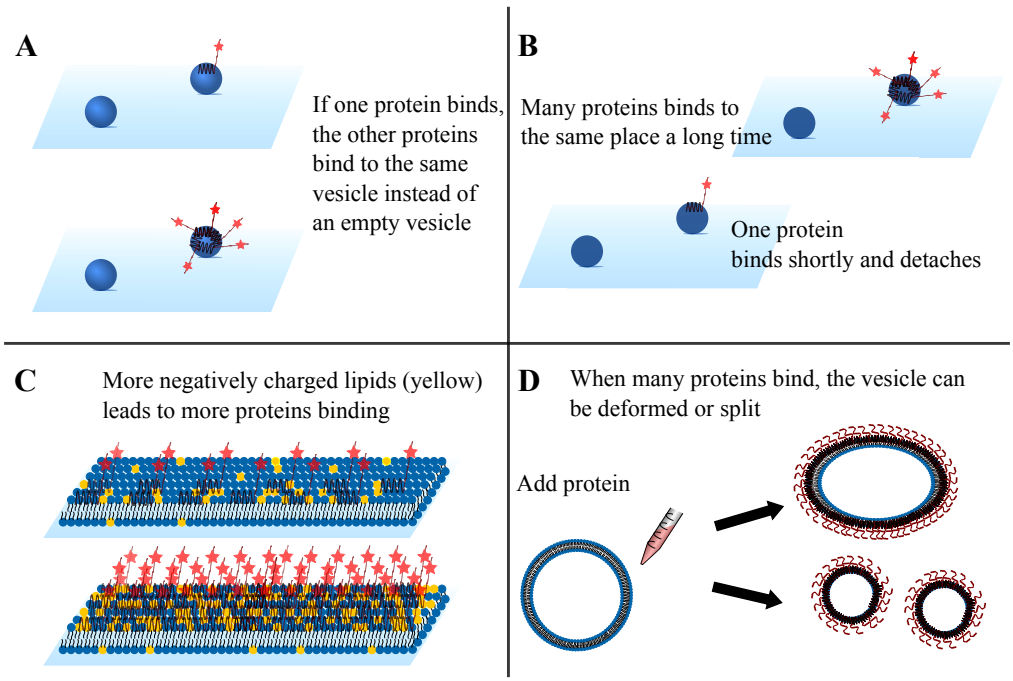

Figure 3: Illustration of the main results.
(A) Protein binds cooperatively, meaning that if one protein binds, other proteins bind to the same vesicle or membrane area. (B) The protein remains bound differently long time depending on the protein concentration in the system, and how many proteins that are bound to the vesicle. (C) When the amount of negatively charged lipids in the membrane increase, more proteins can bind to the membrane. (D) When many proteins bind, the vesicle can deform or split.

fission of vesicles, all depending on the lipid content of the vesicles (Figure 3D).

Altogether, this thesis has contributed to an increased understanding of the interaction between α-Synuclein and lipid membranes. The results show that the interaction between α-Synuclein in several ways are similar to the interaction between lipid membranes and other peripheral proteins. Hence, there are indications that α-Synuclein has a similar role in the healthy body. However, it must be kept in mind that the *in vivo* system is far more complex than the synthetic systems studied in this thesis. This thesis contributes with a piece of the puzzle that, together with previous and future research including *in vivo* studies, leads to a better understanding of the healthy function of α-Synuclein and the degenerative pathway during Parkinson's disease.

Populärvetenskaplig sammanfattning

I takt med att genomsnittsåldern ökar, blir det allt vanligare med neurodegenertrativa sjukdomar såsom Alzheimer's och Parkinson's sjukdom. Den gemensamma nämnaren för dessa sjukdomar är att nervcellerna i vissa delar av hjärnan och nersystemet dör, vilket orsakar symptom som skakningar och nedsatt koordinationsförmåga. De flesta neurodegenerativa sjukdomar kan relaters till proteiner som klumpar ihop sig med varandra och med lipider från lipidmembranen, och bildar stora plack. I Parkinson's sjukdom är det ett protein som heter α-Synuclein, som i den friska kroppen uppträder som enskilda proteiner i området där två nervceller möts, som är en av huvudkomponenterna i placken. Det pågår mycket forskning om α-Synuclein, men faktum kvarstår att vi inte vet särskilt mycket om vare sig sjukdomsförloppet, eller proteinets funktion i en frisk kropp. Syftet med denna avhandling har därför varit att undersöka hur enskilda α-Synuclein interagerar med olika typer av lipidmembran, i hopp om att detta ska öka förståelsen för proteinets funktion i den friska kroppen.

Området där två nervceller möts kallas synaps, och utrymmet mellan ändarna på två nervceller kallas synaptisk klyfta. Signaler passerar från en nervcell till en annan genom utsläpp av neurotransmittorer i den synaptiska klyftan (Figur 4). Neurotransmittorerna är packade i vesiklar,

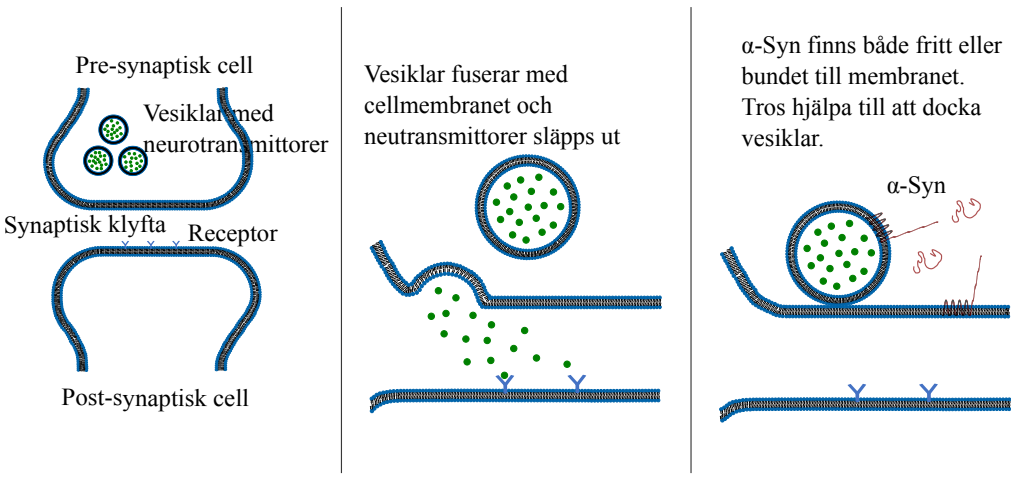

Figur 4: Illustration av en synaps.
Neurotransmittorer släpps ut i den synaptiska klyftan genom fusion av vesiklar och cellmembranet. α-Synuclein, som kan binda till lipidmembran, tros vara delaktig i processen.

små ballonger av lipidmembran. När dessa släppts ut i klyftan mellan nervcellerna binder de till receptorerna på den andra nervcellen, vilket stimulerar en elektrisk signal genom den andra nervcellen. I synapsen finns ett flertal proteiner och protein-komplex som hjälper till att regulera trafiken av vesiklar, genom att binda till lipidmembranen som utgör antingen vesiklar eller plasmamembran. Det har påvisats att α-Synuclein binder till negativt laddade lipidmembran, vilket innebär att det är möjligt att α-Synuclein är ett protein som hjälper till att regulera trafiken av vesiklar. En del proteiner i kroppen binder till lipmembran cooperativt, vilket innebär att om ett protein är bundet till membranet är det större sannolikhet att nästa protein binder brevid. Dessutom ändrar inbindning av proteiner ofta formen på membranet, eller ändrar om ordningen på lipderna i membranet.

Detta projektet har studerat interaktionen mellan enskilda α-Synuclein och lipidmembran med hjälp av fluoroscens-mikroskopi. Det innebär att man fäster syntetiska lipidmembran med en färgmarkör på en yta. De syntetiska membranen kan ha formen av vesiklar eller vara ett platt lipidmembran. När man sedan tillsätter proteiner som har en annan färgmarkör, kan man studera interaktionen på olika sätt genom att illuminera färgmarkörerna, som då emitterar ljus med en viss våglängd (Figur 5). Om man vet hur mycket ljus ett protein avger, kan man exemplevis räkna ut hur många proteiner som har bundit till en viss yta på ett platt membran eller en vesikel, genom att jämföra den totala mängen

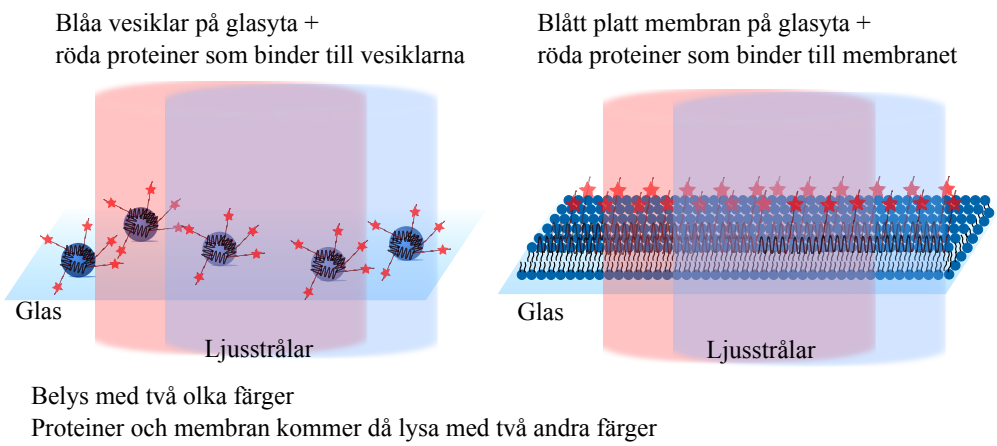

Figur 5: Illustration av de två huvudsakliga metoder som används i avhandlingen.
Vesiklar eller platta lipidmembran märkta med blåa markörer fästs på en glasyta. Protein, märkta med en röd markör, interagerar med lipidmembranen. Genom att belysa systemen med ljus med två olika färger kan man visualisera proteinerna och lipidmembranen, och på så vis studera hur dessa interagerar.

ljus som avges på ytan med hur mycket ljus ett protein avger. Genom att använda denna principen har det visats att α-Synuclein binder cooperativt till både platta membran och vesiklar, även i system med väldigt låg proteinkoncentration (Figur 6A). Det har även visats att proteinet binder till membranet under en relativt lång tid när det finns överskott av lipidmembran och många proteiner binder till samma yta, jämfört med när enstaka protein binder sporadiskt (Figur 6B). Dock samexisterar fritt protein med bundet protein, och även om proteinerna är bundet en längre tid, bytar vissa proteiner plats med varandra.

Membranet behöver även innehålla en viss mängd negativt laddade lipider för att proteinet ska kunna binda till membranet (Figur 6C). Desto fler negativt laddade lipider som finns i membranet, desto fler proteiner kan binda till en viss en yta. Detta gäller upp till den punkt där membranet är saturerat med protein, dvs det inte får plats med fler protein på ytan. Slutligen har det visats att α-Synuclein ensamt inte kan inducera sammansmältning av två membran, men inbindningen av många proteiner

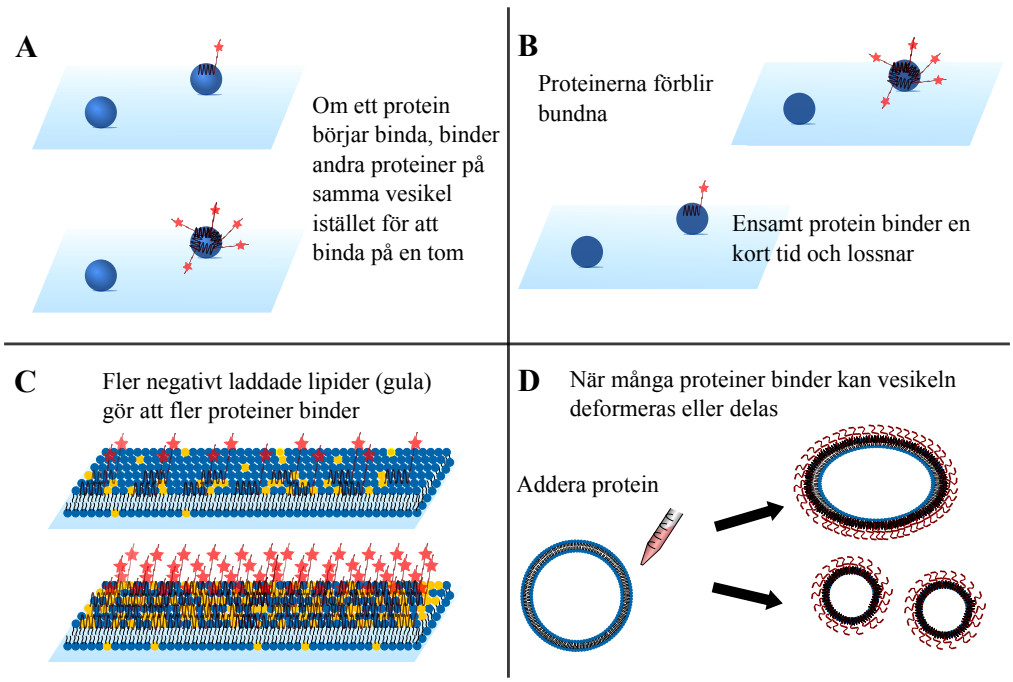

Figur 6: Illustration av huvudresultaten.
(A) α-Synuclein binder copperativt. Detta innebär att om ett protein har bundit, kommer de andra proteinerna binda brevid. (B) Hur lång tid ett protein är bundet beror på proteinkoncentrationen i systemet, och hur många protein som är bundna. (C) Genom att öka antalet negativt laddade lipider i membranet kan fler proteiner binda till en viss yta. (D) Om en vesikel har många protein bundna kan den deformeras eller dela på sig.

till en vesikel kan leda till deformation av vesikeln eller delning av en vesikel till två vesiklar, allt beroende på vilken typ av lipider som vesikeln är uppbyggd av (Figur 6D).

Sammanfattningsvis kan det konstateras att dessa studier har bidragit till en ökad förståelse för interaktionen mellan α-Synuclein och lipidmembran. Resultaten visar att interaktionen mellan α-Synuclein och lipidmembran på flera sätt är lik interaktionen mellan lipidmembran och peripherala proteiner i synsapsen som reglerar vesikel-trafiken. Således finns det indikationer att α-Synuclein har en liknande roll i en frisk kropp. Dock måste det påpekas att denna avhandling har studerat syntetiska system, och att lipidmembranen i kroppen i den intra och extracellulära miljön är betlydligt mer komplexa. Tillsammans med tidigare och fortsatta studier, som även ikluderar studier på kroppsvävnad, bidrar dock resultaten från denna avhandling till ökad förståelse för α-Synucleins funktion i den friska kroppen.

List of publications

This thesis is based on the following publications, referred to by their Roman numerals:

I **Cooperativity of α-Synuclein binding to lipid membranes**
K. Makazewics, S.Wennmalm, B. Stenqvist, M. Fornasier, **A. Andersson**, P. Jönsson, S. Linse and E. Sparr
ACS Chem. Neurosci., 2021, 12, 12, 2099–2109

II **The density of anionic lipids modulates the adsorption of α-Synuclein**
A. Andersson, S. Linse, E. Sparr, M. Fornasier and P. Jönsson
To be submitted

III **Single-vesicle intensity and colocalization fluorescence microscopy to study lipid vesicle fusion, fission, and lipid exchange**
A. Andersson, M. Fornasier, K.Makasewicz, T. Pálmadóttir, S. Linse, E. Sparr and P. Jönsson
Front. Mol. Neurosci., 2022, 15

IV **Time resolved interactions between α-Synuclein and single vesicles below saturating conditions**
A. Andersson, M. Fornasier, S. Linse, E. Sparr and P. Jönsson
Manuscript

Publications not included in this thesis:

Snapshot multicolor fluorescence imaging using double multiplexing of excitation and emission on a single detector
K. Dorozynska, S. Ek, V. Kornienko, D. Andersson, **A. Andersson**, A. Ehn, and E. Kristensson
Sci Rep. 2021, 11, 20454

Author contributions

Paper I: Cooperativity of α-Synuclein binding to lipid membranes

A.A. performed optimization of the TIRF measurements and made the initial measurements of α-Syn adsorption onto SLBs.

Paper II: The density of anionic lipids modulates the adsorption of α-Synuclein

A.A. designed the study together with P.J., M.F. and E.S. A.A performed all experimental measurements and data analysis. A.A wrote the manuscript together with P.J., M.F., E.S and S.L.

Paper III: Single-vesicle intensity and colocalization fluorescence microscopy to study lipid vesicle fusion, fission, and lipid exchange

A.A designed the study together with P.J. A.A performed all measurements and data analysis. A.A. developed the analysis tool with input from P.J., and wrote the manuscript with input from the co-authors.

Paper IV: Time resolved interactions between α-Synuclein and single vesicles below saturating conditions

A.A. designed the study with input from P.J. and E.S. A.A. performed all measurements and data analysis, and wrote the manuscript with input from the co-authors.

An introduction to the nervous system and Parkinson's disease

---

Det har jag aldrig provat tidigare, så det klarar jag helt säkert.

— Okänd

Chapter outline

This chapter will introduce the biological system that is the basis for the studies in this thesis. Initially, neurons and the function of the synapse will be introduced. This is followed by an introduction of neurodegenerative disorders and more specifically Parkinson's disease, which is the medical motivation for studies of α-Synuclein interactions with the lipid membrane.

Neurons and the function of the synapses

Neurons are cells that are the building blocks of the nervous system, and they are responsible for the communication between the brain and the rest of the body. The neurons consist of a cell body with long projections called axons and dendrites. The axon is the output and the dendrites are the input of the neurons. The area where two cells meet is called a synapse, and the space between the two cells is called a synaptic cleft. A signal is passed from one cell to the other by release of neurotransmitters over the synaptic cleft (Figure 7), which is initiated by an electric signal that is passed though the first cell. The electric signal stimulates the voltage-gated calcium channels and calcium ions flow into the cytosol from the extra-cellular environment. The increase of intra-cellular calcium stimulates exocytosis of presynaptic vesicles into the cell membrane and the neurotransmitters can be released into the synaptic cleft [1–3]. Neurotransmitters diffuse across the synaptic cleft between the two cells and bind to receptors on the second, post-synaptic, cell [3]. Binding of the neurotransmitters to receptors on the post-synapse activates the post-synaptic cell and sends an electric signal throughout that cell. When the post-synaptic cell has been activated, the neurotransmitters are released from the receptors and either digested by enzymes in the synaptic cleft or taken up by the first neuron by endocytosis.

Diseases that cause the progressive malfunction and ongoing death of neurons are called neurodegenerative disorders [4, 5]. Neurodegenerative disorders are often connected with symptoms such as tremor, loss of muscle function and dementia [5, 6]. The two most common neurodegenerative disorders are Alzheimer's disease (AD) and Parkinson's disease (PD) [7], which both are connected to the presence of proteins that have aggregated into fibrillar amyloids [8].

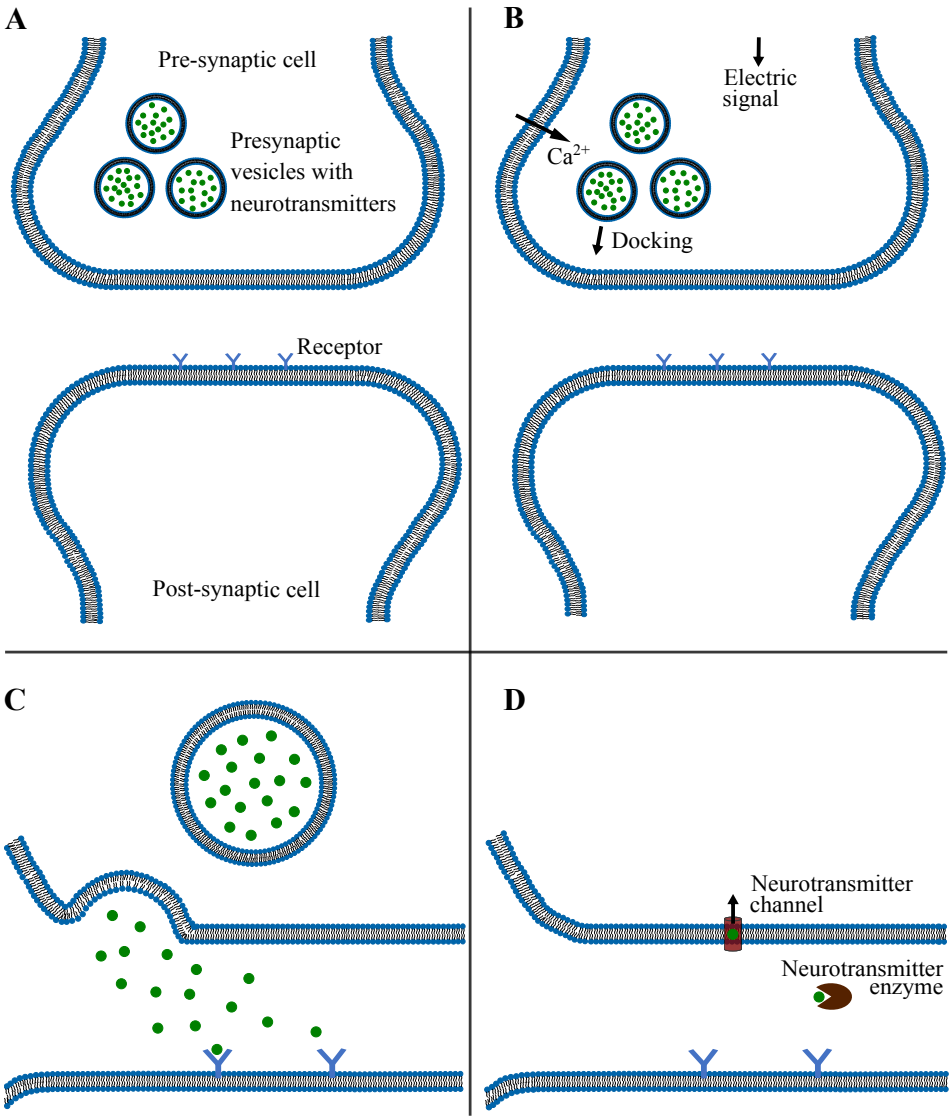

Figure 7: Signalling between neurons.
Signalling between neurons take place at the synapses. The area where two cells meet is called a synapse, and the space between the two cells is called a synaptic cleft. (A) The cytosol of the pre-synaptic cell includes synaptic vesicles loaded with neurotransmitters. (B) When an electric signal reaches the end of the pre-synaptic cell, voltage-gated calcium channels open and Ca^{2+} flow into the the cytosol. The increase of intracellular calcium stimulates exocytosis of presynaptic vesicles. (C) Fusion of the synaptic vesicles with the plasma membrane results in the neurotransmitters being released into the synaptic cleft and bind to receptors on the post-synaptic cell. (D) When the second cell has been activated, the neurotransmitters are released from the receptors and digested by enzymes or taken up by the the pre-synaptic cell.

α-Synuclein and Parkinson's disease

PD is the second most common neurodegenerative disorder. Only a small fraction of PD cases are confirmed familial (approximately 5-10%), while the remaining cases are idiopathic [9–11]. Every year, 8-18 per 1000 people are diagnosed with PD [12], and over ten million people around the world are currently living with PD [7]. The symptoms of PD include motor-symptoms such as tremor, slowness of movement, rigidity, and postural instability [7, 13], but also non-motor symptoms such as depression, apathy and sleep disorders [7, 13, 14]. There is only a minor reduction of the life expectancy when living with PD [15], where the most common reason for a pre-mature death for PD patients is aspiration pneumonia [15, 16]. The loss of muscle control leads to trouble swallowing which results in the patient inhaling small pieces of food that get stuck in the lungs and cause an infection.

The symptoms related to PD have been reported several thousand years back in history on Egyptian papyrus writings. However, it took until 1817 until the symptoms were concluded in a written summary when the British doctor James Parkinson published a report of the symptoms called "An essay on the Shaking Palsy" [17]. Other neurologists continued the study of the disease, one of them was Jean-Martin Charcot who was the one to distinguish between rigidity and weakness [18], and named the disease in honor of James Parkinson. In 1912, Freidrich Lewy published his findings of some microscopic particles in the brains of patients with neurodegenerative diseases in the seminal 1912 publication in Lewandowsky's Handbook of Neurology, particles he called Lewy Bodies [18]. Seven years later, Konstantin Tretiakoff found that it was the substantia nigra part of the brain that was affected [18], and in the 50's it could be concluded that the Lewy bodies were mostly present in the dopaminergic neurons in the substantia nigra part of the brain [19]. The Lewy bodies were later found in several other neurodegenerative diseases [8], and 1997 it was found that the Lewy bodies related to PD mainly consisted of the protein α-Synuclein (α-Syn), [20], which is a short (14 kDa) intrinsically disordered protein that mainly is present in the pre-synapses in the neurons in the substantia nigra part of the brain [21]. The healthy function of α-Syn in the synapses is not yet fully understood, but it is hypothesised to in some manner participate in and regulate the release of the neurotransmitters into the synaptic cleft. It has been proposed that

α-Syn might regulate the size of the vesicle pool [22, 23], or is involved in vesicle recycling [24–26]. Others suggest that the function of α-Syn involves regulation of neurotranmission [27, 28] or that α-Syn is involved in the vesicle trafficking over the synapses by assisting during endo- and exocytosis [29–32].

Aim of the thesis

Deprived of meaningful work,
men and women lose their reason for existence;
they go stark, raving mad.

— Fyodor Dostoevsky

The overall aim of this thesis has been to study the interaction between monomeric α-Syn and lipid membranes, to obtain a better understanding of the physiological role of α-Syn. Many of the previous studies of interactions involving α-Syn have been using bulk techniques, which means that individual events in a heterogeneous sample disappear in a bulk average. Hence, one major aim of this thesis has been to explore the use of fluorescence microscopy single vesicle and single molecule techniques, to study individual events. This includes development of methodology and image analysis tools, which was done in paper III and IV. Using these and other fluorescence microscopy techniques, four main aspects of the interaction between α-Syn and lipid membranes were studied. These four aspects were studied in four different projects, that are presented in paper I-IV. Even though several parallels can be drawn between the projects, they have had four different main aims.

1. The main aim of paper I was to investigate whether α-Synuclein binds cooperatively.

2. In paper II, the main aim was to study how the density of α-Syn adsorbed to lipid membranes was affected by the amount of anionic lipid in the membrane.

3. The main aim of paper III concerned the ability of α-Syn to induce fusion, fission or lipid exchange between vesicles. To study these events, a single vesicle assay was developed. The assay was then used to investigate how fusion, fission and lipid exchange depend on the lipid composition of the membrane.

4. The main aim of paper IV was to study the binding kinetics of α-Syn. This study includes several aspects, such as cooperative binding and the effect of different membrane properties.

Chapter 1

α-Synuclein interactions with lipid membranes

No man should escape our universities
without knowing how little he knows.

— J. Robert Oppenheimer

Chapter outline

The aim of this chapter is to introduce α-Syn and lipid membranes to the reader. The chapter will start with an introduction of lipids and lipid membranes, followed by a short introduction of proteins that will lead to a presentation of the protein of interest in this thesis, α-Syn. The chapter ends with a section that introduces previous research of α-Syn interactions with lipid membranes. Each subsection will end with the questions the previous studies have raised, and how these questions are related to the research output from the papers included in this thesis, which are presented in chapter 3-4.

1.1 Lipids and lipid membranes

Phospholipids are macromolecules that are the main building blocks of cell membranes. A phospholipid has two hydrocarbon chains and one phosphate containing polar head group, which results in an amphiphilic lipid molecule. The amphiphilic property of phospholipids enables the formation of lipid bilayers in polar solvents, where the hydrophobic hydrocarbon chains of the monolayer leaflets are directed towards each other and the hydrophilic phosphate headgroups are directed towards the solvent. A lipid bilayer is approximately 4-5 nm thick [33–35], depending on the length of the hydrocarbon chains and the phase behavior. The fluidity of a lipid bilayer depends on the composition, temperature, pressure and solution conditions. In a uniform fluid bilayer, the lipids move fast in the plane of the membrane with a lateral diffusion of approximately 1-3 $\mu m/s$ [36]. The lipid molecules in the bilayer can also undergo transverse diffusion, which is a flip-flop movement of lipid molecules between the inner and outer leaflet of the bilayer, but this process occurs on much longer timescales due to the energy cost of moving polar groups through the hydrophobic environment in the center of the bilayer.

1.1.1 The plasma membrane

The plasma membrane of animal cells is constructed as a lipid bilayer containing three major types of lipids; phospholipids, glycolipids and cholesterol, where phospholipids are the most abundant type [37]. Some of the most abundant phospholipids found in the plasma membrane are phosphatidylcholine (PC), phosphatidylethanolamine (PE) and phosphatidylserine (PS) [38]. These phospholipids are non-uniformly

distributed between the monolayers, with PC more abundant in the outer leaflet and PS and PE are more abundant in the inner leaflet [39, 40]. PC and PE lipids are zwitterionic, while PS is anionic with a net charge of -1. The lipids can either have two saturated hydrocarbon chains, two unsaturated hydrocarbon chains, or one hydrocarbon chain that is saturated and one that is unsaturated. Two common hydrocarbon chain compositions in cellular membranes are the 16 carbon long saturated chain (16:0), and the 18 carbon long unsaturated chain (18:1).

Among the glycolipids, the most abundant type of lipid are the gangliosides, that are primarily present in the outer leaflet in the plasma membranes [41, 42]. Gangliosides are glycosphingolipids with a sialic acid moiety that is linked to an anionic and relatively large oligosaccharide headgroup. This thesis has been focused on the interaction between α-Syn and lipid membranes consisting of the zwitterionic 1,2-dioleoyl-sn-glycero-3-phosphocholine (DOPC), and 1,2-dioleoyl-sn-glycero-3-phosphocholine (POPC), and the anionic 1,2-dioleoyl-sn-glycero-3-phospho-L-serine (DOPS) and monosialotetrahexosylganglioside (GM1), which are shown in Figure 1.1.

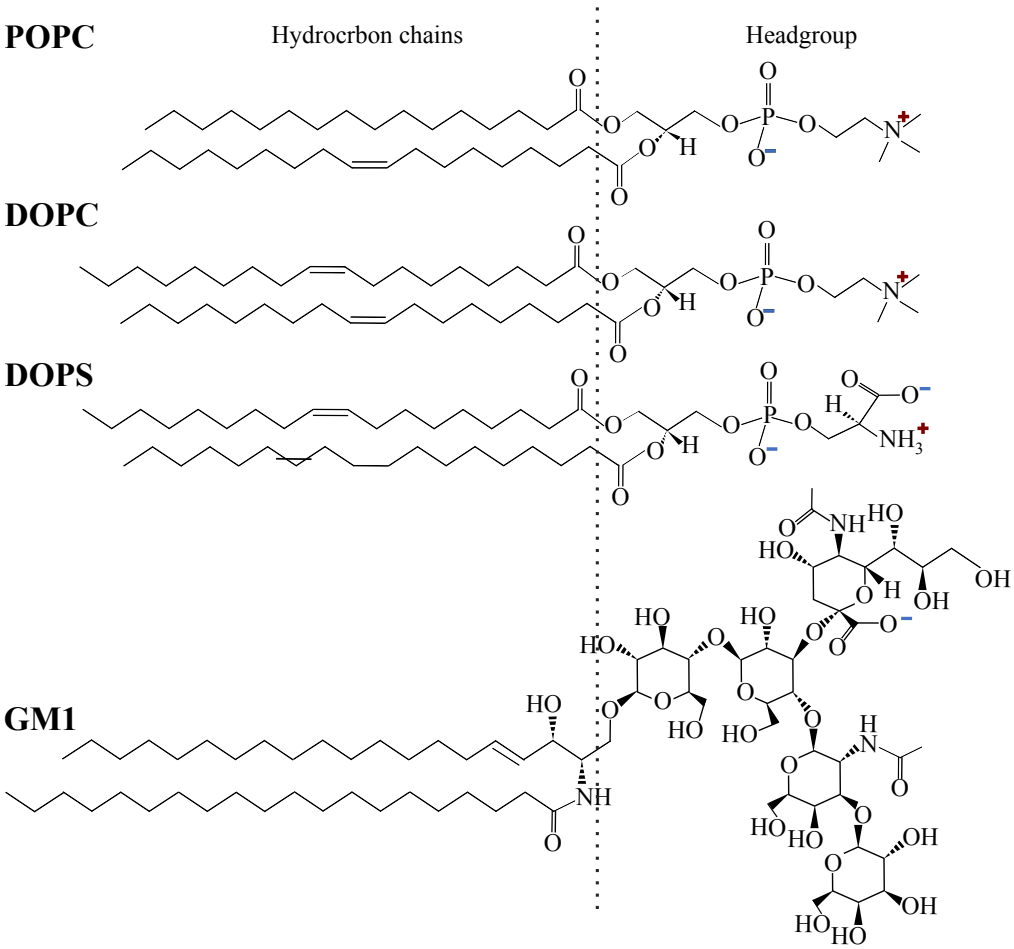

Figure 1.1: Lipids present in the membranes studied in this thesis.
This thesis includes four different types of lipids that can be found in the plasma membrane. POPC, DOPC and DOPS are phospholipids and GM1 is a ganglioside. POPC and DOPC are zwitterionic while DOPS and GM1 are anionic.

1.2 Syntethic lipid membranes

In addition to lipids, the plasma membrane includes different proteins with various functions, that are anchored on the surface or extend through the lipid membrane. To simplify experiments, synthetic model membranes can be used [43]. Small unilamellar vesicles (SUVs) are commonly used to model pre-synaptic vesicles, and supported lipid bilayers (SLBs) can be used to model the plasma membrane (Figure 1.2). Depending on the question to be studied in a specific experiment, different lipids can be incorporated into the bilayer.

1.2.1 Formation of small unilamellar vesicles

SUVs are generally prepared by dissolving lipids from stock solutions to obtain molecular mixing, whereafter the solvent is evaporated and the lipids are resuspended in experimental buffer. When resuspending dry lipids in an aqueous buffer, the lipids can form both unilamellar and multilamellar vesicles (MLVs), which are vesicles consisting of several layers of bilayers, in a large range of sizes [43]. Several methods can then be used to obtain unilamellar vesicles. Two common methods are extrusion [43–45] and ultra-sonication [43]. During extrusion, the lipid solution is pushed through a filter membrane with pores of a certain diameter. If the pore diameter is smaller than the diameter of the MLVs in the solution, the MLVs will break down and form SUVs in a similar size as the pore size. The great advantage of extrusion over sonication is that extrusion generally generates a more monodispersed vesicle solution.

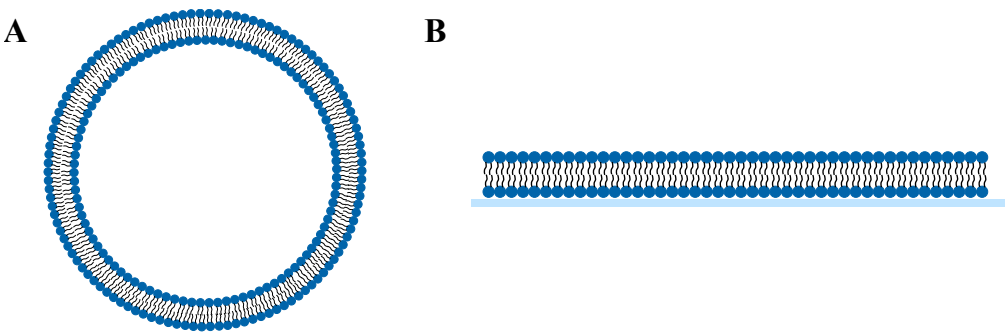

Figure 1.2: Lipid membranes.
Lipid membranes consists of two monolayers with the hydrophobic tails directed towards each other and the hydrophilic headgroups directed outwards. Synthetic lipid membranes are often used to model synaptic vesicles and the plasma membrane.(A) Small unilamellar vesicles are used to model synaptic vesicles. (B) The plasma membrane is often modelled by supported lipid bilayers.

When sonicating the vesicles, the sample is exposed to ultrasound waves that creates microbubbles due to the compression and rarefaction of the wave. The microbubbles quickly disrupt which leads to high local temperature and pressure that induces shear forces on biological material in the sample. The shear forces temporarily disrupt lipids in the MLVs, and when the lipids are rearranged, they eventually form SUVs that are smaller and more stable than the MLVs. Increasing the effect, i.e. the frequency, of the ultra-sonicator results in an increased shear force and a smaller SUV size. The advantage with ultra-sonication is that the vesicles are more robust, and does not age as quickly as extruded vesicles [46]. In this thesis, SUVs have been obtained using ultra-sonication.

1.2.2 Formation of supported lipid bilayers

There are several ways to form a supported lipid bilayer [47, 48]. The three most commonly used methods are (i) deposition of a monolayer on a hydrophilic planar surface by pulling the surface through a water-air interface, and then depositing a second monolayer on the first one [49–51], (ii) hydration of dried lipids on a surface resulting in the spreading of a lipid bilayer [52], and (iii) fusion of SUVs [53, 54] (Figure 1.3). When a sufficiently high concentration of SUVs is added to a solid substrate they rupture and fuse, forming a continuous bilayer. A thin layer of water (1-2 nm) between the SLB and the substrate ensures fluidity and free lateral diffusion of the bilayer [35, 50]. In this thesis, SLBs have been deposited via fusion of SUVs.

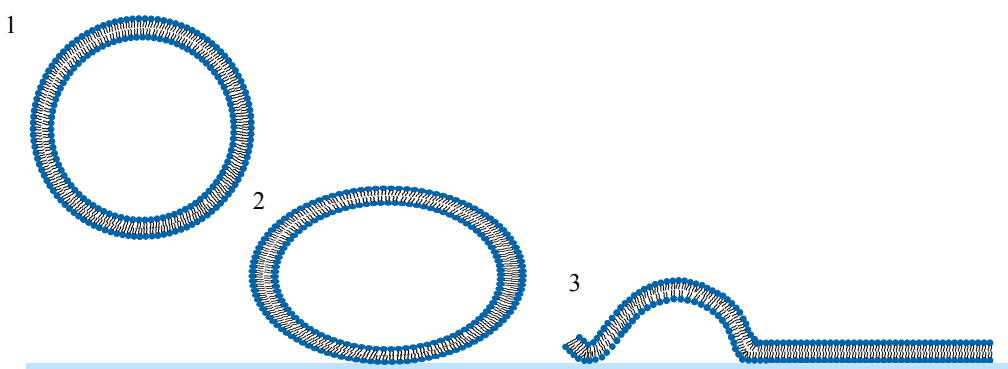

Figure 1.3: Formation of supported lipid bilayers by vesicle fusion.
A high concentration sample of SUVs are are deposited onto a glass coverslide. The vesicles rupture and fuse to form a lipid bilayer.

1.3 Proteins

Proteins have several different roles in the human body. Enzymes, for example, are proteins that facilitate different reactions like digestion, antibodies are proteins that are produced by the immune system in order to fight an infection when a foreign pathogen is detected in the body, and hormone proteins like insulin regulates uptake of glucose in the cells.

Proteins are built up by smaller units called amino acids. Every protein has its own unique amino acid sequence, which gives the protein a unique native fold and their own specific role in the human body. Tertiary and quaternary structures depend on the secondary structure of the protein, which is determined by the molecular groups on the amino acid side chains. One of the most common secondary structures are the left-handed α-helix where the protein chain is forming a spiral around its own axis. The α-helical conformation can be either left-handed or right-handed. In the human body, almost all α-helical conformations are left-handed [55].

Another type of secondary structure is the β-sheet. The β-sheet is a formation where the amino acids are arranged in β-strands kept together by hydrogen bonds between the amino acids in the strands. A strand has a certain direction from the N-terminus to the C-terminus based on how the hydrogen bonds are formed. A sheet with evenly spaced hydrogen bonds along the strands, with an angle in relation to the strand axes, is called a parallel β-sheet, while a sheet with unevenly spaced hydrogen bonds perpendicular to the strand axes is called an anti-parallel β-sheet. Several β-sheets can interact and form a fibril.

Some proteins have a native state that is unfolded, which is called a random coil conformation. The random coil conformation does not have a specific structure but is, as the name suggests, in a random conformation. Proteins with a native unfolded state are called intrinsically disordered proteins (IDPs). These proteins often have many charged and polar residues [56]. Under certain circumstances, however, the IDPs can start to fold and self-aggregate to form β-sheet rich amyloid fibrils and inclusion bodies. The presence of IDP including aggregates has during the last decades been a hallmark of several neurodegenerative diseases [57–59], and the oligomeric α-Syn aggregates have been related to cytotoxicity [60–62].

1.3.1 α-Synuclein

α-Syn is a 140 amino acid long intrinsically disordered pre-synaptic protein that has a net negative charge at neutral and slightly acidic pH. α-Syn is often divided into three main segments (Figure 1.4). The N-terminus part is 60 amino acids long (residue 1-60) and contains both negative and positive residues with an overall positive charge. Many of the known mutations involved in α-Syn pathogenesis are located in the N-terminus part [63]. The NAC region (which has got its name from the Non-Amyloid Component of amyloids formed by the AD-related peptide Amyloid β) consists of residues 61-95. This region is highly hydrophobic and induces the β-sheet structure of amyloid fibrils. Together, the N-terminus and the NAC-region contains 11 repetitive KTKEGV sequences, that enables the formation of an α-helix upon binding to negatively charged lipid membranes [64]. The proline-rich C-terminus part (residue 96-140) is highly acidic at neutral and slightly acidic pH.

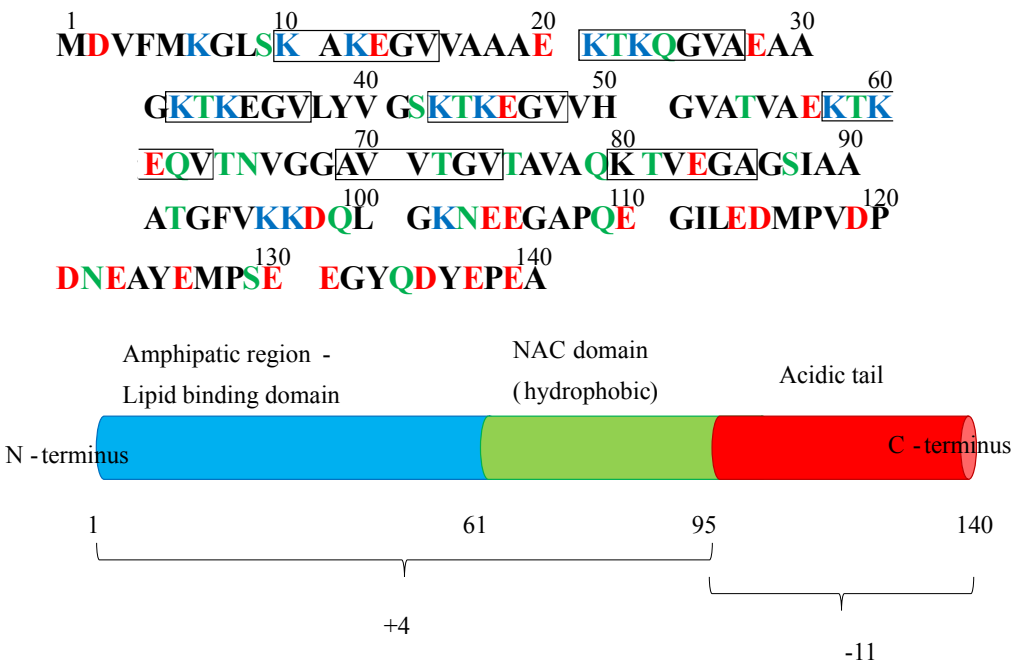

Figure 1.4: α-Synuclein
α-Syn is a 140 amino acid long IDP. The protein has a non-uniform charge distribution, where the N-terminal part has an overall positive net charge and the C-terminal part has an overall negative net charge. The middle region (NAC-region) is highly hydrophobic. Together, the N-terminal part and the NAC-region contains 11 KTKEGV sequences that enables association to negatively charged lipid membranes.

1.4 Interactions between monomeric α-Synuclein and lipid membranes

Due to the repetitive KTKEGV periodic sequences in the N-terminal part and the NAC-region, α-Syn is able to adopt an amphipathic α-helical conformation where the polar residues are separated from the non-polar residues at different faces of the helix [65]. The amphipatic property of the α-helical conformation along with the non-uniform charge distribution of the protein enables α-Syn to bind to negatively charged lipid membranes [64] (Figure 1.5). The non-uniform charge distribution of the protein results in electrostatic attraction between the positively charged N-terminus and the negatively charged lipids in the lipid membrane, which may bring the protein close to the membrane surface and facilitate the membrane association. Due to the amphipatic property of the α-helix, the hydrophobic side of the α-helix is partly buried into the headgroup region of the outer leaflet of the lipid membrane [66], which stabilizes the α-helical conformation. The gradually shifting amphipaticity of the α-Syn α-helices indicates that the binding affinity of the protein is likely to decrease as the amphipaticity decreases in the NAC-region. This has been suggested based on NMR studies that identified two different binding modes of α-Syn [67, 68]. At low L:P ratios, with an excess of α-Syn, two co-existing binding modes were suggested; the short (1-25) α-helix as well as the full membrane binding (1-97) α-helix. At higher L:P ratios, i.e. in systems with α-Syn deficit, all α-Syn were bound by residue 1-97 [67]. Further NMR studies have suggested that there is a third binding mode of α-Syn [69], where the protein is bound by the first 55 residues.

The highly acidic C-terminus is electrostatically repelled by the negatively charged lipids in the membrane and by other nearby membrane-associated proteins, which results in a polymer brush extended into the solvent [70, 71]. Hence, the electrostatic repulsion between the C-termini, and between C-termini and negative charges in the membrane is believed to destabilize the association of α-Syn to the membrane [72]. Studies have shown that increasing the ionic strength in the aqueous environment screens the electrostatic attraction between the N-termini and the negatively charged lipid membrane [73], which results in a decreased number of associated α-Syn [64]. However, the association was not completely screened. This indicates that other factors play a role in membrane association, for example the minimization of exposure of the

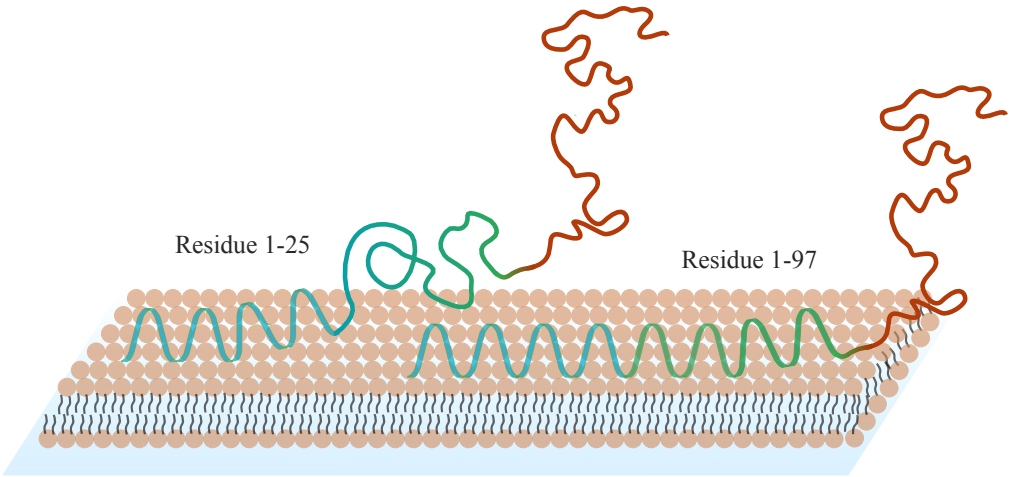

Figure 1.5: Illustration of α-Syn association to lipid membranes.
Upon association, α-Syn adopts an α-helical conformation. The length of the amino acid sequence bound to the membrane depends on the solution and membrane conditions.

hydrophobic interior of the lipid bilayer.

1.4.1 Cooperativity of α-Synuclein binding to lipid membranes

Cooperative binding of protein to a membrane implies that the binding is more favorable to occur when another (of the same kind) protein is already bound to the bilayer as compared to a fully bare membrane. An increase in the binding affinity when there are other proteins already bound is referred to as positive cooperativity, whereas negative cooperativity means a decreased binding affinity.

Cooperative binding was first discovered by Bohr [74], who studied hemoglobin binding to oxygen. This phenomenon has since been studied [75–77], and cooperative binding is now known to be a common phenomenon amongst proteins [78], that enables regulation of different processes *in vivo* at lower concentration of free protein compared to independent binding.

Several studies have shown that α-Syn associates with lipid membranes. However, it has not specifically been investigated whether the α-Syn binding to membrane is cooperative or not. Many previous studies of α-Syn have been based on bulk techniques such as spectroscopy [64, 79, 80] and nuclear magnetic resonance (NMR), [67, 68, 80]. Using bulk techniques, it is not possible to differentiate between protein binding

in patches and protein binding with a uniform spread over the membrane. Only a few studies using single-vesicle techniques have been conducted [81–83], but the data was mainly analysed in terms of bulk average. Further, many studies have investigated the low L:P regime with an excess of α-Syn [64, 67, 68, 72, 80], where the membrane is saturated with α-Syn. Protein that appears uniformly distributed when the membrane is saturated with protein, does not necessarily bind uniformly when there is not enough protein to saturate the membrane. Hence, indications of cooperative binding can be found when studying systems with a deficit of protein.

In paper I, it was shown that α-Syn binds to lipid membrane in a strongly cooperative manner. This conclusion also finds support in several previous published observations. For example, Lee *et al* showed that α-Syn bound to only a few vesicles instead of distributing uniformly over the vesicle sample [84]. Further, cross-linking and Förster Resonance Energy Transfer (FRET) experiments showed cross-linking of over eight α-Syn bound to vesicles [85]. Isothermal titration calometry, where an increasing amount of SUVs was added to a constant α-Syn concentration, showed that increasing the amount of vesicles above the saturation point where all α-Syn was bound, did not result in redistribution of the already bound α-Syn [86]. Further, double electron-electron resonance (DEER), of α-Syn labelled with a probe with an unpaired electron pair binding to vesicles was performed [87]. The minimum distance between the electrons is given by the distance between the electrons when the membrane is saturated with protein. This occurs in the low L:P regime, where there is an excess of protein. The results showed that increasing the amount of lipid membrane in the sample did not change the distributions of the distance between the electrons. This was true for intermediate and high L:P ratios corresponding to conditions where the membrane is saturated with protein, and for conditions with an excess of membrane. This indicates that there was no redistribution of α-Syn when adding excess membrane.

The cooperative binding of the protein is likely of high biological relevance since cooperative binding leads to local accumulations of α-Syn on the membrane [85, 88]. This leads to the questions if an accumulation of protein on the lipid membrane results in a change of membrane properties, for example local changes in membrane spontaneous curvature and rigidity. Such changes may eventually lead to membrane deformation and remodeling. Cooperative binding of α-Syn was studied in paper I,

where binding of α-Syn to SLBs over a wide L:P regime was investigated. Further, cooperative binding is discussed in paper IV, where α-Syn binding kinetics in a dilute system below the saturation point was studied. The results show that α-Syn indeed binds in a cooperative manner, both on vesicles and SLBs. The results are further discussed in chapter 3.1 and 4.3.

1.4.2 Membrane properties affect α-Syn association with lipid membranes

The interaction between α-Syn and lipid membranes depends on several factors, such as the L:P ratio and the membrane composition [64, 89, 90]. For example, previous studies have shown that α-Syn associates with membranes consisting of anionic lipids [89–91], where the amount of bound α-Syn depends on the content of charged lipids. Circular dichroism (CD), spectroscopy studies show that increasing the amount of anionic lipids from 30% to 67% does not significantly increase the amount of α-helical structure [92], which is a characteristic of the membrane-bound state, while NMR studies where the DOPS content was increased from from 15 to 50% increased the fraction of bound α-Syn [93]. Other NMR studies of membranes with various amounts of anionic lipids suggests that increasing the amount of anionic lipids alters the length of the sequence that is bound to the membrane [67, 94].

Previous studies have shown that α-Syn has a higher binding affinity for vesicles with a diameter less than 40 nm compared to vesicles with a diameter of 40-100 nm [64, 66, 82, 86]. This has been explained by that smaller vesicles are more prone to packing defects originating from a high curvature [64, 82, 86, 95–97]. Hence, the hydrophobic interior of the bilayer would experience a higher exposure to the solvent, enhancing binding of an amphipathic helix. This suggestion is strengthened by studies where α-Syn association onto DOPC:DOPS membranes were compared to α-Syn association onto POPC:POPS membranes. It was shown that more α-Syn was associated to membranes consisting of DOPC:DOPS, which was explained by DOPC and DOPS having two unsaturated hydrocarbon chains while POPC and POPS only have one unsaturated hydrocarbon chain. A bilayer consisting of DOPC:DOPS is hence less densely packed, meaning that the hydrophobic interior is more exposed to the solvent compared to a membrane consisting of POPC:POPS, which is suggested to enhance binding of α-Syn [66, 72].

α-Syn is generally considered to associate with membranes containing anionic lipids but not with membranes containing zwitterionic lipids only. However, in several studies, α-Syn association to membranes containing zwitterionic lipids only have been detected [66, 86, 98], but the amount of α-Syn associated to zwitterionic membranes is much lower than the amount of α-Syn associated to membranes containing anionic lipids. It has been suggested that α-Syn binds to membranes consisting of only zwitterionic lipids by binding to defects in the lipid membrane [66, 86]. Hence, it has been suggested that α-Syn association to membranes containing anionic lipids are governed by electrostatic interactions between the N-terminus part and the anionic headgroups in the membrane to a large extent. The association to membranes containing zwitterionic lipids only would instead be driven by interactions between hydrophobic residues in the α-helix and the hydrophobic interior of the membrane at membrane defects. Hence, a higher membrane curvature with more packing defects has been suggested to be a major contribution of increasing the binding affinity for α-Syn association to zwitterionic membranes [66].

Furthermore, it has been suggested that α-Syn has a higher binding affinity to a flexible membrane compared to a more rigid membrane, since α-Syn association likely results in bending of the membrane [99] and membrane remodeling [98, 100]. Hence, α-Syn has been suggested to be both a curvature sensing and curvature inducing protein.

Altogether, α-Syn is considered to associate with lipid membranes containing anionic lipids but not to lipid membranes containing only zwitterionic lipids. Most studies have investigated association onto lipid membranes containing no anionic lipids or large fractions of anionic lipids (30-100% anionic lipids). However, little is known about α-Syn association to membranes consisting of low amounts anionic lipids. Further, the density of α-Syn associated to membranes with various curvature and rigidity has not been investigated thoroughly. These questions have been investigated in paper II, where α-Syn adsorption onto anionic model membranes composed of either planar deposited bilayers that are restricted by the underlying surface, or free deformable bilayers in SUVs. These studies can spread new light on some of the unresolved questions related to α-syn binding to membrane with different rigidity and curvature. The results are further discussed in chapter 3.2-3.3.

1.4.3 Monomeric α-Synuclein induced vesicle fusion, fission and deformation

As mentioned in the introduction, the physiological function of α-Syn is not fully understood, but interactions between monomeric α-Syn and lipid membranes is believed to have a crucial role. Cryo-TEM studies of α-Syn and DOPS containing vesicles have shown how spherical vesicles adopt a prolate shape in presence of α-Syn [101], that first was hypothesized to be a result of vesicle fusion. The hypothesis of α-Syn induced fusion was explained by the double-anchor model, that suggested that α-Syn binding to two vesicles would enable fusion of vesicles. However, the double-anchor model mainly suggests monomeric α-Syn binding to two different vesicles [101, 102], and does not provide direct evidence of α-Syn induced fusion between vesicles. Instead, recent cryo-TEM studies of DOPC:DOPS 7:3 vesicles in presence of α-Syn have shown that the vesicles indeed change shape, but that the number of vesicles and the prolate shape was constant over time [103]. This indicates that the association of α-Syn results in stable deformation of the vesicles, but that the vesicles do not undergo fusion. The results was confirmed by fluorescence cross-correlation spectroscopy (FCCS), experiments that showed neither clustering nor fusion of DOPC:DOPS vesicles in presence of α-Syn [103].

Instead, other studies have shown that α-Syn interactions with vesicles including PG lipids induced membrane remodeling eventually resulting in vesicle rupture [104]. Another study showed that α-Syn binding to membranes containing GM1 resulted in membrane remodeling, where lipids rafts containing GM1 lipids acted as a strong binding mediator [105]. There are also indications that α-Syn induces fission of GM1-containing vesicles during the course of amyloid formation [106]. Hence, prolate shaped vesicles are likely to be fission intermediates.

The disagreement in the previous literature regarding the ability of α-Syn to induce vesicle fusion, fission, clustering and/or deformation [101, 103], leaves a knowledge gap on how α-Syn may induce membrane remodelling processes. This may in turn be important for the physiological role of α-Syn. Previous studies have included different methods to study the above listed mechanisms, yet the results are inconclusive. This led to the development of a fluorescence microscopy-based method that was able to detect fusion, fission and lipid exchange between differently labelled lipid vesicles. The method is presented in paper III and chapter 4.1. Paper

III and chapter 4.2 present results that show that neither fusion, fission or lipid exchange occur for DOPC:DOPS 7:3 vesicles in presence of α-Syn, but vesicles containing GM1 undergo fission in presence of α-Syn.

1.4.4 α-Synuclein binding kinetics

Although the knowledge of α-Syn interaction with lipid membranes has been steadily increasing, little is known about the kinetics of α-Syn binding to lipid membranes. Several methods have been used to try to characterize the kinetics of the binding, but there is a lack of systematic characterization of the exchange rate and binding lifetime for different systems and conditions.

Previous studies of α-Syn binding kinetics in presence of DOPC:DOPS vesicles indicate that the binding lifetime is in the range of ms in a system with an excess of protein [69]. Another study suggested that the exchange rate is between 50-700 s^{-1} for SUVs with various amount of anionic lipids [66]. There are also indications that α-Syn remains bound for seconds or longer at the saturation point where there is neither excess or deficit of α-Syn [72]. Other studies of a system with an excess of protein have suggested that the binding lifetime may vary depending on the length of the amino acid sequence bound to the membrane [67]. To further investigate the binding kinetics for systems below saturation conditions, and study how the membrane charge density affects the binding kinetics, single vesicle interactions between DOPC:DOPS containing SUVs and α-Syn were studied in paper IV. A method to investigate the binding lifetime of membrane-associating proteins, as well as new insights regarding the binding kinetics of α-Syn, will be further discussed in chapter 4.3.

Chapter 2

Fluorescence microscopy

The definition of insanity is doing the same thing over and over again and expect different results.

.....

Two things are infinite: the universe and human stupidity; and I'm not sure about the universe.

— Albert Einstein

P.S Do not scare the lab elf. D.S.

Chapter outline

The aim of this chapter is to give the reader an introduction to fluorescence microscopy and the methods used in this thesis. The chapter will start with some basic concepts of microscopy and then continue with fluorescence probing and fluorescence microscopy. Finally, the microscopy methods used in this thesis will be discussed.

2.1 Microscopy

Conventional light microscopy is a method widely used in the field of life sciences. The method relies on light being focused onto a sample by a magnifying objective, and viewed through an eyepiece. The simplest version of light microscopy is bright-field microscopy, where a light absorbing sample is illuminated from below, resulting in an image built up by light transmitted through the sample with dark fields corresponding to the sample. The opposite version to bright-field microscopy is dark-field microscopy, where the image is built up by light scattered from the sample. This results in a setup that collects light at an angle from the sample, with bright fields are light scattered by the specimen of interest. The benefits of these techniques is that they are easy to set up, and it is possible to visualize living tissue non-intrusively and without any modifications to the sample [107].

The magnification of the sample depends on the lenses in the objective and is described as

$$M = \frac{d}{f_0} \tag{2.1}$$

where f_0 is the focal length of the objective lens and d is the distance between the back focal plane of the objective and the focal plane of the eyepiece. The angle a lens can spread or collect light from is given by the numerical aperture (NA) [108]. The NA is a dimensionless number that is related to the focal length of the lens and the refractive index of the medium the light is propagating through as

$$NA = n\sin(\theta) \approx n\frac{D}{2f} \tag{2.2}$$

where n is the refractive index of the medium, D is the diameter of the lens, f is the focal length and θ is the half-angle over which the lens can collect light.

The resolution of a conventional optical microscope is diffraction-limited, i.e. the resolution of the system is limited by the wavelength of the emitted light [109]. Emission from a small molecule passing through circular apertures will be diffracted and interfere with itself, resulting in a ring-like pattern. This pattern is known as the "airy disc", and can be described by a point spread function (PSF). The distance for constructive or destructive interference is given by Bragg's law

$$m\lambda_0 = 2d\sin(\theta) \tag{2.3}$$

where m is the order of the interference maximum/minimum and d is the distance between two objects scattering light. This means that the minimum distance two point objects can be resolved at is

$$d = \frac{\lambda_0}{2\sin(\theta)} = \frac{\lambda}{2n\sin(\theta)} = \frac{\lambda}{2NA}. \tag{2.4}$$

Hence, the small point source will appear as a larger spherical disc (first maxima of the diffraction pattern) surrounded by bright rings on the sensor of the imaging system. For very small apertures, where the aperture size is in the same range as the wavelength of the light or smaller, the resolution limit is given by the Rayleigh criterion. The Rayleigh criterion states that "two images are just resolvable when the centre of the diffraction pattern of one is directly over the first minimum of the diffraction pattern of the other". For two circular objects, where the first minimum occurs at a distance 1.22 θ from the centre, the minimum resolvable distance is translated to

$$d = \frac{1.22f\lambda}{nD} = \frac{0.61\lambda}{NA}. \tag{2.5}$$

The objective is usually either an air or oil objective, meaning that the medium between the objective lens and the glass cover slide with the sample is either oil or air. Air objectives are typically used in bright-field microscopy where the illumination is propagating in one axis and the demands on resolution and magnification are not as high. When higher resolution or magnification is needed, oil objectives are beneficial. An oil objective has a larger numerical aperture, meaning that the objective can collect light in a larger angle which increases the resolution.

2.2 Fluorescence probing

An atom have several electronical energy levels. When electrons in an inner electron energy level is excited to an outer level, they will spontaneously de-excite to the lower electron energy level and emit photons. For large molecules with a large number of different atoms, the electron energy levels are more similar to a continuum than discrete levels, and is usually called an energy band. The atoms in the molecule can vibrate within the bond or rotate around the bond depending on the excess energy of the molecule. Except for the electronical energy levels, the vibrational and rotational movement between two or several atoms in a molecule that share electrons in a covalent bond, give rise to vibrational and rotational energy levels. When electrons in a molecule are excited by photons that does not match the transition between two electron energy levels, they can be excited to a vibrational and in some cases a rotational level. Two atoms in close proximity, either inter-molecularly but especially intra-molecularly when the energy levels are shared, can transfer energy in a non-radiative transfer between different energy states instead of a radiative decay emitting a photon (Figure 2.1). Intra-molecularly, the most common non-radiative decay is vibrational relaxation where an electron is de-excited to a lower vibrational level within the energy level due to loss of thermal energy. Due to the overlap of vibrational and electronical energy levels at high energies the electron can undergo internal conversion. Internal conversion is a non-radiative decay where an electron is transferred between vibrational levels in two different electronic energy levels. While the previous mentioned transitions occurs between levels with the same spin multiplicity, the electron can also undergo transition from a singlet to a triplet state, known as inter-system crossing. This transition is not allowed according to quantum mechanical rules, and have a very low probability to occur.

Except for the non-radiative decays, the electron can be de-excited to a lower energy state emitting a photon. The most common type of emission is fluorescence where the molecule is emitting light with a longer wavelength than the incident light exciting the molecule. The loss of energy before fluorescing comes from either thermal relaxation or internal conversion. If the electron undergo inter-system crossing from a singlet to a triplet state from which there are no allowed transitions, the electron will remain in that energy state longer. The electron can either get rid

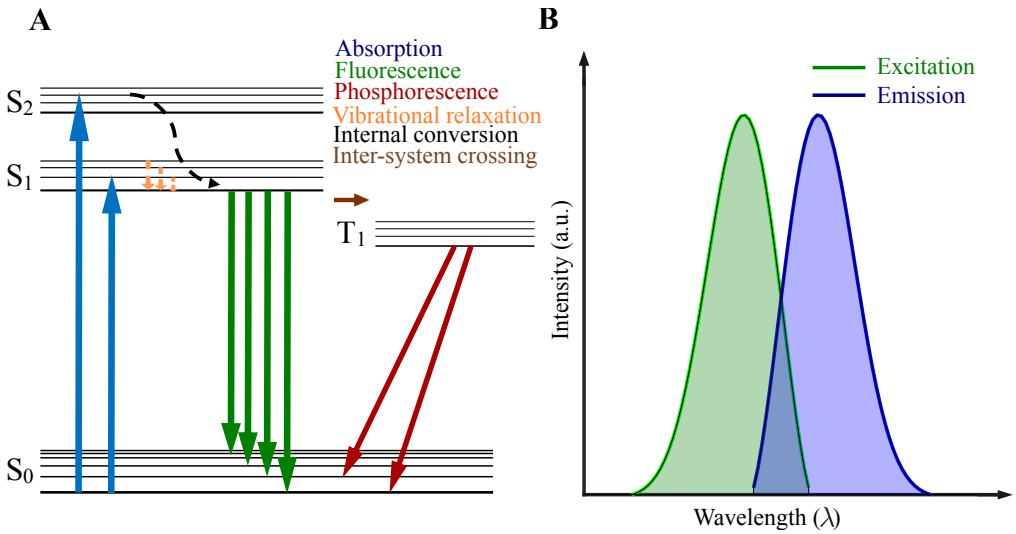

Figure 2.1: Illustration of the different radiative and non-radiative processes possible when exciting a molecule with light.
(A) Radiative decay only occurs when the electron undergoes a transition between two electron energy levels. Non-radiative decays can occur when the electron undergoes a transition between two electron energy levels (for example internal conversion), as vibrational relaxation within an electron energy level, or as inter-system crossing. (B) Losses of energy due to non-radiative decays result in a longer wavelength of the fluorescent light compared to the excitiation light.

of the excess energy by thermal relaxation or staying in the energy state until de-exited by photon emission called phosphorescence.

In order to visualize different biological systems under the microscope or using spectroscopy, different fluorescent markers are used. A fluorescent marker is a molecule that absorbs light with a certain wavelength and emits light of a longer wavelength. The excitation and emission wavelengths depend on the atoms and the structure of the molecule, simply which electrons that are excitable and how they are bound to different atoms within the molecule. The ideal fluorescent marker has distinct excitation and emission spectra, have a high quantum yield, and a steady-state emission. Further, the fluorescent marker should not affect the molecules it is attached to, and should itself not be easily affected by varying solution conditions [110].

2.3 Fluorescence microscopy

In order to visualize small structures in the field of life sciences, with a higher contrast, fluorescence microscopy might be used [111–113]. The advantage with fluorescence microscopy is that unwanted light can be filtered out using dichroic mirrors and filters, and staining of molecules and membranes are relatively easy [114]. The drawback with fluorescence microscopy is that as soon as the molecules of interest is stained by a dye, the properties of the molecule might be affected. For example, dyes are often charged, and adding charged dyes to a normally uncharged molecule as for example a lipid, would change the properties of a stained lipid bilayer compared to an unstained lipid bilayer containing the same lipids.

In comparison to simpler optical microscopy techniques that uses broadband light sources, fluorescence microscopy often uses different types of lasers with wavelengths corresponding to the excitation wavelength of the dye. This enhances the image contrast since it is then possible to filter out excitation light from fluorescence emission when imaging the sample.

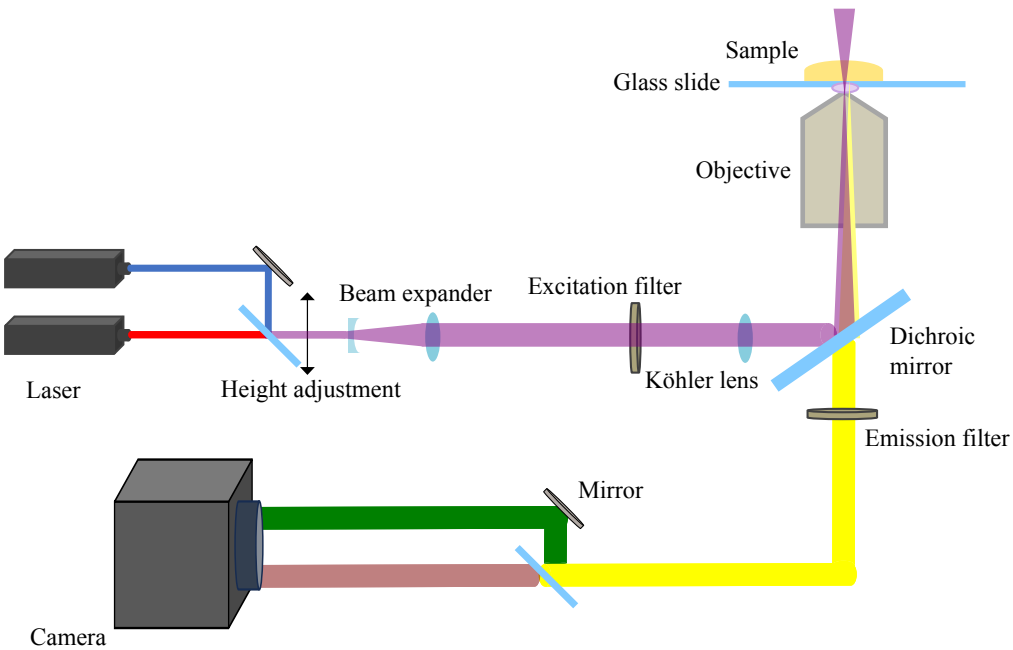

Figure 2.2: Schematic drawing of the microscopy setup.
The illuminating light beam passes an excitation filter that filters out stray light before being reflected to the sample by a dichroic mirror. Fluorescence from the sample is transmitted by the dichroic mirror and collected by a CCD camera.

Further, fluorescence microscopy normally uses an inverted microscope where the excitation light is illuminating the sample from below, and the emission light is reflected back and imaged onto a detector instead of through the eyepiece. A typical setup for fluorescence microscopy consists of an inverted microscope where a light beam can be guided into the microscope by a set of lenses and mirrors and illuminate the sample. The fluorescence is then separated from the excitation light by a dichroic mirror and collected by a sensor, usually a CCD or a CMOS camera. An excitation filter is often used in order to avoid stray light from the surroundings reaching the sample, and an emission filter is used to avoid light of other wavelengths than the fluorescence emission reaching the sensor (Figure 2.2).

An issue to take into account when working with high-intensity lasers and fluorophores is photobleaching, which occurs when the fluorophores are damaged by the high-intensity radiation and loses their ability to fluoresce [115]. On the molecular scale, the excited electron is transferred to a forbidden state via inter-system crossing. The long lifetime of the forbidden state means that the fluorophore has time to undergo reactions with neighboring molecules. These reactions can for example result in cleaving of covalent bonds that irreversibly alters the photochemical properties of the fluorophore. In order to minimize the risk for photobleaching the laser intensity and exposure time of laser irradiance should be minimized.

2.4 Total internal reflection fluorescence microscopy

A common method of fluorescence microscopy is epi-illumination fluorescence microscopy, which is widely used in the field of life sciences [111–113]. The name originates from the Greek word "epi" that means "same", which simply means that the sample is illuminated from the same side as where the fluorescence is detected. Illuminating the sample from below, the emitted fluorescence is hence directed back through the objective and transmitted through the dichroic mirror and then collected by the detector. The light that is not absorbed by the sample is transmitted straight through the sample, resulting in a decreased risk of excitation light being collected by the detector which reduces the signal-to-noise ratio (SNR). The drawback is that fluorescent probes throughout the axis of illumination (z-axis) will be excited. In conventional microscopy, where one only wants to illuminate and image the (x,y)-plane at the focal plane of the objective lens, fluorescent emission from other planes at the z-axis will increase the background light of the image and decrease the SNR.

2.4.1 Principles of total internal fluorescence microscopy

In order to reduce the background signal from planes higher up in the sample, total internal reflection fluorescence microscopy (TIRFM) can be used. The method was first used by Ambrose [116], and is based on total internal reflection giving rise to an evanescent field. When light is passing an interface between two different media it will be refracted due to the difference in refractive index, n, i.e. the difference in speed the light has through the different media. If the light is propagating from a denser (high n) to a more rare (low n) medium the light can be totally internal reflected if the angle of incidence θ_i is large enough (Figure 2.3).

Using an oil objective together with an aqueous sample fixed on a glass cover slide, the light will propagate from a denser to a rarer medium. The light beam must hence be directed toward the glass at an angle so that the light is totally internally reflected at the interface between the glass slide and the sample (Figure 2.4A). The refraction at an interface is given by Snell's law

$$n_{glass} \sin(\theta_i) = n_{sample} \sin(\theta_c) \tag{2.6}$$

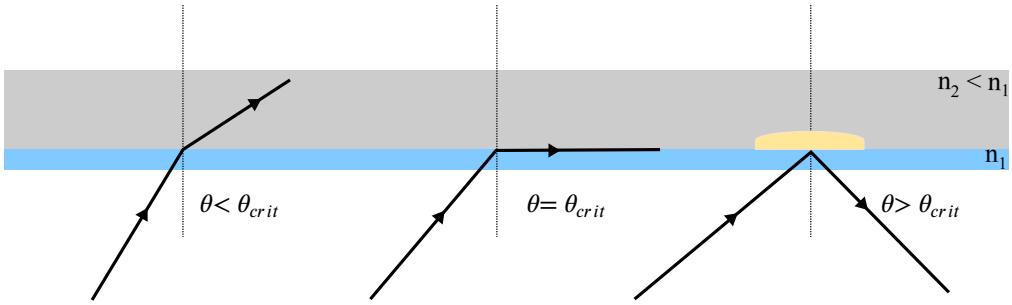

Figure 2.3: Schematic illustration of how changing the incident angle cross over from refraction to total internal reflection.
When the incident angle is smaller than the critical angle, the light will mainly be refracted in the second medium. At an angle equal to the incident angle, the light will mainly propagate along the interface. Increasing the incident angle will lead to total internal reflection, with a reflection angle equal to the incident angle.

from which the critical angle θ_c can be calculated [117]. With a refractive index of the glass as 1.518 and assuming the refractive index of an aqueous sample is around 1.330, the incoming angle of the illuminating light for total internal reflection would be ca 61°. Even though no light is propagating into the second media (the sample), the reflected light generates an electromagnetic field in the second media (Figure 2.4B). The electromagnetic field has the same frequency as the electromagnetic wave describing the incident light beam [118], and is described by

$$I_z = I_0 e^{-z/d} \tag{2.7}$$

where z is the distance from the glass-sample interface and d is the penetration depth, [118],

$$d = \frac{\lambda}{4\pi\sqrt{n_1^2 sin^2(\theta_1) - n_2^2}}. \tag{2.8}$$

Since the intensity of the field decays exponentially from the interface and diminishes at a range of approximately 100-200 nm, only the dyes closest to the interface will be excited by the light. This supresses background light when studying SLBs, docked vesicles or other systems where only the volume closest to the glass surface is of interest [119]. Hence, the method increases the SNR compared to a bright-field microscope and confocal microscopy, with a penetration depth that is approximately a tenth of the depth of the planes using confocal microscopy.

The possibility to change the angle of the incoming light can be implemented into an inverted microscope where the light is guided into

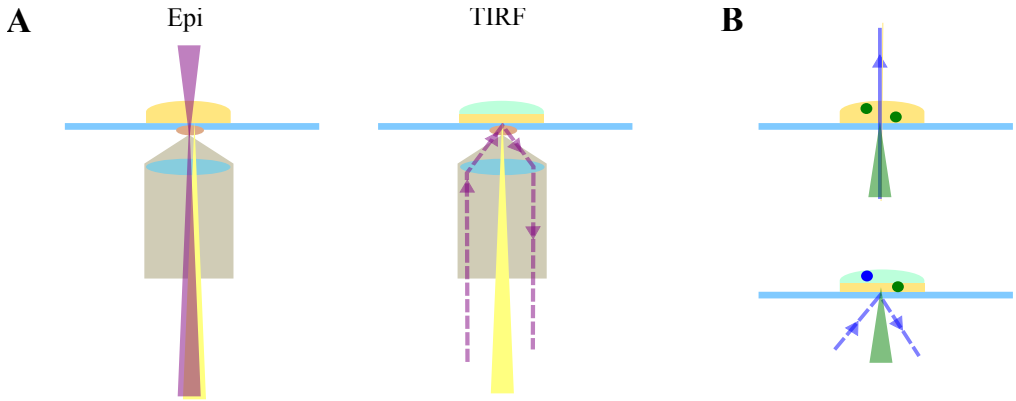

Figure 2.4: Altering between TIRF and epi mode.
(A) Adjusting the incident angle of the illuminating light alters the microscopy setup between epi and TIRF mode. (B) When the setup is in epi mode, the illumination light propagates through the sample and excites fluorophores through the full sample depth. When the setup is in TIRF mode, the total internal reflection yields an evanescent wave that decays with sample depth. Hence, only the fluorescent species closest to the surface are excited.

the microscope by lenses on an optical table. Instead of directing the light beam directly into the microscope, the light will be directed orthogonal to the microscope entrance and go through a translational stage which can be built using two mirrors. The first mirror will direct the light in ca 45°back in the opposite direction of the microscope entrance, whereas the second mirror will be directed approximately 180°towards the first mirror, directing the light into the microscope entrance. If the light is orthogonal to the microscope entrance before the translational stage and the two mirrors are directed ±45°in relation to the incoming beam, facing each other, the light will enter the microscope along the axis of the objective and the setup will be put in epi-illumination mode. Changing the angle of one of the mirrors will result in a beam that enters the microscope with an angle to the objective axis, and the setup can be put in TIRF mode (Figure 2.5).

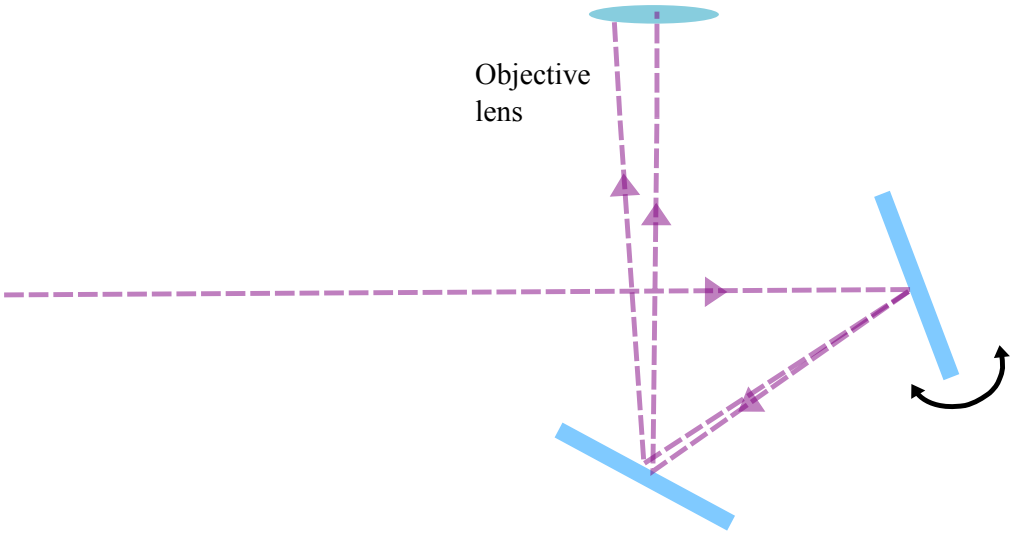

Figure 2.5: Illustration of a translation stage.
By adjusting one of the mirrors, the angle of the light entering the microscope will be altered and the setup can be changed between epi and TIRF mode.

2.4.2 Fluorescence recovery after photobleaching

Fluorescence recovery after photobleaching (FRAP) was first used by Axelrod et al [120], and can be used to study the lateral diffusion of a fluorescently labelled SLB (Figure 2.6A) or fluorescently labelled molecules, for example proteins, associated to the SLB [121–123]. The method relies on the permanent bleaching of fluorescent molecules due to photochemical alteration when exposed to a high intensity light source [115]. By increasing the intensity and focusing the laser beam used to illuminate the sample, the fluorescent components within the illuminated area are bleached (Figure 2.6B). In a fluid bilayer, the lipid molecules will diffuse, resulting in the lipids with bleached fluorescent markers becoming more and more spread out in the bilayer (Figure 2.6C), until the the bilayer is homogeneously bright again (Figure 2.6D). Studying the normalized average intensity within the bleached area over time, it can be seen how the intensity decreases to zero when bleached, and then slowly recovers as more and more non-bleached molecules are diffusing into the area (Figure 2.6E).

The intensity recovery profile depends on the mobility of the bilayer [120, 124]. A bilayer with a high mobility will recover quicker than a less mobile bilayer and hence have a sharper gradient compared to the less

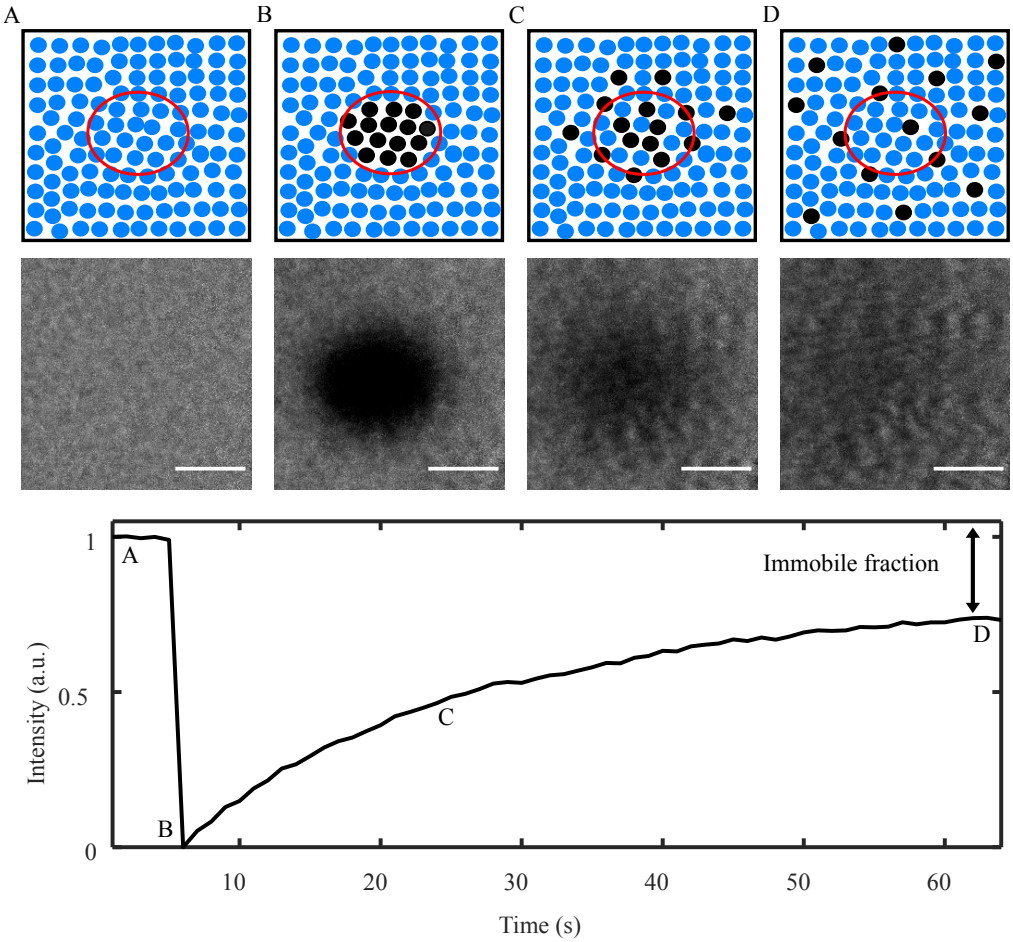

Figure 2.6: Fluorescence recovery after photobleaching.
(A-D) Illustration and corresponding microscopy images of a FRAP measurement. The scale bar on the images are 10 μm. (A) A bilayer is deposited onto a glass substrate. (B) Lipids with fluorescent markers are bleached in small area. (C) As the lipids are diffusing the bleached molecules will spread out in the bilayer, until the brightness of the bilayer is homogeneous (D). (E) Intensity recovery profile of the bleached area.

mobile bilayer. From the gradient of the recovery profile, the 2-dimensional diffusion constant, D, can be obtained. Another factor affecting the recovery is the amount of immobile molecules in the bilayer, which can be obtained from the difference in intensity before bleaching and after recovery. Two common reasons for an SLB to become immobile is through interactions between lipid molecules or associated molecules and the glass cover slide through defects in the bilayer, or for associated molecules like ligands to partly immobilize the bilayer due to the interaction between the ligand and the lipid molecules in the bilayer.

2.4.2.1 Analysis of FRAP recovery curve

The recovery profile of the FRAP curve is generally obtained by subtraction of the background intensity and correcting for general bleaching of the fluorophores in the bilayer [125]. This is done by obtaining the background level outside the sample, and another intensity recovery curve at a reference area which is not bleached [48, 125, 126] (Figure 2.7). Hence, the recovery curve is calculated as

$$I_R(t) = \frac{I_{Bleach}(t) - I_{BG}(t)}{I_{Corr}(t) - I_{BG}(t)} \tag{2.9}$$

where $I_{Bleach}(t)$ is the mean intensity in the bleached area as a function of time (green curve), $I_{Corr}(t)$ is the mean intensity in the correction area as a function of time (red curve), and $I_{BG}(t)$ is the background level as a function of time (blue curve). In this way, the recovery curve is normalized to the average intensity in the sample at each time point.
The recovery curve can be normalized once, as described above, or twice,

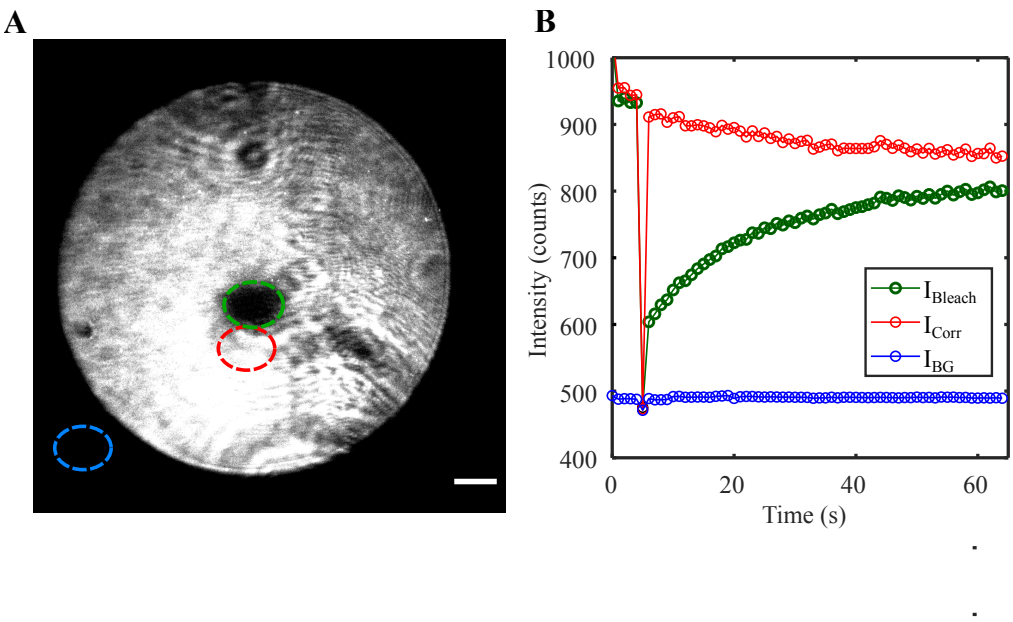

Figure 2.7: Analysis of FRAP recovery curves.
(A) The recovery curve is obtained by measuring the average intensity in the bleached area (green), a correction area outside the bleached area (red) and the background level (blue). The scale bar is 20 μm. (B) The average intensity in the different areas over time. The intensity profile from the correction area is used to correct for general bleaching in the sample over time, which leads to a decreased fluorescence intensity.

as

$$I_R(t) = \frac{(I_{Bleach}(t) - I_{BG}(t)) - (I_{Bleach}(0) - I_{BG}(0))}{(I_{Corr}(t) - I_{BG}(t)) - (I_{Bleach}(0) - I_{BG}(0))} \tag{2.10}$$

where $I_{Bleach}(0)$ is the intensity in the bleached region at time point zero and $I_{BG}(0)$ is the background at time point zero. This results in a recovery curve where the initial intensity is normalized to 1 and the point of bleaching is normalized to 0 [126] (Figure 2.6E). When the FRAP curve is normalized, the mobile and immobile fractions can be obtained. If the initial intensity is normalized to 1 and the time of bleaching is normalized to 0, the mobile fraction, M, corresponds to the plateau, and the immobile fraction IM = 1 - M [126] (Figure 2.6E). To obtain the accurate value of M, the recovery curve is often fit to an exponential function [126, 127]. However, the recovery curves are not always accurately described by exponential functions [126, 128]. If the recovery curve is normalized twice to contain values between 0 and 1, it can be fitted to a converging function

$$I_{R,fit}(t) = M\left(1 - \frac{1}{1 + t/t_{1/2}}\right). \tag{2.11}$$

The above mentioned analysis has described qualitative analysis of recovery curves, used to obtain the mobile and immobile fractions. Generally, FRAP analysis is divided into qualitative analysis and quantitative analysis, where the latter includes curve fitting to obtain either information regarding diffusion or kinetics [126, 127]. Quantitative fitting of the recovery curve fit the data to a single exponential function including information about the 2-dimensional diffusion constant [126, 129] or the association and dissociation constants using a single [127], or a double exponential function [126, 128].

In this thesis, FRAP data has been qualitatively analysed using recovery curves normalized by Eq(2.10). FRAP has been used in paper I and II to ensure a successful deposition of a fluid bilayer. Further, in paper II, FRAP has been used to obtain the immobile fraction of proteins associated to a membrane using Eq(2.11).

2.5 Single vesicle and single protein imaging

Studying biological processes often requires evaluating processes on the single molecule level. In colloidal systems where the molecules of interest often are in the range of nanometers, it is difficult to image molecules and interactions between different particles with conventional optical microscopy techniques [130]. Electron microscopy techniques are often used to image shape and structure of small particles. The principles of an electron microscope are similar to an optical microscope, but the former uses an electron beam as energy source instead of light. Since the electron microscope often uses wavelengths below 1 nm they give more than 100 times better resolution compared to an optical microscope, which generally is limited by the optics [131]. The drawback with electron microscopes are that they are expensive, sensitive to their environment and often requires extensive sample preparation.

2.5.1 Optical super-resolution techniques

An alternative to electron microscopy, that offers sub-diffraction limited resolution, are optical super-resolution techniques. There are several different methods of super-resolution techniques, but the two most common are stochastic (localization) microscopy and deterministic techniques. Stochastic techniques are based on isolating the emitting particle and fitting the signal to the gaussian PSF, from which the center position can be determined. Two common stochastic methods are STochastic Optical Reconstruction Microscopy (STORM) [132], and Photo-Activated Localization Microscopy (PALM) [133], that use samples with several sets of fluorophores that are activated and imaged separately.

Deterministic techniques are based upon selective activation or de-activation of a fluorophore that is obtained using an inhomogeneous beam profile. The two most common deterministic techniques are REversible Saturable OpticaL Fluorescence Transitions (RESOLFT) microscopy and STimulated Emission Depletion (STED) microscopy [134], which can be seen as the reverse version of RESOLFT. While RESOLFT rely on selective activation of fluorophores, STED uses selective de-activation of the fluorophores.

2.5.2 Single molecule imaging

Another alternative to study processes on the nanometer scale is single molecule imaging. Single molecule detection using microscopy techniques was first observed by Hirschfeld in the 1970s [135]. Detection of single molecules using fluorescence microscopy includes attaching one or more fluorescent markers onto one molecule [136, 137] and then image single molecules using fluorescence microscopy techniques. The fluorescence emission from the molecule is imaged as a spot, whose size depends on the PSF characterized by the optical system. If a high spatial resolution is required, the spot can be fitted to a 2-dimensional gaussian function [138], which is fundamental during single particle tracking (SPT) [139].

Single molecule imaging of molecules in low concentrations does not only enable single particle tracking over time [140]. Single molecule imaging is also of great importance when studying molecular mechanism that otherwise would risk being hidden in the bulk average of a heterogeneous sample [141], for example when studying the kinetics between lipid membranes and particles [142]. Instead of focusing on a high spatial resolution of the molecules, the ability to detect changes in the total intensity of single entities and colocalize differently labeled entities enables studying protein aggregation [143] and folding [144], fusion of vesicles [145, 146], and interactions between protein and vesicles [147, 148]. When the position and intensity of the single molecules or single vesicles are obtained, changes in intensity can be detected [149–153], as well as spatial and temporal colocalization [142]. Further, by obtaining the intensity of a single molecule, the number of molecules on a densely packed surface can be calculated [154]. In this thesis, detection of single protein and single vesicles and their intensities have been fundamental to all four papers.

2.5.2.1 Single protein imaging to calculate the density of proteins associated to a supported lipid bilayer

Measurements of single proteins have been of great importance in paper I and II where the average intensity of monomeric proteins have been used to estimate the total number of proteins bound to a lipid membrane. Single proteins were detected as will be described in chapter 4.1, and the average intensity of single proteins on glass slides was calculated (Figure 2.8 A,B). Knowing the average single protein intensity, the total amount of proteins on the membrane (Figure 2.8 C,D), could be calculated as described by

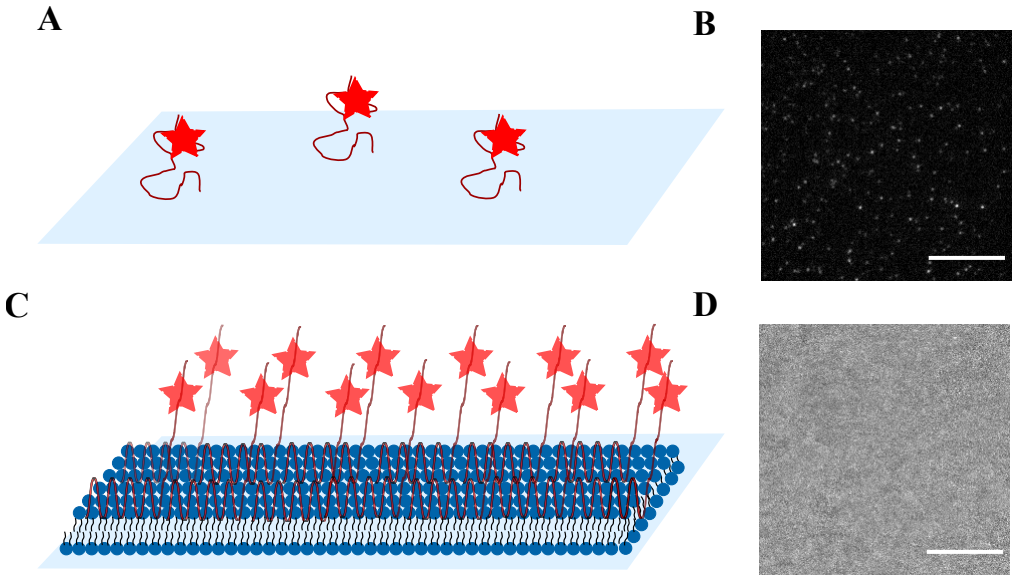

Figure 2.8: Single protein measurements to calculate protein density.
(A) Single proteins bound to a glass surface. (B) Single proteins imaged on a glass slide. The protein concentration is ca 10 pM and the scale bar is 10 μm. (C) SLB saturated with proteins. (D) SLB saturated with protein. The scale bar is 10 μm.

Junghans *et al* [154]. Hence the density of proteins adsorbed to a bilayer was calculated by

$$\rho = \frac{I_{int,SLB}}{I_{int,SP} C A_{pix} n_{pix}} \tag{2.12}$$

where $I_{int,SLB}$ is the total intensity of proteins adsorbed on the SLB, C is the fractional conversion factor if different neutral density filters are used, $I_{int,SP}$ is the intensity of one protein, A_{pix} is the pixel area and n_{pix} is the number of pixels covered by the SLB.

2.5.3 Single vesicle imaging

Single vesicles are commonly imaged using TIRFM [149]. The image analysis in this thesis rely on detection of single vesicles, which includes obtaining the position and intensity of a single vesicle. Further, the ability to detect changes in intensity, and being able to colocalize differently labelled vesicles or proteins have been fundamental to the studies performed in paper III and IV. Studying interactions including single vesicles is often conducted by docking vesicles to a passivated surface [152, 153, 155]. In paper III and IV (chapter 4.2-4.3), single vesicles have been docked to a passivated surface using a biotin-streptavidin linkage.

2.5.3.1 Tethering lipid vesicles to a glass surface

Vesicles can commonly be attached to a glass surface by using a buffer containing NaCl that enhances electrostatic attraction between the glass and the vesicle, which otherwise would be repulsive due to net negative charges of both the glass and most lipid membranes of interest. However, during experiments with α-Syn, salt has been shown to inhibit the interaction between the lipid membranes and the protein [156]. Tethering of vesicles onto a glass slide can instead be obtained by passivating the glass cover slide by a Poly-L-Lysine(PLL)-g-PEG-biotin and streptavidin layer, which has been used in several TIRFM studies of single vesicles [149–151]. Vesicles can then be docked to the surface by incorporation of biotin into the vesicle membrane, that binds to the streptavidin [157] (Figure 2.9).

The passivation of the surface is carried out by adding a solution consisting of PLL-g-PEG:PLL-g-PEG-biotin (100:1) in a total concentration of 0.1 mg/mL, PBS, pH 6.5 to a silica well attached to a piranha cleaned glass slide. After incubation, excess molecules are washed away with buffer, and streptavidin (0.1 mg/mL in PBS, pH 6.5) is added to the well. Finally excess streptavidin is washed away with experimental buffer. The positively charged PLL backbone is electrostatically attracted to the glass surface that is negatively charged in a aqueous environment. This results in the PEG-chains extending into the solvent like a brush, where the conformation of the PEG chain depends on the relation between the Flory radius of the PEG,

$$R_F = \alpha N^{3/5} \tag{2.13}$$

where α is the ethoxy unit and N is the extent of PEG polymerization, and the distance between the grafting points for two PEG chains can be calculated by

$$D = 2\sqrt{\frac{S}{N\pi}}, \tag{2.14}$$

where S is the total surface area of PLL in the sample. During all measurements included in this thesis, the surfaces have been passivated using PLL(20)-g[3.5]-PEG(2) and PLL(20)-g[3.5]-PEG(2)/PEG(3.4)-biotin(20%). Eq (2.13-2.14) then yields $R_F = 3.5$ nm, and $D = 6$ nm. According to Shi *et al* [158], the PEG chain takes a brush formation where the brush thickness is given by

$$L = \frac{N\alpha^{5/3}}{D^{2/3}}, \tag{2.15}$$

which means that the thickness of the PEG brush during the experiments included in this thesis is 2.4 nm.

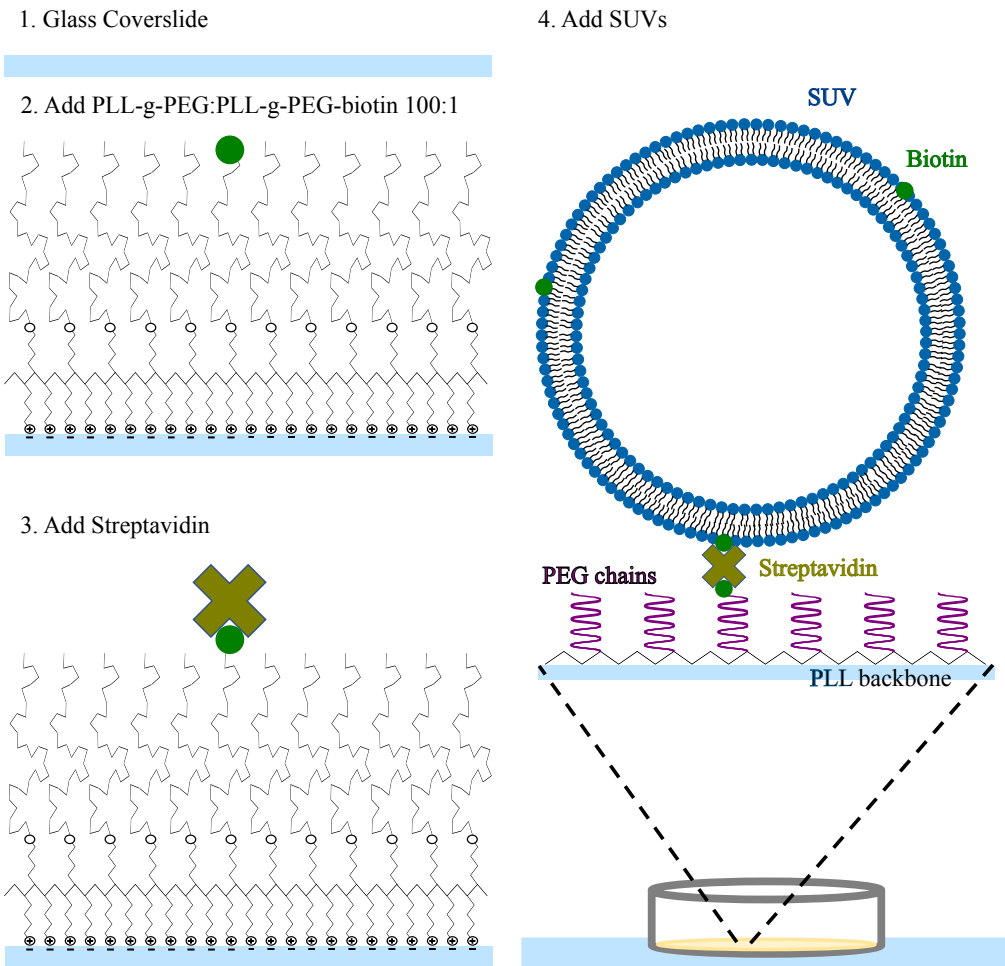

Figure 2.9: Docking of vesicles to a glass surface.
To enable imaging of vesicles, the vesicles were docked to a passivated glass surface. Biotinylated Poly-L-Lysine was added to a piranha cleaned glass coverslide and left to incubate for 30 min (step 2). Thereafter, excess molecules were washed away and a streptavidin solution was added to the well and left to incubate (step 3). After excess streptavidin was washed away, vesicles containing biotinylated lipids could be docked to the surface (step 4).

Overall, the height of the passivated surfaces can be estimated to be approximately 10-12 nm with the PEG chain in a brush conformation. Hence the height of the passivated surface does not have a major effect on the ability to illuminate the lipid vesicles that are docked to the surface, with a loss of ca 10% of the incident light according to Eq(2.7).

Chapter 3

α-Syn association with lipid membranes

Both the man of science and the man of action
live always at the edge of mystery, surrounded by it.

— J. Robert Oppenheimer

Chapter outline

This chapters mainly covers fluorescence microscopy studies of α-Syn association with SLBs. The chapter starts with α-Syn association with SLBs performed to study cooperative binding of monomeric α-Syn. The chapter continues with studies of α-Syn association with SLBs with different charge density, and ends with a comparison of experiments performed using SLBs and SUVs with same lipid composition.

3.1 Cooperative binding of α-Syn upon association with SLBs

In paper I, cooperative binding of α-Syn to vesicles of various sizes was studied by FCCS, confocal microscopy and cryo-TEM. Initially, cooperative binding was studied by confocal microscopy using non-labelled GUVs. Fluorescently labelled α-Syn was added to giant unilamellar vesicles (GUVs), at L:P ratios corresponding to an excess of membrane, showing that some GUVs had many α-Syn associated while others had no α-Syn bound. When more protein was added, all vesicles were covered by protein, showing that all vesicles had the ability to bind α-Syn. Further, FCCS measurements of fluorescently labelled SUVs and α-Syn labelled with a different fluorescent marker were performed. The α-Syn concentration was kept constant, and SUVs were added in a range from L:P=10:1 to 2000:1. For low L:P ratios, where there was an excess of α-Syn, the number of SUVs and the number of SUVs with adsorbed α-Syn was equal. Increasing the number of SUVs above the saturation point (here L:P = 200:1), did not result in an increased number of SUVs with adsorbed α-Syn even though the total number of vesicles increased. Hence, it could be concluded that α-Syn bound to vesicles in a cooperative manner. To quantitatively investigate cooperative binding on a more rigid membrane, TIRFM experiments of α-Syn added to SLBs were carried out.

3.1.1 Measuring the density of adsorbed α-Syn

An SLB was deposited to a piranha cleaned glass surface attached to a silica well by fusion of vesicles. The SUVs used to deposit the SLB consisted of POPC:DOPS 7:3, and included 0.5 wt% fluorescently labelled lipids (AF488-PE) to enable FRAP measurements of the SLB. The well was left to incubate for one hour before washing away excess SUVs. To ensure a successfully deposited mobile SLB, FRAP measurements were performed

before the addition of α-Syn. Titrations of α-Syn were then performed at concentrations between 0.1 - 1000 nM. After addition of α-Syn, the system was left to incubate for 15 minutes before imaging. Single protein measurements to calculate the α-Syn density, as described by Eq (2.8), were performed before each measurement.

The raw data images of the titrations can be seen in Figure 3.1A. Calculating the α-Syn density for the different concentrations using Eq (2.8) resulted in a binding curve with a rapid increase in the number of bound protein above 10 nM (Figure 3.1B). From Figure 3.1B, a slow linear increase of the number of bound proteins can be seen for concentrations below 5 nM. The rapid increase in the α-Syn density levelled out at approximately 8000 proteins/μm^2 for α-Syn concentrations around 100 nM. The data is re-analysed before included in the thesis, resulting in an updated absolute value of the α-Syn density.

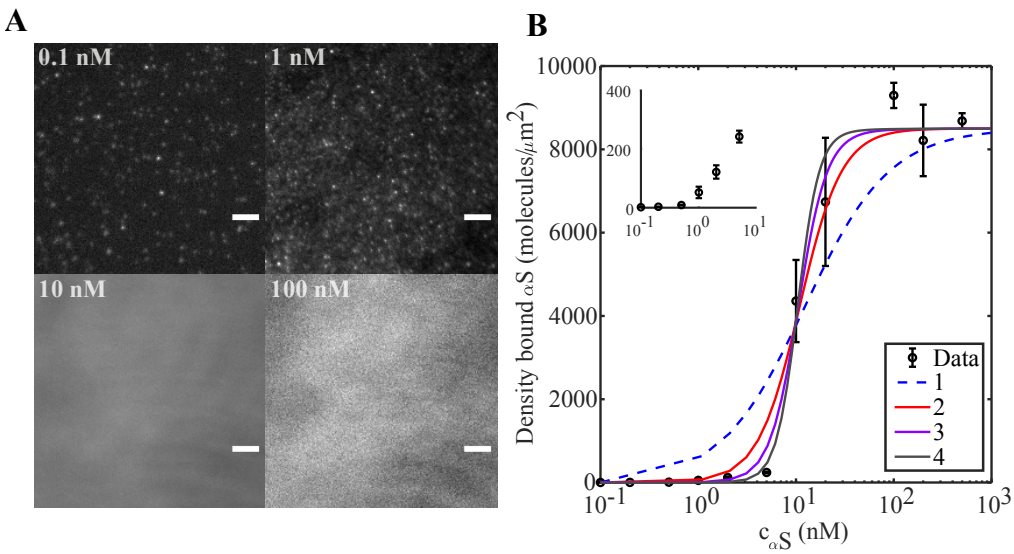

Figure 3.1: Cooperative binding of α-Syn onto SLBs.
(A) Fluorescent signal from a POPC:DOPS 7:3 SLB incubated for 15 min with 0.1 nM α-Syn (top left), 1 nM α-Syn (top right), 10 nM α-Syn (bottom left) and 100 nM α-Syn (bottom right). The scale bars are 5 μm. (B) Density of α-Syn bound to an SLB for concentrations between 0.1-500 nM. The dotted blue line shows a fit of the Adair equation (eq 3.1) for one binding site and corresponds to independent binding. The red, purple, and gray lines represent fits of the Adair equation with two, three, and four coupled binding sites, respectively. The data is mean $\pm$ SD for two to three separate measurements. The figure is adapted version of re-analysed data, originally published in paper I.

3.1.2 α-Syn binds cooperatively upon SLB association

The degree of cooperativity can be determined from the shape of the binding curve [159–161], where an increased gradient indicates positive cooperative binding [78]. The binding curve can be fitted to the Adair equation [162]

$$\Gamma = \Gamma_{max} \frac{\sum_{k=1}^{N} \left(k c^k \prod_{j=1}^{K} K_j \right)}{N \left(1 + \sum_{k=1}^{N} \left(c^k \prod_{j=1}^{K} K_j \right) \right)} \tag{3.1}$$

where c is the protein concentration, N is the number of binding sites and K_i is the macroscopic binding constant for cooperative binding. Hence, to investigate the binding behaviour of the protein, the data was fitted to the Adair equation for 1-4 different binding sites. One binding site corresponds to independent binding and multiple binding sites corresponds to positive cooperative binding, where an increased number of binding sites corresponds to a stronger cooperative binding. The fits in Figure 3.1B show that assuming 1 binding site does not fit the data well, while assuming 2 binding sites majorly improves the fit. Assuming 3-4 binding sites results in a minor improvement of the fit.

3.1.3 Discussion

Altogether, it can be concluded that α-Syn binds cooperatively in an environment with membrane excess under the conditions investigated. The results presented above and in paper I shows that α-Syn binds cooperatively on both vesicles and more rigid planar membranes like SLBs. This agrees with previous suggestions that protein binding in patches leads to formation of protein domains on the membrane [85, 88, 163], which eventually may result in membrane deformation and remodeling. The cryo-TEM experiments in paper I indeed showed that protein association resulted in vesicle deformation. However, from the SLB experiments presented above it can be concluded that cooperative binding is also present in systems including more rigid membranes with a limited ability to deform. Membrane deformation induced by binding of protein might enhance cooperative behavior, but is not a requirement for cooperative binding.

The molecular origin of the cooperativity remains unknown, but might be explained by several factors. One possible explanation is that binding of one α-Syn leads to an increased solvent exposure of the hydrophobic interior of the membrane. Hence, the enthalpic cost of binding is reduced when binding in proximity to another protein compared to binding at a new location. Another explanation might be that the cooperative binding has a smaller effect on, for example, reduced lateral diffusion of the membrane, which might be minimized if the protein binds in a more concentrated area. As discussed by Lee et al, cooperative binding may be related to the physiological function of α-Syn [84], which is suggested to involve membrane remodeling [98, 100], possibly related to vesicle trafficking.

3.2 α-Syn association with SLBs with various membrane charge densities

The SLB measurements performed in paper I gave new insights on the association of α-Syn with membranes containing 30% DOPS. In paper II, studies of α-Syn association with membranes with various anionic lipid composition and membrane deformability was conducted. The main research questions investigated were

- What is the minimum amount of anionic lipids needed for α-Syn association?
- How does an increased amount of anionic lipids in the membrane affect α-Syn association?
- At what α-Syn density is the membrane saturated with proteins for different membrane compositions?

The measurements in paper II were carried out using TIRF microscopy to do single protein measurements and FRAP measurements of α-Syn adsorption onto SLBs, and CD spectroscopy measurements to study α-Syn adsorption onto SUVs. Both the SLBs and SUVs consisted of POPC:DOPS, where the amount of DOPS varied between 0 and 30%.

3.2.1 Measurements of α-Syn adsorption to SLBs

Measurements of α-Syn association with SLBs were carried out by depositing SLBs in silica wells attached to piranha cleaned glass cover slides, and then add an excess amount of α-Syn to the system (μM) (Figure 3.2A). The system was left to incubate for 5 minutes, whereafter non-adsorbed α-Syn was washed away by rinsing the well with experimental buffer (Figure 3.2B), to obtain an SLB saturated with α-Syn (Figure 3.2C). The amount of α-Syn adsorbed to the bilayer was calculated by Eq(2.8) (Figure 3.2D). The intensity of a single protein was obtained from single protein measurements made previous to the SLB measurements.

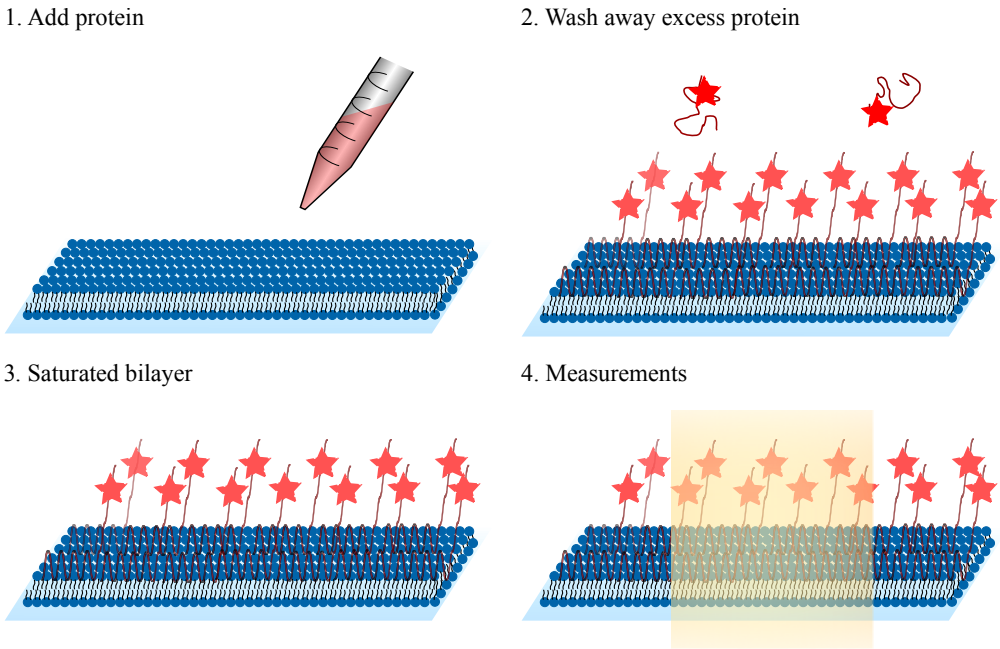

Figure 3.2: Measuring α-Syn association with SLBs.
Measurements were performed by adding an excess amount of α-Syn to an SLB. After incubation, non-adsorbed proteins were washed away with experimental buffer to obtain a saturated bilayer with a minimum amount of unbound α-Syn. FRAP measurements of the SLB was performed before and after addition of α-Syn, and of the α-Syn channel after adsorption of protein.

3.2.2 The density of adsorbed α-Syn depends on the lipid composition

From the FRAP measurements of the α-Syn channel, the immobile and mobile fractions could be obtained by normalizing the recovery curve as described by Eq(2.10), and fitting the data to Eq(2.11). From the recovery profiles and the fit (Figure 3.3A-B), it could be concluded that approximately 89 $\pm$ 7% of the α-Syn adsorbed to membranes containing only zwitterionic lipids were immobile, indicating that the protein, that is highly surface active, was in fact adsorbed to the glass surface at defects in the membrane. From the raw data (Figure 3.3C), it can be seen that increasing the amount of DOPS in the membrane increased the number of α-Syn molecules adsorbed to the bilayer. Taking only mobile protein into account, there was a significant increase in protein density when the membrane contained 5% DOPS, accompanied with a clear increase in the intensity recovery as shown in Figure 3.3D. There was no significant increase in mobile protein density between 0 and 1% DOPS. The amount

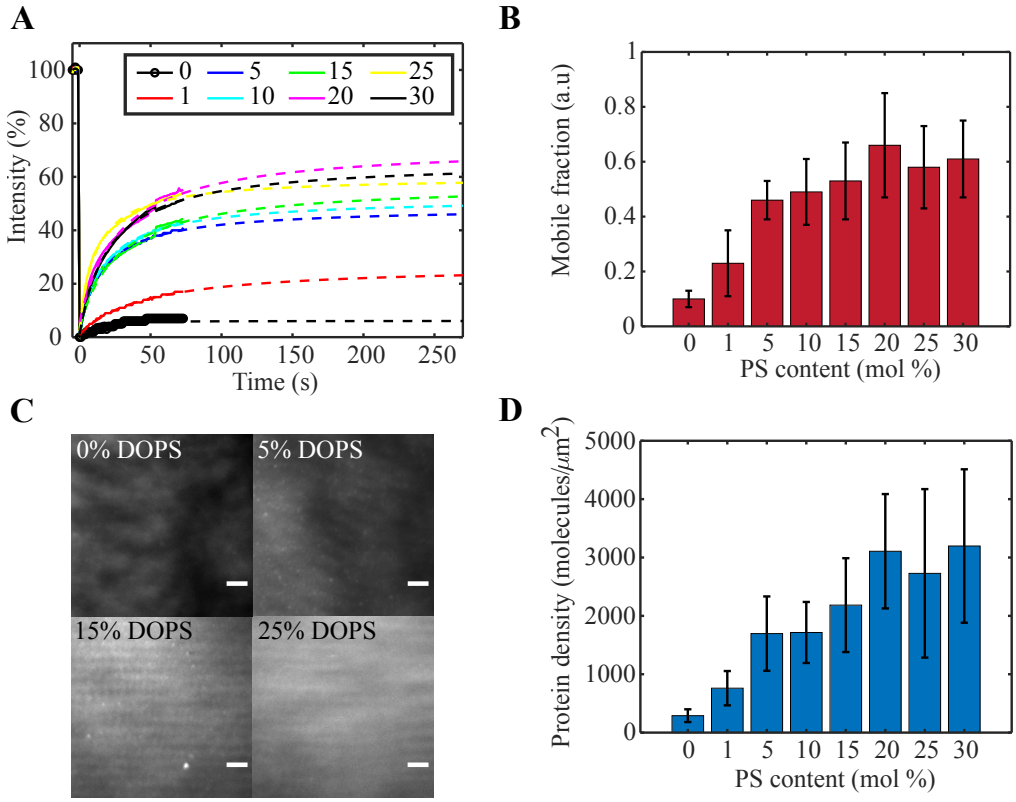

Figure 3.3: Density of α-Syn associated to SLBs.
(A) Fits of the average recovery profiles for α-Syn. The recovery profiles are fit to Eq(2.11). The recovery profiles are mean $\pm$ SD of 3-13 measurements. (B) The fraction of mobile α-Syn at SLBs with varying DOPS content. The data are mean $\pm$ SD from 3-13 separate experiments. (C) Raw data images of protein adsorbed to membranes containing 0, 5, 15 and 25% DOPS. The scale bar is 5 μm. (D) The density of mobile α-Syn adsorbed to the SLBs with varying DOPS content. The data is mean $\pm$ SD from 3-13 separate experiments.

of adsorbed α-Syn increased until the SLB contained 20-30% DOPS, where the α-Syn density levelled out at approximately 3000 mobile proteins/μm^2. Hence, increasing the charge density resulted in an increased α-Syn density, meaning that more α-Syn could be bound to the same membrane area.

3.2.3 α-Syn adsorbed to membranes both diffuse on the membrane and exchange with unbound α-Syn

FRAP measurements of α-Syn associated with SLBs with different membrane compositions were mainly performed to obtain the immobile and mobile fractions, and hence enable investigation of the α-Syn

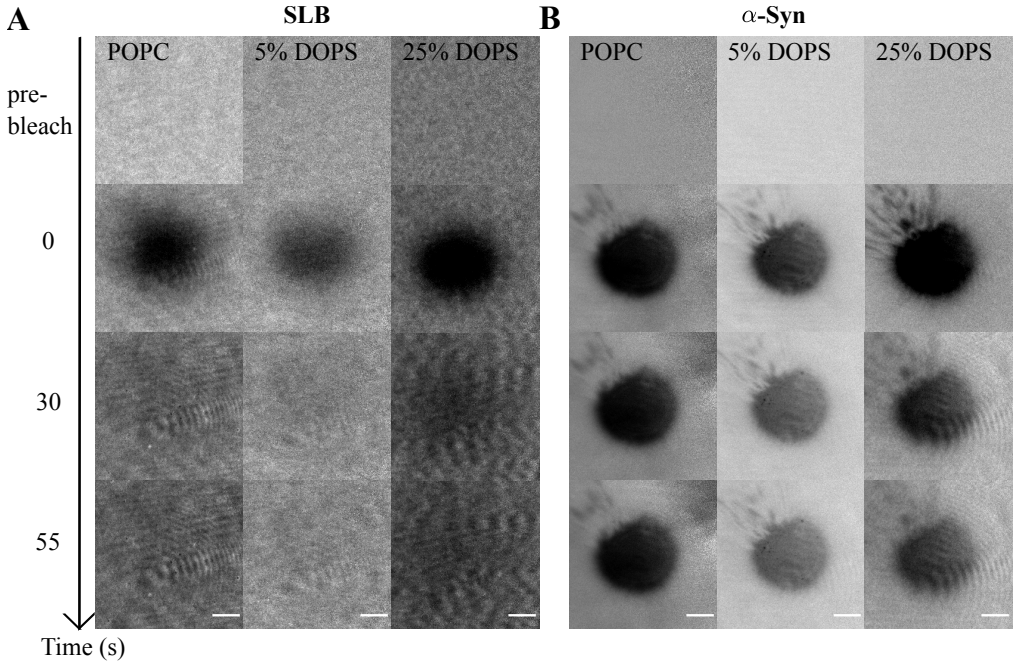

Figure 3.4: Raw data from FRAP measurements.
(A) Raw images from FRAP measurements of SLBs containing 0, 5 and 25% DOPS. The scale bars are 10 μm. (B) Raw images from FRAP measurements of α-Syn adsorbed to SLBs containing 0, 5 and 25% DOPS. The scale bars are 10 μm.

density adsorbed to the membrane and not to defects. Further, FRAP measurements of the SLBs were performed before and after α-Syn adsorption, mainly to ensure a successful deposition of a mobile SLB. Studying the raw images of the FRAP measurements (Figure 3.4), of the SLB before α-Syn adsorption, it can be seen how the recovery is smooth which indicates recovery by diffusion of lipids. Comparing the images of the SLB to images of the α-Syn channel (Figure 3.4B), there is only a minor recovery of the bleached area. Further, during the recovery, the edges of the bleached area remains sharp, indicating that a part of the recovery is due to exchange of α-Syn.

Studying the recovery profiles of the α-Syn compared to the SLB before and after protein addition (Figure 3.5), the shape of the recovery curves of the α-Syn indicate that the proteins diffuse on the membrane to some extent, but that a large part of the recovery is likely due to exchange of proteins. Further, the recovery profiles of the SLB after α-Syn adsorption indicates that SLBs with a high DOPS content recover slower after adsorption of α-Syn. Since the fluorescently labelled lipids are

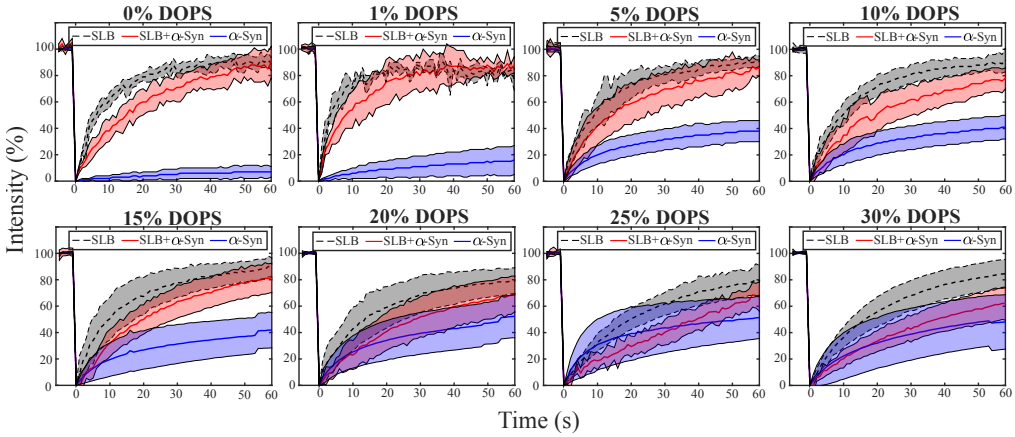

Figure 3.5: FRAP recovery profiles.
Average FRAP recovery profiles for SLBs with various DOPS content before (black) and after (red) α-Syn adsorption, and α-Syn adsorbed to SLBs (blue). The shaded areas are standard deviations. The data is mean $\pm$ SD from 3-13 separate experiments.

zwitterionic, they are most likely present in the bare parts of membrane that is not directly in contact with α-Syn. Hence, the results indicate that not only the local mobility of the membrane might be affected by protein association in domains [164]. Association of a high protein densities may even affect the overall lipid lateral diffusion as previously suggested [165, 166]. However, it should be noted that only a minor decrease in mobility is observed and the membrane is, in fact, still mobile and carry the characteristics of a fluid membrane. More importantly, α-Syn adsorption does not immobilize the lipid components in the membrane, even when the membrane is saturated with α-Syn.

3.2.4 Discussion

As discussed in chapter 1, previous studies have often investigated the interaction between α-Syn and lipid membranes containing 30% anionic lipids or more, whereas cellular membranes contain less than 30% anionic lipids [167–172]. The results presented in paper II shows that association occurs with membranes containing 5% DOPS but not with membranes containing 1% DOPS. Hence, the results suggest that the membrane needs to contain a certain amount of anionic lipids for association to occur. The cellular membranes contain up to 30% anionic lipids [167, 168], which are more abundant in the cytosol-facing leaflets [39, 40, 173]. Hence, the amount of anionic lipids in the lipid membrane is likely important for the distribution of α-Syn between different cellular membranes. However,

to exact quantify the amount of anionic lipids needed for association, interactions with membranes containing low amounts of anionic lipids need to be studied further.

The results presented above show that an increased amount of anionic lipids in the membrane results in more α-Syn being able to adsorb to the membrane, until the membrane contains around 20-25% DOPS after which the α-Syn density levels out. That the α-Syn density increases with an increasing amount of anionic lipids show that the electrostatic attraction between the anionic lipids and the N-terminus part of α-Syn is an important factor for α-Syn association with membranes. The binding of α-Syn is likely to be partly electrostatically driven, and partly driven by hydrophobic amino acid residues and fatty acids being less exposed to the solvent. The saturation behavior with respect to DOPS content implies that other factors than the membrane charge density are important in regulating the adsorption behavior at these conditions, likely including electrostatic repulsion between anionic C-terminal segments that extend into the solution at the membrane interface [72].

3.3 α-Syn association with SUVs with various membrane charge density

To validate that α-Syn did not associate with membranes containing less than 5 % DOPS was not related to the specific type of model system, the same phenomena was studied in a completely different model system composed of SUVs with DOPS content varying between 0-30% (paper II). The SUVs had a diameter of approximately 40 nm, which can be compared to the estimated radius of a random coil of a 140 amino acid protein (ca 15 nm), meaning that the membrane interface is a curved surface on the length scale relevant in comparison to the incoming protein. Furthermore, unlike the SLBs, the vesicles are deformable and may change shape upon protein association. The packing of lipids is also expected to differ between the curved membrane in the vesicles and the SLBs. All these differences may affect the protein association. The questions to be studied were

- At what DOPS content can binding be detected (Figure 3.6A)?
- What is the protein density at the saturation point (Figure 3.6B)?
- Is the density of associated α-Syn different for SUVs compared to SLBs?

3.3.1 Circular dichroism spectroscopy

Circular dichroism is a method commonly used to study protein conformations [174–176]. The method is based on that chiral molecules absorb left and right circularly polarized light differently, a property that is called to be "optically active". Circularly polarized light is light that it "chiral", i.e. the electrical field vector rotates around the axis of propagation compared to linearly polarized light where the electrical field vector oscillates in a single plane. Left and right circularly polarized light represents the two different directions around the propagation axis; left-hand circularly polarized (LCP), light rotates counter clockwise (with the propagation towards the observer) and the right-hand circularly polarized (RCP), light rotates clockwise around the propagation axis. LCP and RCP components with equal magnitude superpose each other in such a way that it sums up to linearly polarized light with twice the amplitude as the RCP or LCP component alone. In an optically active medium, LCP light and RCP light are absorbed differently. After linearly polarized

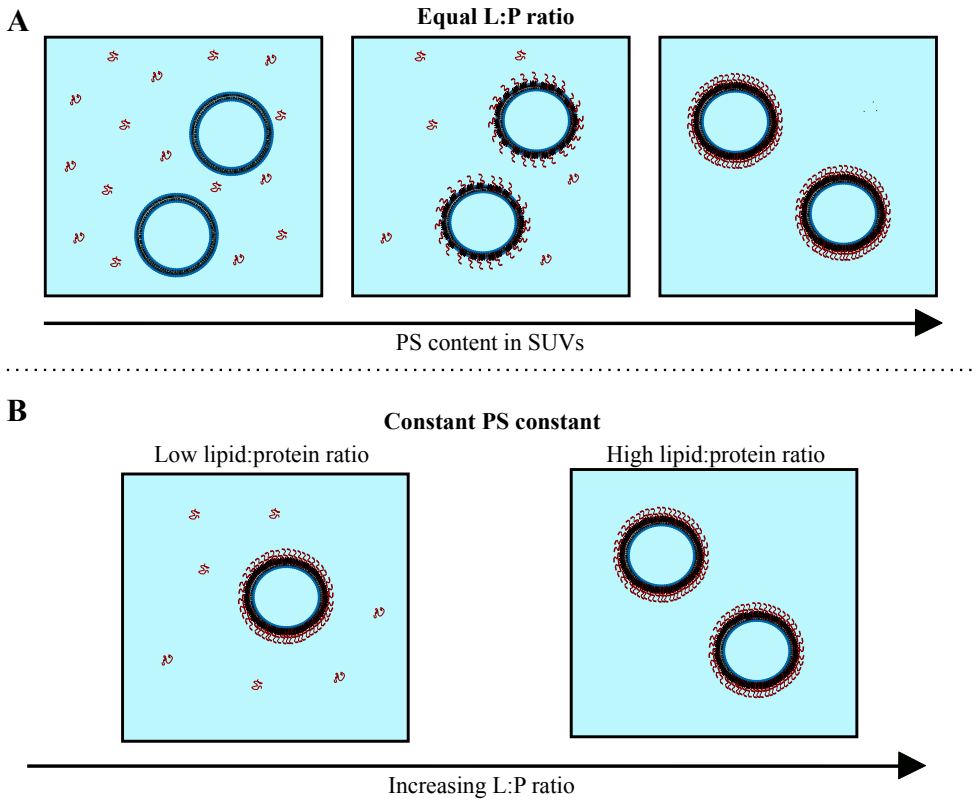

Figure 3.6: Illustration of the research questions studied by CD spectroscopy.
(A) The DOPS content required for binding was obtained by studying when binding started to occur. (B) The L:P ratio needed for saturation was studied by adding an increasing amount of SUVs to a given protein concentration.

light has passed through an optically active medium, the LCP and RCP components have been absorbed in different amounts and have different electrical field vector magnitudes. Hence, the light will be elliptically polarized and the difference in absorbance is given by Beer-Lambert's law. The circular dichroism of a molecule is measured as the difference in absorbance, ΔA, between RCP and LCP light, and is usually converted to millidegrees (mdeg), as

$$[\theta_{mdeg}] = 1000\Delta A \frac{180ln10}{4\pi} = 32982\Delta A, \tag{3.2}$$

or mean residue ellipticity as

$$MRE = \frac{\Delta AM3298.2}{lc}, \tag{3.3}$$

where M is the mean residue weight, l is the path length and c is the protein concentration.

Intrinsically disordered proteins have low ellipticity above 210 nm, and negative ellipticity around 195 nm. When the amide chromophores are aligned upon folding, their optical transitions are shifted or split which results in a change in the relative absorption between the RCP and LCP components. Hence, the secondary structure of proteins can be studied using CD spectroscopy [177]. When an IDP changes from a random coil conformation to an α-helical conformation, the spectrum changes from a characteristic random coil spectrum with a minimum around 195 nm to the characteristic spectrum with minima at 208 nm and 222 nm [175, 178].

3.3.2 α-Syn in free and bound state

The measurements of α-Syn association to SUVs were performed by studying the change in the CD spectrum when adding an increasing amount of lipids to a constant α-Syn concentration. The lipid concentration in the sample was varied to correspond to L:P ratios between L:P = 30:1 to L:P = 680:1. α-Syn in solution (free protein) has a random coil conformation which has a characteristic CD spectrum shown in Figure 3.7. Upon association to lipid membranes, when the protein adopts an α-helical conformation, the CD spectrum changes. When a maximum amount of protein is bound, adding more lipids will no longer alter the CD spectrum. This will from now on be referred to as the saturation point, which yields a spectrum shown in Figure 3.7B. Studying the alteration of the CD spectrum when increasing the amount of SUVs with a given DOPS content, the L:P saturation point for that membrane composition could be obtained. However, this assumes that the protein binds with the same sequence, which is a reasonable assumption for systems with an excess of membrane, but not for systems with membrane deficit [67].

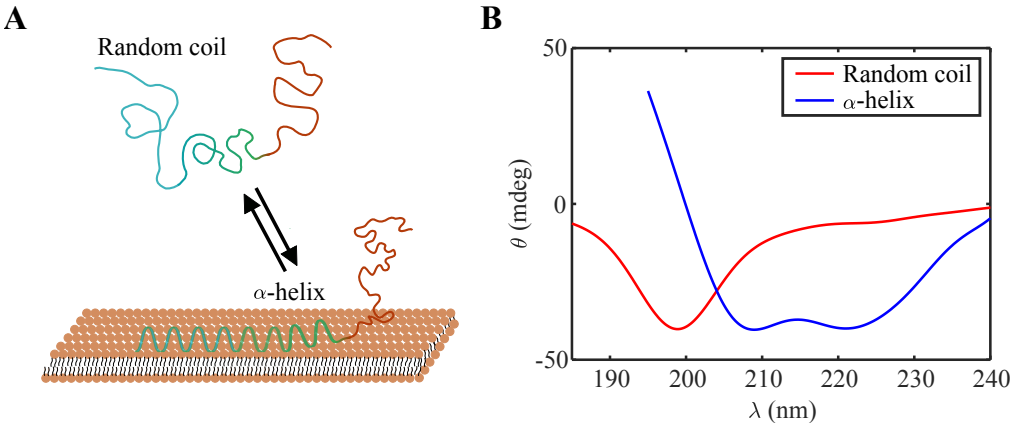

Figure 3.7: Studying secondary structures of protein using CD spectroscopy
(A) When α-Syn binds to a membrane the first 97 residues can adopt an α-helical conformation. (B) The change from a random coil conformation (red curve), to a major part of the protein adopting an α-helical conformation (blue curve), can be detected as changes in the CD spectrum.

3.3.3 α-Syn association with SUVs with various membrane charge density

The CD spectra for samples of α-Syn and SUVs (0-30% DOPS) in L:P ratios 60:1 to 680:1 are shown in Figure 3.8. For samples of 0-1% DOPS there was no binding observed at any L:P ratio. However, binding of a fraction of the protein was detected at the lowest L:P ratio studied, L:P = 30:1 for SUVs containing 5% DOPS. Hence, it could be confirmed that, for the lipid compositions and solution conditions studied, 5% DOPS was required for detectable binding to occur.

Increasing the L:P ratio resulted in an increased amount of bound α-Syn, for SUVs with 5% DOPS or more. For membranes containing 20% DOPS, there was no change in the spectra for L:P ratios 200:1 and higher. By plotting the MRE (Eq(3.3)), at 222 nm as a function of the L:P ratio for all membrane compositions investigated, the L:P ratios where the MRE reached a plateau was found (Figure 3.9A). The L:P for saturation could then be plotted as a function of DOPS content in the membrane, showing how the L:P for saturation decreased with increasing DOPS content (Figure 3.9B).

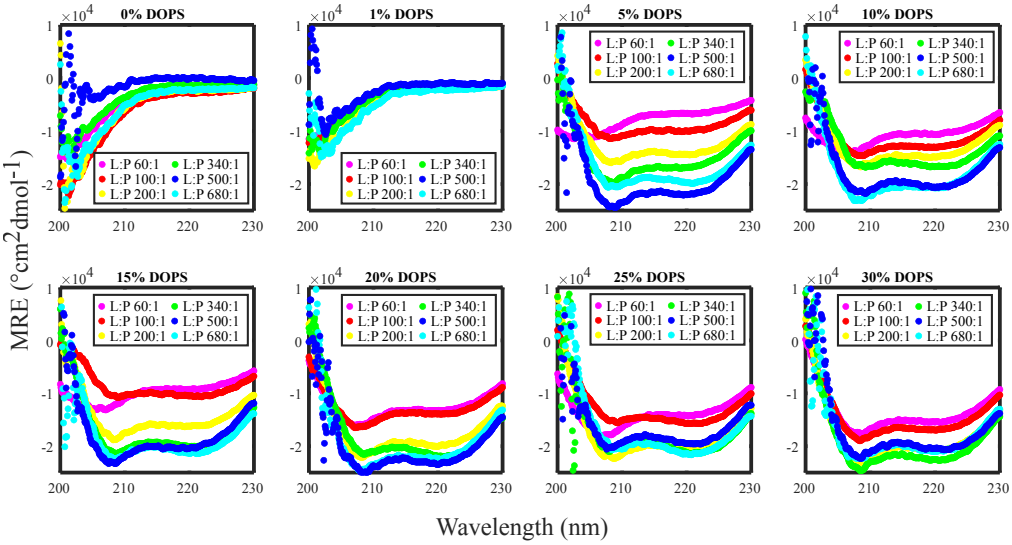

Figure 3.8: Raw data from CD spectroscopy measurements of α-Syn and SUVs.
Representative MRE as a function of wavelength for samples with vesicles containing 0-30% DOPS between L:P = 60:1 and L:P = 680:1.

3.3.4 Linear combinations can be used to obtain the fraction of saturation

The CD spectrum can be described as a linear combination of known reference spectra [176, 179]. Previously, linear combinations assuming only two states, membrane bound and free protein, have been used to describe samples where bound and free protein co-exist [180, 181]. The reference spectra have been a spectrum corresponding to a maximum amount of bound protein and a spectrum with 100% free protein.

In paper II, all spectra of SUVs and α-Syn were fitted to a linear combination of a reference spectrum with a maximum amount of bound protein (saturation), and a reference spectrum for 100% free protein using a least squares method. Figure 3.10A shows an example of raw data at L:P ratio 100:1 fitted to a linear combination of the reference spectrum for free protein and saturation. The reference spectrum for free α-Syn was a spectrum of 100% POPC SUVs and α-Syn at L:P ratio 200:1. The reference spectrum for saturation was a spectrum of POPC:DOPS 75:25 and α-Syn at L:P ratio 200:1. These spectra were chosen as reference spectra for several reasons. First, a sample containing SUVs will be affected by light scattering on the SUVs. Hence, the reference spectrum for 100% free protein needs to be a sample containing SUVs to account for the

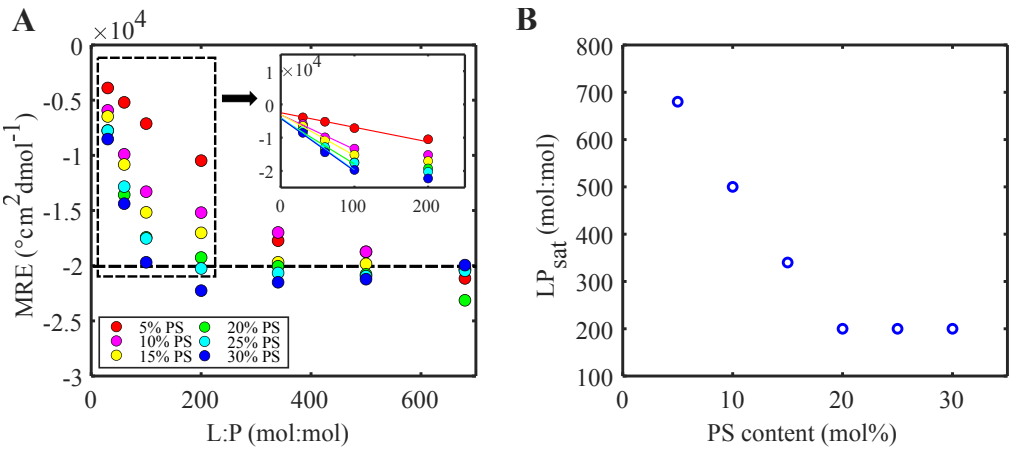

Figure 3.9: L:P saturation point for SUVs with various DOPS content.
(A) The MRE at 222 nm as a function of L:P ratio. The values are an average of 2-5 measurements. (B) From (A), the intersection between the MRE222 and the reference value for a saturated sample could be obtained. L:P ratio required for saturation could then be plotted as a function of DOPS content.

scattering of light, but where no protein is bound. Further, samples with an L:P ratio over 340:1 were affected by scattering to a large extent in the low wavelength regime, meaning that the reference spectra should be a sample with L:P 340:1 or lower. Second, the fraction of α-helical content was studied by studying the change of the spectra when increasing the lipid content in the sample. Hence, the reference spectrum had to be a spectrum where increasing the lipid content did not alter the spectrum. For SUVs with high DOPS content, this happened at L:P 200:1. This means that the reference spectrum for a maximum α-helical content needed to be a spectrum of a sample of SUVs containing at least 20% DOPS, at L:P 200:1 or 340:1. The spectrum with an MRE at 222 nm closest to the average MRE at 222 nm for the saturated spectra was the spectrum of DOPS 75:25 at L:P 200:1 ($MRE_{222} = -2e^{-4}$).

The results confirmed that the spectra can be represented by a linear combination of these two states, and that no signs of α-helix, a characteristic of the bound protein, could be confirmed for the vesicles with 0 and 1 % DOPS. Vesicles containing 5% DOPS showed an average of approximately 20% saturation at L:P ratio 30:1 (Figure 3.10B). The average fraction of saturation for a given L:P ratio increased with increasing DOPS content in the SUVs. For SUVs containing 20-30% DOPS, saturation was reached around L:P = 200:1, which agrees well with the results presented in Figure 3.9.

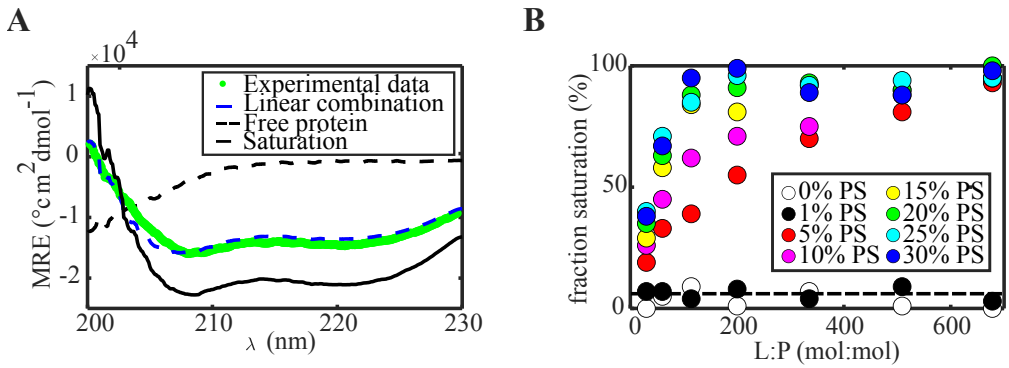

Figure 3.10: Linear fits of raw data.
(A) Examples of raw data at L:P 100:1 fitted to a linear combination of a spectrum of 100% free α-Syn, and a spectrum where a maximum amount of bound α-Syn (saturation), using a least squares method. The percentages of saturation in the legend is the fraction of saturation that was obtained by the fit.(B) Increasing the amount of DOPS increased the amount of bound protein. Bound protein could not be detected in samples with 0-1% DOPS, while samples containing $\geq$ 5% DOPS had protein bound at L:P 30:1

3.3.5 Estimating the α-Syn density adsorbed to SUVs

The density of α-Syn adsorbed to SUVs was calculated by

$$\rho_{SUV} = \frac{n_{prot}}{A_{tot}}, \tag{3.4}$$

where n_{prot} is the number of α-Syn molecules in the sample, and A_{tot} is the total accessible membrane area,

$$A_{tot} = \frac{n_{lipid} A_{lipid}}{2}, \tag{3.5}$$

where n_{lipid} is the number of lipids in the sample obtained from the L:P ratio at saturation, and A_{lipid} is the average lipid area for the different membrane compositions. Assuming a lipid area of 0.64 and 0.65 nm^2 for POPC and DOPS respectively [182, 183], the density of adsorbed α-Syn was estimated to 5000 - 15000 proteins/μm^2 (Figure 3.11A). This is a factor 3-5 more compared to the density of adsorbed α-Syn onto SLBs with the same compositions.

The estimations of the density of adsorbed α-Syn assumes that all α-Syn in the sample are bound to membrane (either SUVs or SLBs) with no co-existence between free and bound protein, which is not completely true considering the transient binding of peripheral protein [184, 185], and previously reported results regarding exchange between free and membrane bound α-Syn [67, 69]. However, previous studies on similar

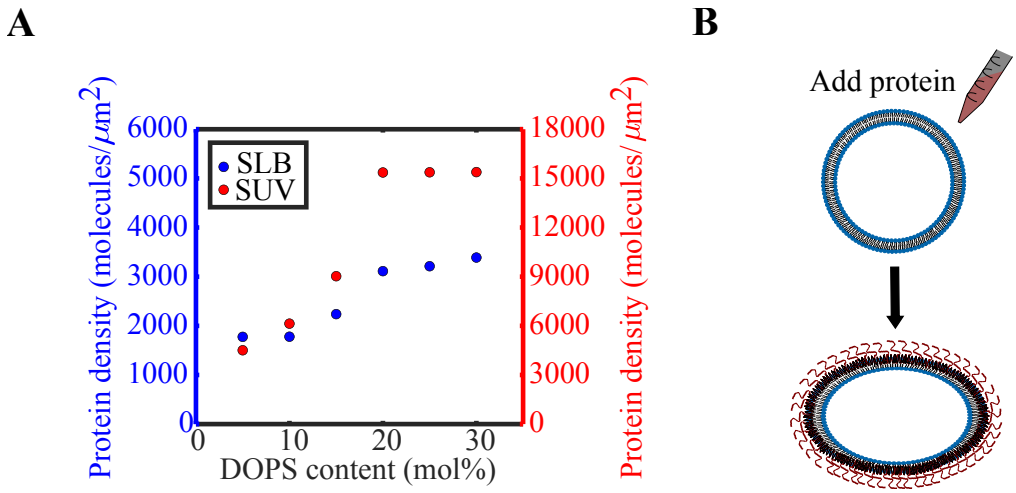

Figure 3.11: α-**Syn density adsorbed to SLBs and SUVs.**
(A) Protein density for SLB compared to SUVs. The left scale shows the α-Syn density adsorbed to SLBs (blue), and the right scale shows the α-Syn density on SUVs (red). One step on the right scale corresponds to 3 steps on the left axis. (B) SUVs are flexible whereas SLBs are more rigid. Hence, SUVs can deform upon protein adsorption.

systems have shown that for systems with an excess of lipid membrane, virtually all proteins are associated to the membrane [81]. Hence, the estimates performed above provides reasonable estimates of the α-Syn density adsorbed to the membrane and should thus be comparable to the SLB studies in chapter 3.2.

3.3.6 Discussion

The CD spectroscopy measurements of α-Syn and SUVs with various DOPS content showed that α-Syn did not bind to membranes containing 1% DOPS, but to membranes containing 5% DOPS or more. Further, it was shown that membranes containing 20-30% DOPS reached saturation at L:P 200:1, which agrees well with previous results [69].

Comparing the density of adsorbed α-Syn on SUVs with the density of α-Syn adsorbed to SLBs, the SUVs had approximately a factor 5 more α-Syn adsorbed when the membranes contained 20% DOPS or more. One major contributor to the difference in the adsorbed α-Syn density can be that the bilayer in the vesicles is rather easily deformed (Figure 3.11B), while the deposited SLB is highly limited to undergo deformation. This agrees with previous studies that have shown that α-Syn adsorption onto SUVs induce membrane deformation [101, 103], of SUVs containing 30% DOPS in a system with an excess of protein. As the lowest energy state

appears to be the deformed membrane, the gain in energy for protein adsorption is expected to be larger for the membrane where adsorption and bending can occur simultaneously, as compared to a membrane with a limited ability to deform.

Chapter 4

Studies of interactions between monomeric α-Syn and single vesicles

---

The most damaging phrase in the language is
"It's always been done this way."

— Grace Hopper

Chapter outline

This chapter concerns fluorescence microscopy studies of interactions between monomeric α-Syn and single vesicles. Initially, the different aspects of image analysis, and the assay to study single vesicle interactions developed in paper III, will be presented. The chapter continues with studies of vesicle fusion, fission and lipid exchange between vesicles that was investigated in paper III. Finally, the chapter covers the binding kinetics of α-Syn that was studied in paper IV.

4.1 Single vesicle detection and colocalization

The fundamentals of the image analysis in this thesis is detection of single spots, which includes obtaining the position and intensity of a spot. After obtaining the position and intensity, the changes in intensity and position can be studied [149, 150]. This can, for example be used to study fusion of vesicles [145, 146], and interactions between protein and vesicles [147].

4.1.1 Single vesicle and molecule detection

In this thesis, single vesicle and single protein detection have been of great importance. An assay to detect and colocalize single vesicles was developed in paper III, and has been the basis of the image analysis performed in all papers.

4.1.1.1 Raw data processing

Raw data from .tiff-files, (Figure 4.1A), was loaded into Matlab as 2 or 3-dimensional matrices and filtered by a low-pass filter. The background was subtracted from all images using a rolling ball algorithm. The algorithm was first developed by Sternberg [186], and is since then commonly used during image analysis, of for example single vesicles [187]. First, the pixel specific background was found by looping a rolling ball algorithm defined by

$$BG = [col] - \sqrt{r^2 - (kdx)^2} \tag{4.1}$$

over each column of the image, where [col] is a column in the two-dimensional image, r is the radius of the rolling ball, k is the current pixel and dx is the spacing of sample points. The edge constraints giving the start and end point of the rolling ball was defined as $K = floor(r/dx)$. The background image was filtered by a median filter over a 3x3-pixel

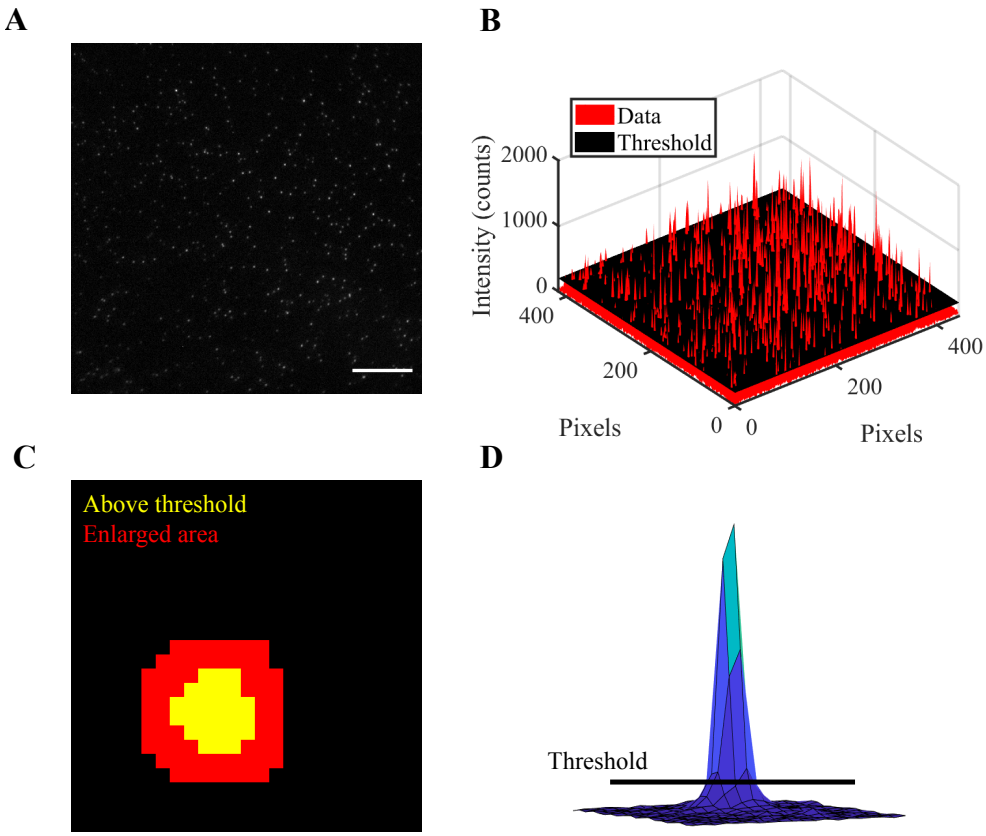

Figure 4.1: Single vesicle detection.
(A) Image of vesicles in one channel. The scale bar is 10 μm. (B) Images are analysed in Matlab 2020b and can be plotted as 3-dimensional surfaces with the fluorescence intensity on the z-axis. The black surface shows the pixel-specific threshold and the red surface shows the fluorescence intensity. The red peaks above the threshold is the detected vesicles. (C) To ensure that the total intensity is obtained, the area of the detected vesicle is enlarge. Otherwise, the bottom of the peak will be excluded as illustrated in (D), and the total intensity will be incorrect. The figure is an an adapted version, originally published in paper III.

area and then subtracted from the raw data image. To finalize, the background-subtracted image was subjected to a Gaussian filter.

The vesicles or single molecules could then be identified by creating a binary mask of the pixels that passed an intensity threshold (Figure 4.1B), depending on a user-set signal-to-fluctuation ratio (SFR) as

$$I(r)_{th} = SFR \cdot 2(I_{median}(r,:) - I_{min}(r,:)) \tag{4.2}$$

where $I(r)_{th}$ is the threshold intensity, $I_{median}(r,:)$ is the row median intensity and $I_{min}(r,:)$ is the row minimum intensity. This means

that the fluctuation level was chosen as twice the difference between the median and minimum intensity row vectors of the two-dimensional image, with a minimum value of zero. The threshold is hence pixel specific which eliminates issues with uneven background intensities due to in-homogeneous background illumination.

The neighboring pixels in the binary mask, i.e., a "spot" represents a single vesicle or single molecule. Every spot was enlarged by a pixel window that created an enlarged ring around the detected spot (Figure 4.1C). The enlargement was performed to include the edges of the spot that might not pass the threshold (Figure 4.1D). Using a 5x5 pixel enlargement window, a single pixel that passes the threshold would be enlarged to a 5x5 pixel spot, and a 3x4 spot is enlarged to 7x8 spot. Finally, the intensity of all pixels corresponding to a spot was summed to obtain the total intensity I_{int} as

$$I_{int} = \sum_{i=1}^{n} I_{pix}(i) \tag{4.3}$$

where I_{pix} is the intensity in every pixel in the spot. Since the same enlargement is applied to all spots in a data set, the additive effect is equal for all spots. If no enlargement is done, failing to include the edges of the spot would lead to greater differences in the I_{int} due to the spread in the intensity distribution of the vesicle or single molecule population.

4.1.2 Colocalization

The ability to detect colocalization has been of great importance in paper III and paper IV. In paper III, colocalization between two differently labeled vesicle populations (blue and red) was used to detect fusion and lipid exchange between vesicles. In paper IV, colocalization between differently labeled vesicles (blue) and proteins (red) was used to estimate binding lifetime of α-Syn bound to vesicles.

4.1.2.1 Spatial colocalization

In paper III, the vesicle populations were simultaneously imaged onto two channels on the same image using a Hamamatsu Gemini Dual View. The vesicles in the two channels were then detected as described in chapter 4.1 for each channel separately. When the vesicles in the two channels were detected, colocalization between the vesicle populations were detected by two different methods; position detected colocalization and intensity detected colocalization. The two methods to detect colocalization

are described in Figure 4.2, where Figure 4.2A shows the fictional case where 3 vesicles of 7 are both blue and red-labelled. The first method, position-detected colocalization, detects colocalized vesicles by comparing the center positions (black dots in Figure 4.2B) of the vesicles in the two channels. One of the channels is chosen as reference channel, and the center positions of the reference channel with a user determined search radius (black dashed circles in Figure 4.2B), is applied to the second channel.

The program then search within the search radius to find center positions from the second channel. Hence, if the user chooses to use the red channel as the reference channel, the program applies the red vesicle center positions with search radius to the blue channel, and search for blue vesicles with center positions within the search radius. During intensity-detected colocalization, the mask from one channel (red circles in Figure 4.2B) is

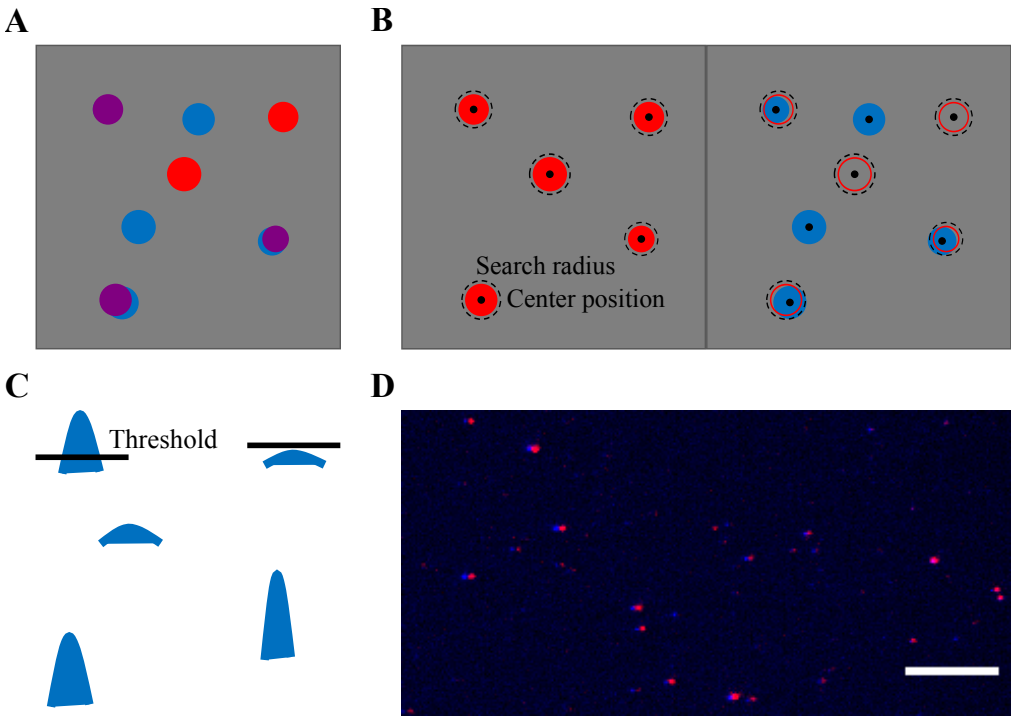

Figure 4.2: Intensity and position-detected colocalization.
(A) Illustration of an overlay of the red and the blue channel, showing that 3 of 7 vesicles are both blue and red labelled. (B) Illustration of the two channels where the center positions and search radius from the red channel has been applied onto the blue channel to obtain position-detected colocalization. Further the outlines (red circles) show how the mask from the red channel is applied onto the blue channel. (C) To obtain intensity-detected colocalized vesicles, the integrated intensity within the red circles in the blue channels must be higher than the threshold (D). Image of raw data overlay of a sample where 100% of the vesicles are both blue and red-labelled. The scale bar is 10 μm. The figure is an an adapted version, originally published in paper III.

applied on the second channel and I_{int} within the red circles in the second channel is calculated. If this integrated intensity in the second channel is above a threshold ($I_{th,int}$) given by

$$I_{th,int}(\sigma) = SFR * I_{BG}(\sigma) \tag{4.4}$$

where $I_{BG}(\sigma)$ is the size dependent background of a spot, the vesicles are considered colocalized (Figure 4.2C). An example of a sample with vesicles that are both blue and red labelled (100% colocalization) can be seen in Figure 4.2D.

The accuracy of the colocalization was investigated by measuring vesicle samples where blue, red or both blue and red-labelled vesicles were mixed in different molar ratios. The ratios were chosen to correspond to 0%, 25%, 50%, 75% and 100% of vesicles containing both dyes and thus mimicking fusion events. The results are presented in paper III, and shows that both methods agree well with theoretical values, although position detected colocalization is preferable for samples with low colocalization and intensity-detected colocalization is preferable for samples with high colocalization. A reason for this is that intensity-detected colocalization is better at detecting small or unfocused vesicles from the data that the position-detected colocalization could miss. However, for samples with low colocalization, position-detected colocalization is preferable whereas intensity-detected colocalization tends to find "false" vesicles from the background.

To compensate for differences in positional alignment, the channels can be drift corrected using a reference sample with vesicles labelled with both colors (100% colocalization). The images of the channels are then cross-correlated (Figure 4.3A) and the drift offset between the channels is obtained by finding the maxima in the correlation matrix (Figure 4.3B). One of the images is then drift corrected by adjusting the position of the image in the 2-dimensional space by the offset in relation to the other image (Figure 4.3C-D).

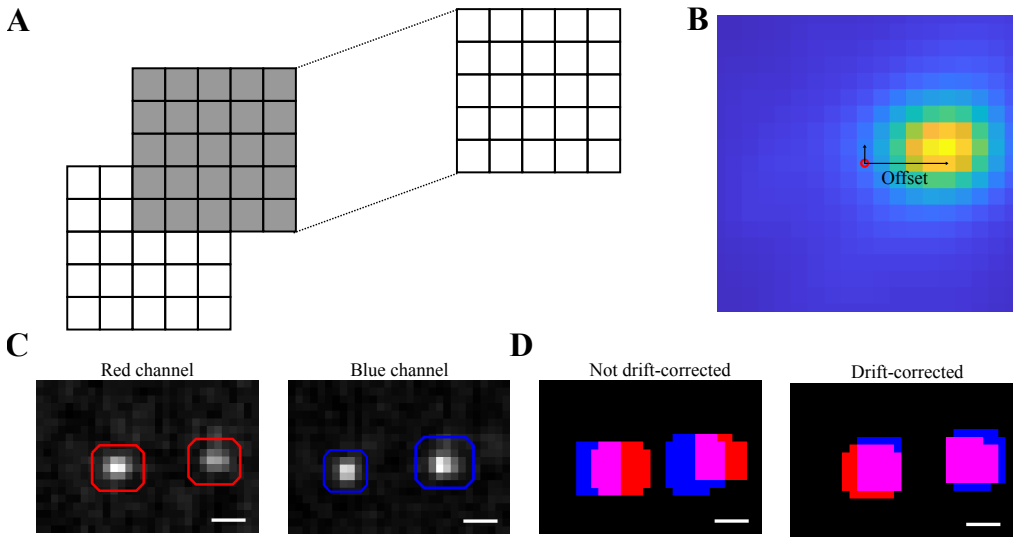

Figure 4.3: Drift-correction between the red and blue channel.
(A) Misalignment between the channels are compensated for by drift-correction. The images from the two channels are cross-correlated and the maxima in the correlation matrix gives the offset between the images (B). (C) Images of two vesicles in the red and the blue channel. The scale bars are 1 μm. (D) Overlay of the mask from the two vesicles in (C) before and after drift correction. The scale bars are 1 μm.

4.1.2.2 Temporal colocalization

The above section has described the spatial colocalization between vesicles imaged in two different channels, performed in paper III. In paper IV, colocalization between blue-labelled vesicles and red-labelled protein was performed both spatially and temporally. Temporal colocalization was done by position-detected colocalization between proteins in different frames (Figure 4.4A). This enabled studying the binding kinetics by tracking the time a vesicle was colocalized with protein. Further, it was possible to track and compare the number of vesicles that were colocalized with protein in every frame (momentary colocalization) to how many vesicles that had been colocalized with protein after a certain time had passed (accumulative colocalization) (Figure 4.4B).

Simultaneously, the intensity-detected colocalization was used to study the time dependent intensity profile of the protein channel in those spots where a vesicle was docked (Figure 4.4C). From the intensity profiles, it is possible to detect step-wise bleaching that gives information about the number of proteins bound to every vesicle.

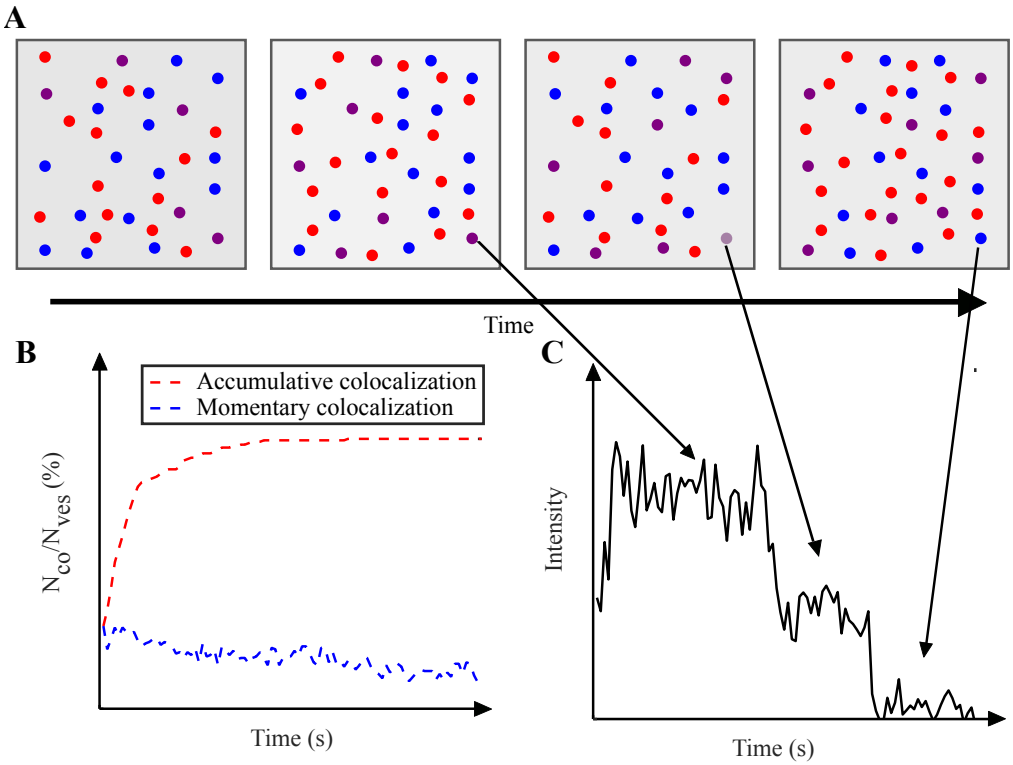

Figure 4.4: Temporal colocalization between image frames.
(A) To detect temporal colocalization, vesicles (blue) and proteins (red) were first position-colocalized in every frame. When colocalization (purple) within the frames were performed, colocalization of α-Syn between frames was performed in a similar manner. (B) This means that it was possible to study how different vesicles were colocalized with proteins in different frames, yielding a momentarily and accumulated colocalization. (C) Intensity-detected colocalization can be used to study the time-dependent intensity profile of vesicle positions in the protein channel. This makes it possible to detect stepwise bleaching, corresponding to the intensity of one protein. The figure is an adapted version from paper IV.

4.1.3 Discussion

In paper III, a single vesicle assay used to detect vesicle fusion, fission and exchange between vesicles was developed. Single vesicle studies are of great importance to study interactions between vesicles and proteins that would otherwise disappear in a bulk average. The first to study fusion of vesicles using TIRF was Weber, who studied SNARE mediated vesicle fusion *in vivo* [145] using a FRET pair. Since then, studies of single vesicle interactions have been commonly performed in various ways. However, while there are several options for analysis of FRAP data [124, 188, 189], or single particle tracking [190–193], user friendly analysis tools able to do the full analysis of the interactions presented in paper III and IV are scarce or lacking. Hence, the single vesicle assay was developed, which was used

not only in paper III but also paper IV to study binding kinetics of α-Syn using temporal colocalization.

The detection of these events rely on the detection of the position and intensity of single vesicles. By studying colocalization of vesicles, vesicle fusion and lipid exchange can be detected, and by studying changes in intensity, vesicle fission can be detected. In paper IV, the assay was adjusted to study kinetics of monomeric α-Syn interactions. The assay can easily be adjusted to be used for FRET studies, which might be used for further studies of protein-vesicle interactions, vesicle docking and vesicle fusion.

4.2 Vesicle fusion, fission and lipid exchange between vesicles

Due to the inconclusive discussion of previous research regarding vesicle fusion, fission, clustering and deformation described in chapter 1, the main aim of paper III was to investigate if α-Syn induces vesicle fusion, fission, clustering or lipid exchange between vesicles. This was done using the single vesicle assay presented above. The main research questions in paper III were

- Does α-Syn induce vesicle fusion, fission or lipid exchange between vesicles containing anionic DOPS?
- Does α-Syn induce vesicle fusion, fission or lipid exchange between vesicles containing anionic GM1?

To study the α-Syn induced vesicle fusion, fission and lipid exchange between vesicles, blue-labelled vesicles and red-labelled vesicles consisting of DOPC:DOPS 7:3 were incubated with α-Syn at different L:P ratios (50:1 - 400:1) for up to 48 hours. The samples were docked to a glass surface as described in chapter 2.5 and imaged after 0h incubation, 24h incubation and 48h incubation. The images were then analysed using the method described in chapter 4.1. If fusion or clustering between vesicles was occurring, the number of vesicles in the sample would decrease, along with an increase of fluorescence intensity in one channel or colocalization of the vesicle in the red and the blue channel (Figure 4.5A). If there was lipid exchange between vesicles, the total number of vesicles would be unchanged, but a fraction of vesicles would be colocalized in both channels and hence the intensity in respective channel would decrease (Figure 4.5B). If the vesicles had undergone fission, the total number of vesicles would increase along with a decrease in fluorescence intensity (Figure 4.5C). Hence, the assay would be able to detect fusion, clustering, fission and lipid exchange, but not be able to differentiate between fusion and clustering.

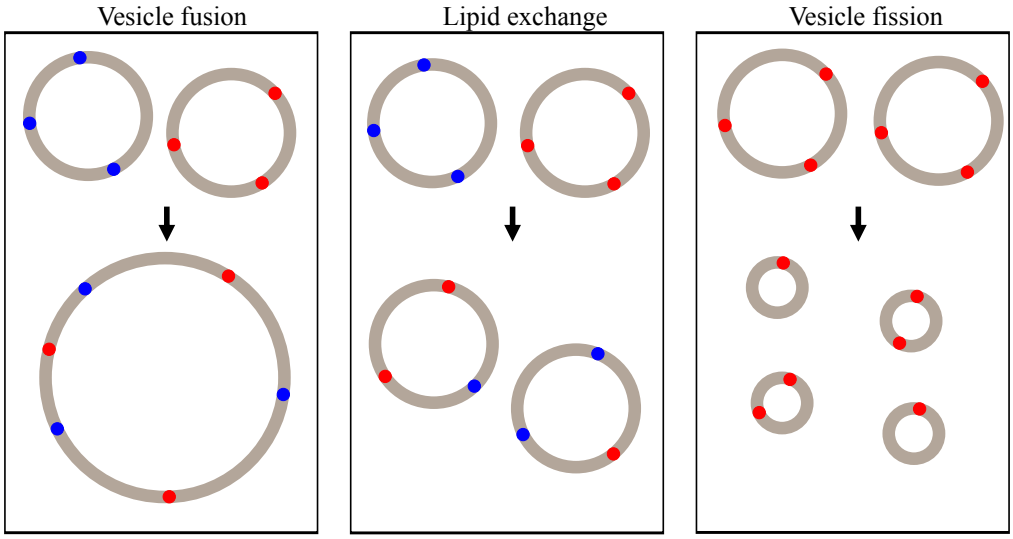

Figure 4.5: Illustration of the consequences of vesicle fusion, lipid exchange between vesicles, and vesicle fission. (A) Vesicle fusion would yield increased fluorescence intensity, decreased vesicle population and colocalization of vesicles in the red and blue channel. (B) Lipid exchange between vesicles would result in an unchanged vesicle population, but colocalization of vesicles in the two channels. (C) Vesicle fusion would lead to an increased vesicle population and a decreased fluorescence intensity.

4.2.1 Lipid exchange

In order to detect lipid exchange a new variable called I_{tot}, normalized to the background intensity of a spot of corresponding size, was defined as

$$I_{tot}(\sigma) = \frac{I_{int} - I_{BG}(\sigma)}{I_{BG}(\sigma)}. \tag{4.5}$$

Since I_{tot} is normalized to the background intensity corresponding to the size of the spot, the variable is independent of vesicle size and more sensitive to changes in the relative summed intensity, which is a necessity when detecting minor changes in intensity that arises from lipid exchange between vesicles. The background intensity was calculated for every image by randomly choosing hundred spots with sizes of the spots vary from 10 to 100 pixels, from places where no vesicles are detected (Figure 4.6A-B).

Figure 4.6C shows the normalized integrated intensity I_{tot} (Eq. 4.5) for detected vesicles in the red and blue channels when the positions obtained in the blue/red channel are being used as a mask. This was done for samples with 0% theoretical lipid exchange (no vesicles are both red and blue) and 100% theoretical lipid exchange (all vesicles are both red and blue) to validate the method. Detected vesicles refer to vesicles that are

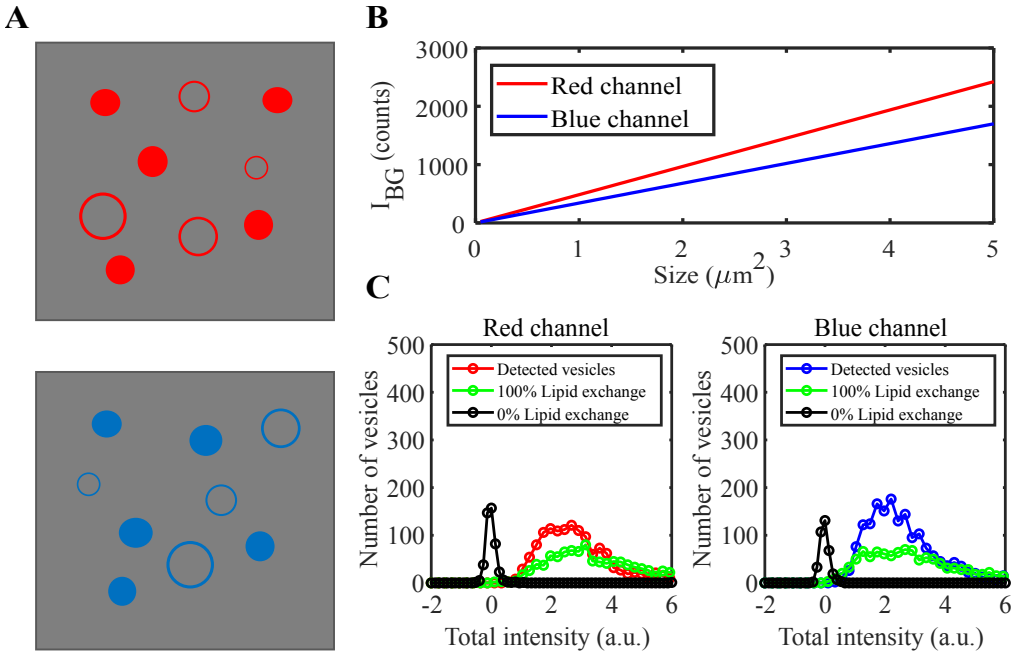

Figure 4.6: Detecting lipid exchange between vesicles.
(A) The size-dependent background intensity I_{BG} was calculated for spots of various sizes from areas with no vesicles (non-filled circles). (B) I_{BG} plotted as a function of spot size. (C) The integrated intensity I_{int} of detected spots (filled circles in (A)), was normalized to I_{BG}, creating the variable I_{tot}. Hence, by studying how I_{tot} increases, lipid change can be detected. The figure is an an adapted version, originally published in paper III.

detected in the red/blue channel and 0 and 100% exchange refers to when the mask from the blue/red channel is applied to the red/blue channel for samples with 0% and 100% lipid exchange. The results in Figure 4.6C shows that it is possible to distinguish between samples consisting of 0 and 100% lipid exchange, and that it is possible to detect shifts in the distribution, indicating lipid exchange. The ratio between the average I_{tot} for the sample, $<I_{tot,sample}>$, and the average I_{tot} for detected vesicles, $<I_{tot,ves}>$, can then be used to estimate the lipid exchange in the sample.

4.2.2 Monomeric α-Syn induces fission in GM1 containing membranes but not in DOPC:DOPS membranes

Initially, vesicles consisting of DOPC:DOPS 7:3 were incubated with α-Syn to different molar ratios (Figure 4.7A). After incubation, vesicles were docked to a piranha cleaned glass slide as described in chapter 2.5 (Figure 4.7B). Vesicles were then imaged in two channels simultaneously (Figure

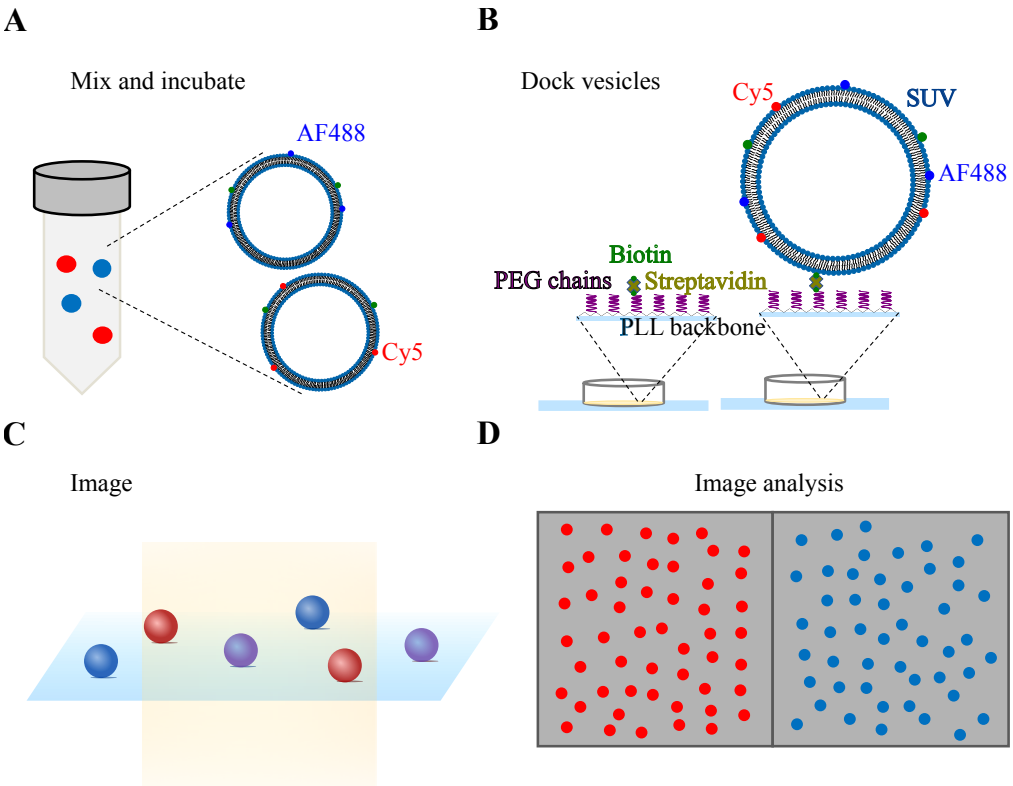

Figure 4.7: Studying vesicle fusion, fission and lipid exchange.
(A) Vesicles labelled with either red or blue fluorescent dyes were mixed with each other and incubated with α-Syn. (B) After incubation, the vesicles were docked to a passivated glass coverslide. (C) The vesicles were imaged onto two channels simultaneously. (D) After measurements, the images were analysed as described in chapter 4.1.

4.7C-D) and the images were analysed as described in chapter 4.1.

Figure 4.8A shows an image of a sample of differently labelled vesicles incubated with α-Syn. No visible colocalization can be seen. Further, there were no statistically significant difference in integrated intensity, I_{int}, or number of vesicles between vesicles incubated in absence and presence of α-Syn in any of the two channels (Figure 4.8B). Measurements of vesicles containing DOPC:DOPS 7:3 incubated with α-Syn showed no statistically significant difference in lipid exchange or colocalization over 48 hours compared to control vesicles incubated in absence of α-Syn (Figure 4.8C-D). Hence, it can be concluded that there was no detectable fusion, clustering, fission or lipid exchange between DOPC:DOPS 7:3 vesicles induced by α-Syn. Altogether, this indicates that α-Syn does not induce any vesicle fusion, fission or lipid exchange

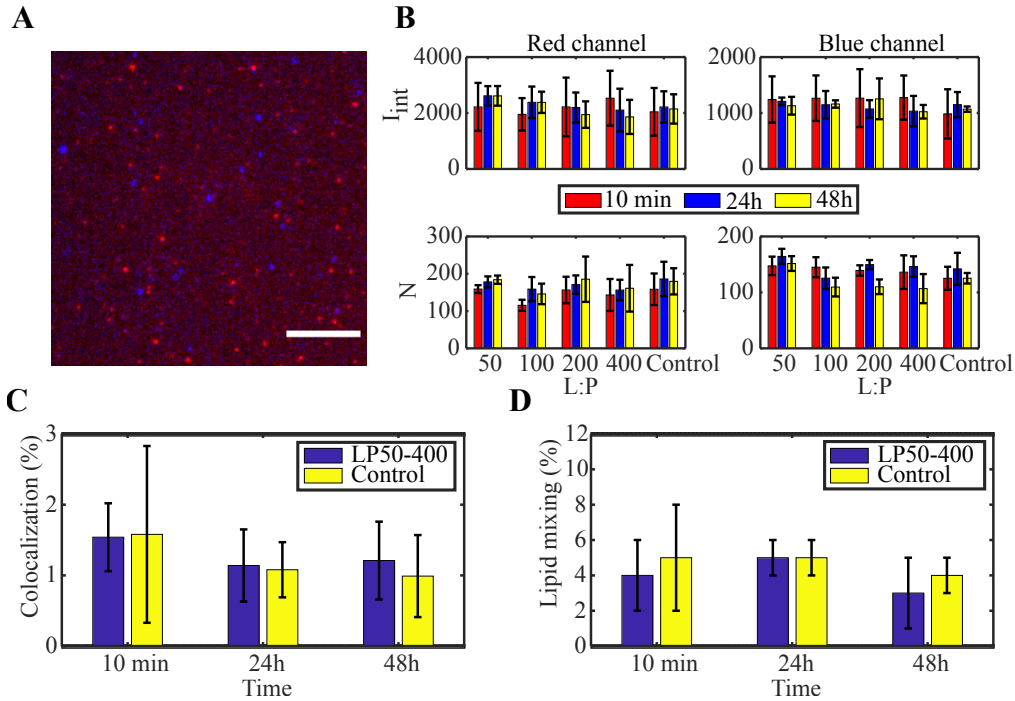

Figure 4.8: Measurements of DOPC:DOPS 7:3 vesicles.
(A) Image of two populations of differently labelled vesicles after incubation with α-Syn. The scale bar is 10 μm. (B) Results of the integrated intensity I_{int} and number of vesicles after incubation with α-Syn for 0, 24 and 48 hours. There is no significant difference between control vesicles and samples incubated in L:P ratio 50:1 - 400:1. (C) Colocalization of vesicles incubated in presence and absence (control) of α-Syn. (D) Calculated lipid exchange of vesicles incubated in presence and absence (control) of α-Syn. There is no significant difference between control vesicles and vesicles incubated in presence of protein. The figure is an an adapted version, originally published in paper III.

within 48h in vesicles consisting of DOPC:DOPS 7:3.

Due to previous indications that association of α-Syn induces fission of vesicles containing ganglioside lipids [106], some of the anionic PS was exchanged to anionic GM1 to obtain vesicles with a composition of DOPC:DOPS:GM1 7:2:1, with 1 mol % red-labelled lipids. The number of vesicles and the fluorescence intensity was obtained before and after incubation with α-Syn at a L:P ratio 200:1 for up to 24 hours (Figure 4.9A). Control vesicles incubated in absence of protein were imaged at the same time as the vesicles incubated with α-Syn (Figure 4.9B). After 10 min, the average fluorescence intensity per vesicle decreased with a factor two (Figure 4.9C). Simultaneously, the number of vesicles had increased with approximately a factor two (Figure 4.9D). Hence, on average, every vesicle had undergone fission and split into two within 10 minutes. The control vesicles incubated in absence of protein remained unchanged in population

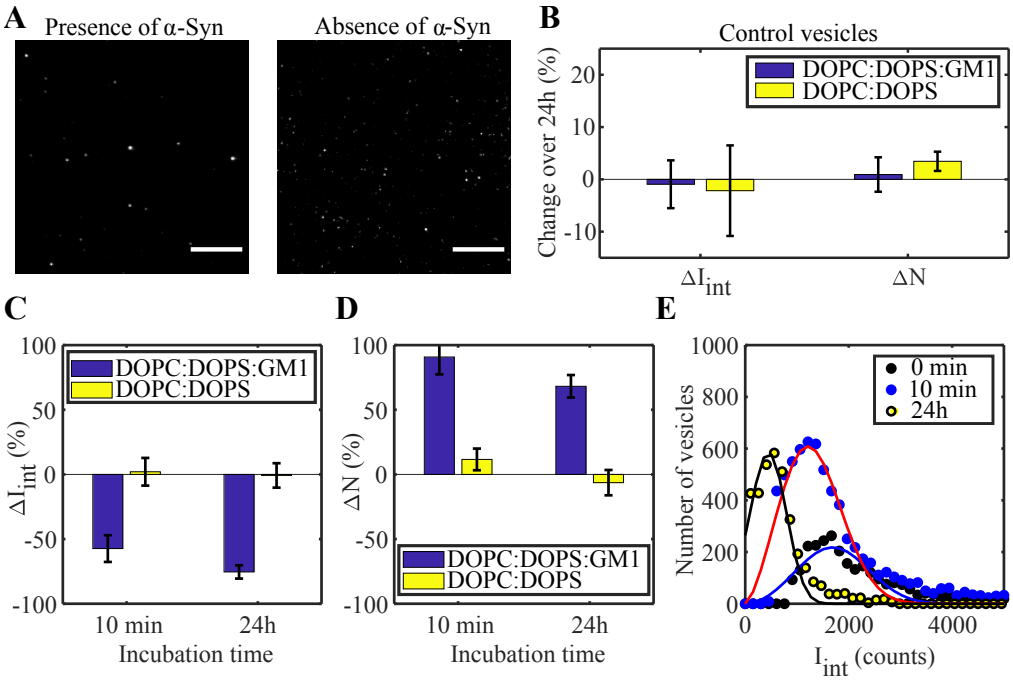

Figure 4.9: Measurements of DOPC:DOPS:GM1 7:2:1 vesicles.
(A) Image of vesicles incubated in absence (left) and presence (right) of α-Syn after 10 minutes. After 10 minutes, the number of vesicles are reduced and less bright. (B) Relative change of number of vesicles and integrated intensity for control vesicles incubated in absence of α-Syn. (C) Relative change in integrated intensity over 24 hours for vesicles incubated in presence of α-Syn. (D) Relative change in number of vesicles over 24 hours for vesicles incubated in presence of α-Syn. (E) Intensity distribution of vesicles incubated with α-Syn for 10 minutes, 24 hours and 48 hours. The figure is an an adapted version, originally published in paper III.

size and average intensity (Figure 4.9B). Incubating the samples for 24 hours resulted in an increase in number of vesicles with a factor 1.7 and a 75% decrease in fluorescence intensity (Figure 4.9C-D). From Figure 4.9E, it can be seen how the population histogram is shifted to the left, indicating that the vesicles have undergone fission several times and reached sizes that are too small to detect with the system used. This suggestion is further strengthened by an approximately 60% drop in total intensity of the sample after 24h, compared to a minor change in total intensity within 10 minutes.

4.2.3 Discussion

The results in paper III, where DOPC:DOPS vesicles were incubated with α-Syn, showed that α-Syn does not induce detectable vesicle fusion, fission or lipid exchange between DOPC:DOPS 7:3 vesicles in L:P ratios 50:1 - 400:1 within 48 h. These findings agree with previous suggestions that

presumed vesicle fusion of DOPS containing vesicles [101] can be explained by shape deformations of vesicles upon protein adsorption [103]. However, including GM1 to the vesicles resulted in immediate fission, in agreement with previous cryo-TEM results [106].

α-Syn induced fission of GM1-containing SUVs may be due to the more conical shape of the GM1 headgroup compared to the phospholipids that results in a different packing parameter. Hence it is likely that the spontaneous curvature is differently affected upon protein association, which may include a lower energy barrier for fission [105]. Overall, these results indicate that it is more likely that vesicle deformation of DOPC:DOPS vesicles are fission intermediates than fusion intermediates, as previously discussed [69]. Altogether, α-Syn alone does not induce vesicle fusion or lipid exchange between vesicles, but could regardless assist during exo- and endocytosis in the neuron.

4.3 α-Syn binding kinetics on a single vesicle level

In order to obtain further knowledge regarding the binding kinetics in systems below saturation conditions, investigate cooperative binding at low protein concentrations, and further study the number of α-Syn adsorbed to a vesicle, paper IV studied individual interactions between α-Syn and SUVs with different membrane charge densities at low protein concentrations. The main research questions that were investigated were

- How many proteins are bound to a vesicle at an overall low protein concentration?
- Is the binding cooperative at an overall low protein concentration?
- How long is the lifetime of the binding?
- Is binding kinetics affected by membrane composition (charge density) and protein concentration?

The binding kinetics were studied by docking fluorescently labelled vesicles (blue), consisting of DOPC:DOPS 7:3 or 9:1 to a passivated glass surface (Figure 4.10). Non-docked vesicles were washed away and the docked vesicles were imaged. After imaging the vesicles, fluorescently labelled α-Syn (red), was added in various concentrations. Using TIRF microscopy, videos of the α-Syn bound to SUVs could be recorded with a temporal resolution of 40 ms.

4.3.1 Vesicle and α-Syn detection

Images of the vesicles and background images were loaded into Matlab as single .tiff files, and timelapses of the α-Syn channel were loaded as .tiff stack files. During the first step of the analysis, vesicles were detected as described in chapter 4.1. The second step of analysis consisted of background subtraction, that was performed by imaging a background image of the α-Syn channel with equal exposure time as the timelapses that were recorded during measurements (Figure 4.10B). By recording a background image for background subtraction, the exposure time dependence of the background level were taken into account. Simultaneously, the sample was confirmed to be free from contamination that could have been mistaken as α-Syn. After imaging the background,

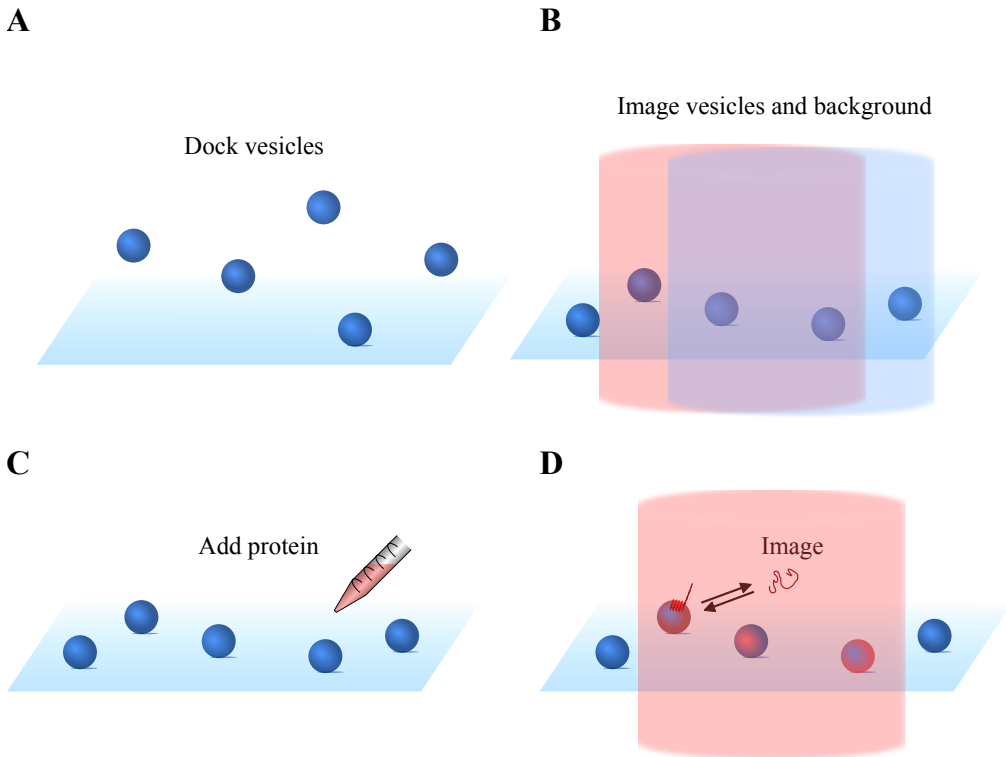

Figure 4.10: Illustration of the measurement procedure.
(A) Vesicles are docked to a passivated surface. (B) Vesicles and the background image of the α-Syn channel are recorded. (C) α-Syn is added to the well. (D) Time lapses of the α-Syn channel are recorded.

α-Syn was added to the well (Figure 4.10C), and time lapses of the α-Syn channel was recorded (Figure 4.10D). α-Syn was then detected in all frames as explained in chapter 4.1, using a user-determined threshold. SUVs and α-Syn were colocalized in every separate frame using position colocalization as described in chapter 4.1. The maximum difference of the center of SUVs and α-Syn spots was 3 pixels in both x and y-direction. After colocalization between vesicles and α-Syn in every frame, α-Syn were colocalized between frames in the same way. From α-Syn colocalization between frames, the continuous time a vesicle was colocalized with α-Syn was obtained, which is referred to as the colocalization time. Simultaneously, the intensity profiles at the positions where a vesicle was docked was tracked in the α-Syn channel (intensity-detected colocalization). From the intensity profiles, stepwise bleaching was detected. The average bleaching step was used to determine the intensity corresponding to one α-Syn molecule and used to calculate the number of α-Syn molecules interacting with a vesicle.

4.3.2 Binding lifetimes of α-Syn associated with single lipid vesicles

To study the binding kinetics, low α-Syn concentrations (30 pM), were added to the docked vesicles, and time lapses were recorded. Studying the intensity profiles, two different type of interactions between α-Syn and lipid membranes could be identified. The first, and most common, type of interaction involved one or two α-Syn molecules and lasted for 40-80 ms (Figure 4.11A). This means that the sample mainly contained many short-lived interactions between vesicles and one or two α-Syn molecules. This type of interaction is referred to as a short interaction. However, there was also a fraction of vesicles with a longer binding lifetime. These interactions had high initial intensities, which were reduced by bleaching in several steps, and are referred to as long interactions (Figure 4.11B). The long interactions generally included association of several α-Syn molecules that remained bound. The average lifetime of the binding was approximately 70 ms (Figure 4.11C-D). Increasing the protein concentration to 300 pM resulted in intensity profiles similar to the intensity profiles obtained for 30 pM α-Syn. However, both the number of short and long interactions increased, as well as the average binding lifetime.

The findings regarding the binding lifetime show that there are different binding alternatives for α-Syn. Trying to quantify a general average binding lifetime on those premises would mean that one would draw conclusions based on the average of a heterogeneous sample. Instead, the discussion should be kept to the separate indications of the two interaction types, and the coexistence of them. The presence of a sub-population of vesicles with several α-Syn molecules associated that eventually bleach, while other vesicles have no α-Syn bound, strongly indicate cooperative binding even in a dilute system. Further, when binding cooperatively in a system where there is not enough α-Syn to saturate the membrane, α-Syn remains bound for seconds or longer. On the contrary, random binding of single α-Syn molecules experiences a shorter lifetime, in the range of ms. Lifetimes in the order of ms has previously been observed in systems with membrane deficit [66, 69].

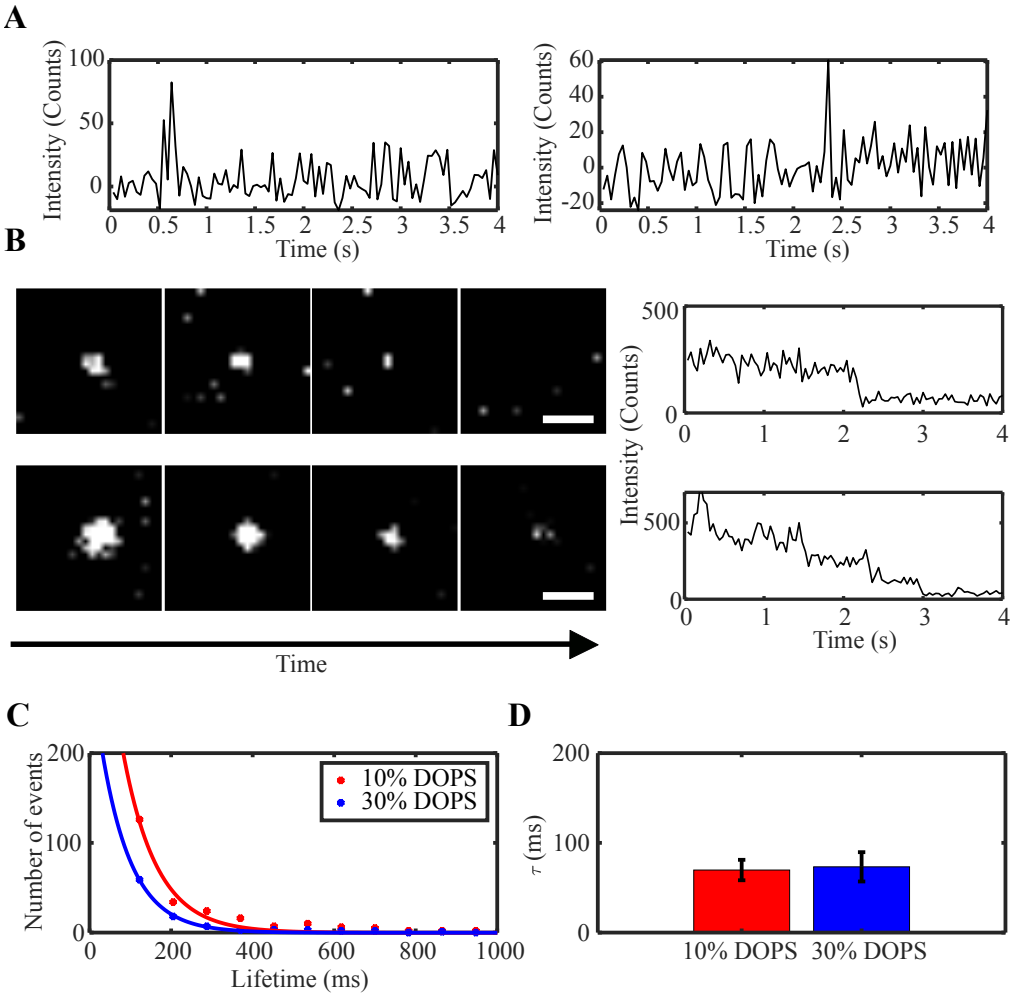

Figure 4.11: Binding lifetimes of α-Syn.
(A) Representative time traces showing short interactions. (B) Raw data images and the corresponding time traces showing long interactions. (C) Representative lifetime distributions for SUVs consisting of 10 and 30% DOPS (D) Average lifetimes for SUVs containing 10 and 30% DOPS. The data are mean ± SD of 10-12 measurements. The figure is adapted from paper IV.

4.3.3 α-Syn co-exist in free and membrane bound states

The fraction of momentary colocalized vesicles and the accumulative colocalization for vesicles containing 10 and 30% DOPS and α-Syn concentrations of 30 pM can be seen in Figure 4.12A. The initial colocalization for a system with 30 pM α-Syn was approximately 10%, and all vesicles had been colocalized with α-Syn within 4 s. During the 4

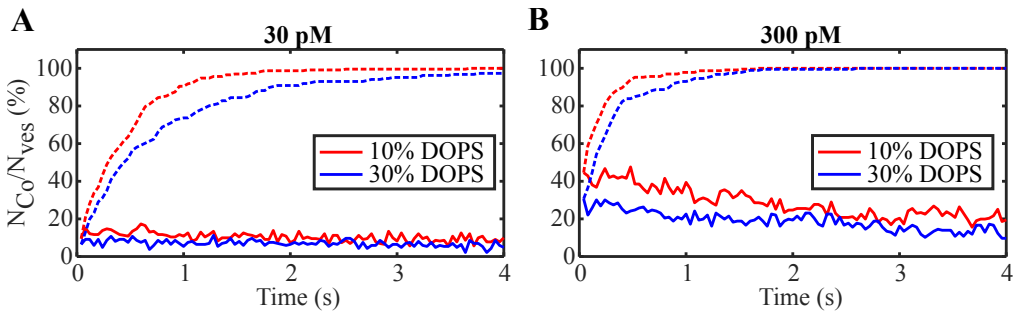

Figure 4.12: Momentarily and accumulative colocalization.
Representative momentarily and accumulated colocalization for SUVs consisting of 10 and 30% DOPS for 30 pM (A) and 300 pM α-Syn (B). The figure is an adapted version of figures included in paper IV.

seconds images were recorded, between 5000 - 10 000 interactions between α-Syn and vesicles were detected. In general, approximately 10% of those were long interactions where protein remained bound for seconds, while 90% of the interaction were short. This shows that α-Syn associates with different vesicles at different time points, meaning that α-Syn in the free and the membrane bound state co-exist in the sample.

Increasing the α-Syn concentration to 300 pM resulted in 100% of the vesicles being colocalized almost twice as fast (Figure 4.12B). The fraction of short interactions also decreased to 80%. Furthermore, there was a significant increase in the number of vesicles colocalized with protein and the number of α-Syn associated to the vesicles compared when adding only 30 pM α-Syn.

4.3.4 Estimating the number of α-Syn molecules associated with a vesicle

One of the aims was to quantify the number of α-Syn molecules that are bound to the vesicles. The results showed that, for vesicles that were colocalized with α-Syn, the average number of α-Syn molecules per vesicle was 2 and 5 α-Syn for 30 and 300 pM α-Syn respectively (Figure 4.13A). There were no significant differences between the number of vesicles colocalized with protein or the number of α-Syn associated with vesicles between vesicles containing 10 and 30% DOPS at a given α-Syn concentration. Instead, a significant increase in the number of α-Syn per vesicle was observed when increasing the protein concentration in the sample (Figure 4.13A). The vesicles used in paper IV had a 60 nm diameter, yielding a surface area of 0.0113 μm^2. An average of 2-5 α-Syn

per vesicle corresponds to a protein density of ca 180-440 proteins/μm^2. Comparing these results to the results presented in paper II, there are two major differences. First of all, the relative increase in α-Syn density when increasing the DOPS content in the membrane is much lower in the dilute system investigated in paper IV. This indicates that initial binding of α-Syn to the vesicles is less sensitive to DOPS content than binding at saturating concentrations.

The second difference between the results in paper II and IV is the overall lower density of α-Syn associated with a vesicle in paper IV. From the CD spectroscopy measurements in paper II, the protein densities on the vesicles were estimated to 5000 and 15000 protein/μm^2 for vesicles containing 10 and 30% DOPS respectively. This corresponds to 70 and 170 proteins per vesicle, if the vesicle diameter is 60 nm. The major reason for the overall low number of associated α-Syn is that the system studied in paper IV uses protein concentrations far below saturation conditions. The dissociation constant of α-Syn, which gives the concentration where the

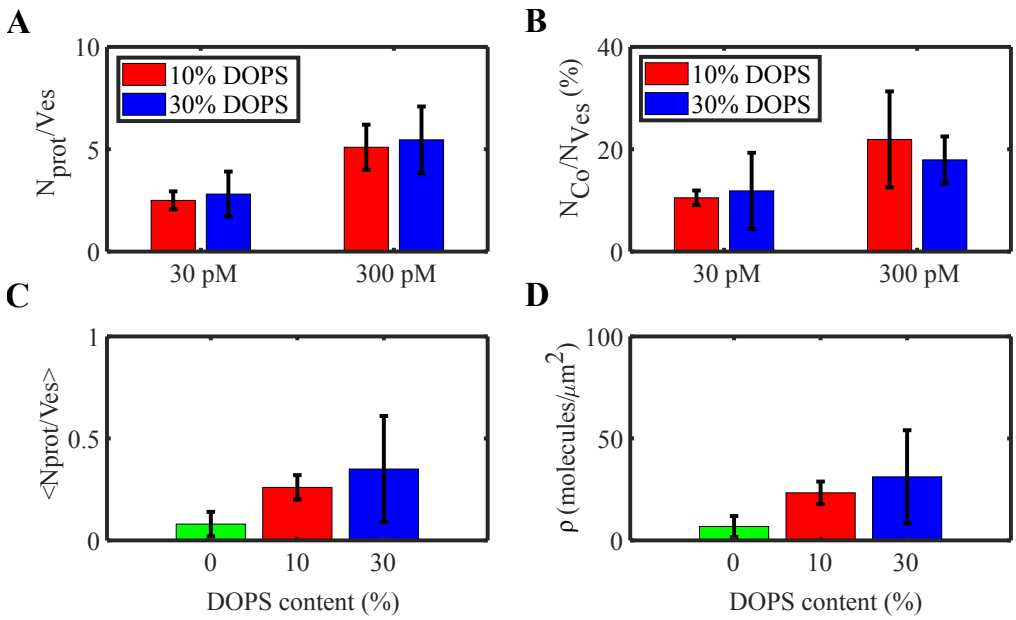

Figure 4.13: Estimating the number of α-Syn bound per vesicle.
(A) Number of proteins/vesicle when 30 and 300 pM protein was added. The data are mean ± SD of 3-15 measurements. The data are mean ± SD of 3-15 measurements. (B) Fraction of colocalized vesicles and number of vesicles detected/protein for 30 and 300 pM protein. (C) Average number of proteins per vesicle for samples containing 30 pM protein. The data are mean ± SD for 3-12 different measurements. (D) Number of proteins per total vesicle area for samples with 30 pM protein. The data are mean ± SD for 3-12 different measurements. The figure is adapted from paper IV.

system is in equilibrium, is expected to be in the range of 10-50 nM, which is more than a factor 100 higher than the overall protein concentration in paper IV.

Another factor that may contribute to a lower number of associated α-Syn is that the protein is surface active. Eventual losses of protein due to binding to the wall of the well can have large effect on the final protein concentration in conditions when the overall protein concentration is very low, and in conditions with high surface area to bulk volume. A third parameter that may also contribute is the vesicle size and the passivated surface. Considering that the passivated surface have a height of ca 10 nm, and the vesicles are 60 nm in diameter, the upper side of the vesicles is 70 nm above the glass surface. At this height there is a 60% decrease in the illumination intensity, meaning that it might not be possible to excite all α-Syn bound to the upper part of the vesicle effectively. Furthermore, it is not certain that the bottom area of the vesicle is accessible for protein binding due to steric repulsion of the PEG layer.

4.3.5 Discussion

In paper IV, the binding kinetics of α-Syn was studied for membranes with two anionic lipid compositions and two low α-Syn concentrations. From the results it could be concluded that in systems with α-Syn concentrations well below saturating conditions, there are two types of interactions; fast interactions with a lifetime in the range of ms and long interactions with lifetimes in the range of seconds. The results in paper IV are in agreement with previous studies that have observed binding lifetimes of α-Syn onto vesicles in the range of ms [66, 69], as well as α-Syn that remains bound for seconds or longer in a system with an equilibrium of α-Syn and lipid membrane [72]. This indicates that there is not a constant exchange rate of α-Syn interactions with membranes. Instead, the exchange rate likely depends on protein concentration, which means that the local protein concentration at the membrane interface might affect the exchange rate between free and bound α-Syn in a native system.

Altogether, the results showed that binding is cooperative also at overall low α-Syn concentrations and that the binding of the protein is dynamic, with membrane-bound and unbound α-Syn co-existing. The concentration of α-Syn *in vivo* is suggested to be in the range of μM [194]. Cooperative binding of α-Syn in the range of pM along with the co-existence of and exchange between free and membrane bound states

suggest that the role of α-Syn in the healthy body could involve transient binding related to vesicle trafficking, as previously discussed [63].

Concluding remarks

Dreyfus definierar expertis som förmågan att intuitivt agera baserat på erfarenhet. En expert kan således tolkas vara en person som baserat på hög grad av erfarenhet, agerar utan att behöva tänka.

Naturvetenskapen besitter den högsta erfarenheten i att undersöka hur världen fungerar. Jag hoppas dock att jag aldrig blir en expert.

The overall aim of this thesis was to investigate interactions between monomeric α-Syn and different lipid membranes, not only in bulk but also using single vesicle and single molecule imaging techniques. In paper I, cooperative binding of α-Syn on SLBs were studied. Paper II studied association of α-Syn to SUVs and SLBs with varying membrane charge density to obtain knowledge about how membrane properties affect adsorption, and more specifically if there is a difference in the number of protein that can bind to membranes with different properties. In paper III, a single vesicle assay used to study fission, fusion and lipid exchange between vesicles was developed. This assay was then used to study α-Syn induced fusion, fission and lipid exchange between vesicles consisting of DOPC:DOPS and DOPC:DOPS:GM1. Paper IV investigated the binding kinetics of α-Syn in dilute systems, for vesicles with different membrane charge density. Adding together the information obtained by those four studies, some summarizing conclusions this thesis has contributed to, can be made.

α-Syn binds in a cooperative manner

From the results in paper I, it can be concluded that α-Syn binds in a cooperative manner. This is true both for vesicles of various size and SLBs. In paper IV, the results indicate cooperative binding in dilute systems with an α-Syn concentration three orders of magnitude lower than the typical *in vivo* concentrations.

α-Syn association requires a certain charge density, and the density of bound protein increase with an increasing membrane charge density

In paper II, it was shown that α-Syn does not associate to membranes containing 1% DOPS but to membranes containing 5% DOPS. Increasing the amount of DOPS in the membrane resulted in an increased density of adsorbed α-Syn.

α-Syn does not induce fusion of vesicles, but association of α-Syn might result in membrane deformation or fission

In paper III α-Syn induced fusion between vesicles was studies. The results showed no fusion of vesicles containing DOPC:DOPS 7:3 occurred

within 48 hours under given solution conditions. However, α-Syn induced fission of vesicles consisting of DOPC:DOPS:GM1 7:2:1 at L:P ratios 200:1. Considering the lack of evidence for α-Syn induced fusion in the literature, α-Syn alone does most likely not induce fusion between vesicles *in vivo*, but instead deforms the membrane as previously suggested. Whether the vesicles are stable fission intermediates or undergo fission likely depends more on the chemical composition of the lipids incorporated in the membrane, and not only on the total amount of anionic lipids.

Previous studies have shown that DOPC:DOPS 7:3 vesicles are deformed upon association of α-Syn to vesicles consisting of a high fraction of anionic lipids (30%), at saturating conditions. The results in paper II indicated that more flexible membranes are able to bind more α-Syn. This was true for membranes with a various amount of DOPS incorporated. This indicates that association of α-Syn likely results in membrane deformation, also for membranes with lower amounts of anionic lipids.

α-Syn binds with different binding lifetimes and co-exists in free and membrane bound state

From the results in paper IV, it can be concluded that α-Syn binds with differently long binding lifetimes. In a system below saturation conditions, both short-lived interactions involving 1-2 α-Syn and long-lived interactions where several α-Syn are bound can be observed. Further, when studying α-Syn association in paper II (saturation conditions), the raw data images and the recovery profiles indicated that a part of the recovery was due to exchange between protein, although the major part of the protein remained bound for up to a minute. Altogether, these findings suggest that α-Syn co-exist in free and membrane bound states and binds either shortly (ms) or in the range of seconds or longer.

4.3.6 Outlook

This thesis does not only lead to new insights, but gives rise to some new questions of interest to study in the future. First of all, it would be interesting to investigate α-Syn binding to membranes containing 1-5% anionic lipids more thoroughly. Comparing the amount of anionic lipids required for binding in a synthetic system to the fraction of anionic lipids *in vivo*, can provide information about which membranes α-Syn is able to associate with in the cell.

Another aspect to investigate further is the binding kinetics of α-Syn, both in systems above and below saturation conditions. Due to the indications of a wide distribution of binding lifetimes, these studies should initially be performed using a method capable to detect individual events. Thus, further studies could be conducted by developing the method used in paper IV further. In order to overcome the limitation in temporal resolution when studying systems with an excess of α-Syn, a high speed camera and a binned image could be used. Such systems could also be combined with FRET to obtain spatial information of the interaction. Studying the binding kinetics in a system with high concentrations (μM) fluorescently labelled protein, FRAP should be avoided due to the high bulk signal that easily could be mistaken for bound α-Syn. However, further studies of binding kinetics in a system with low concentrations (pM-nM) of α-Syn could include FRAP measurements of α-Syn association with SLBs.

References

Det har jag gjort en gång en hel dag och då fick jag i mej så mycket lärdom, så det ligger och skvalpar inne i skallen än idag.

— Pippi Långstrump i "Pippi Långstrump går ombord"

1. Südhof, T. C. & Rothman, J. E. Membrane fusion: grappling with SNARE and SM proteins. *Science (New York, N.Y.)* **323,** 474–477 (2009).
2. Rizo, J. & Xu, J. The Synaptic Vesicle Release Machinery. *Annual Review of Biophysics* **44,** 339–367 (2015).
3. Südhof, T. C. The synaptic vesicle cycle: a cascade of protein–protein interactions. *Nature* **375,** 645–653 (1995).
4. Technology networks. *Technology networks* Accessed: 2023-06-09. https://www.technologynetworks.com/neuroscience/articles/pathophysiology-of-neurodegenerative-diseases-new-approaches-for-investigation-and-recent-advances-357227.
5. JPND Research. *JPND Research* Accessed: 2023-06-09. https://neurodegenerationresearch.eu/what/.
6. UT Southwestern Medical. *UT Sothwestern Medical* Accessed: 2023-06-09. https://utswmed.org/conditions-treatments/neurodegenerative-disorders/.
7. Parkinsons foundation. *Parkinsons Foundation* Accessed: 2023-06-09. https://www.parkinson.org/.
8. Dugger, B. N. & Dickson, D. W. Pathology of Neurodegenerative Diseases. *Cold Spring Harbor perspectives in biology* **9** (2017).
9. Dauer, W. & Przedborski, S. Parkinson's Disease: Mechanisms and Models. *Neuron* **39,** 889–909 (2003).
10. Deng, H., Wang, P. & Jankovic, J. The genetics of Parkinson disease. *Ageing Research Reviews* **42,** 72–85 (2018).
11. Lesage, S. & Brice, A. Parkinson's disease: from monogenic forms to genetic susceptibility factors. *Human Molecular Genetics* **18,** 48–59 (2009).
12. De Lau, L. M. L. & Breteler, M. M. B. Epidemiology of Parkinson's disease. *The Lancet Neurology* **5,** 525–535 (2006).
13. Jankovic, J. Parkinson's disease: clinical features and diagnosis. *Journal of Neurology, Neurosurgery and Psychiatry* **79,** 368–376 (2008).

14. Parker, K., Lamichhane, D., Caetano, M. & Narayanan, N. Executive dysfunction in Parkinson's disease and timing deficits. *Frontiers in Integrative Neuroscience* **7** (2013).

15. Poewe, W. The natural history of Parkinson's disease. *Journal of Neurology* **253,** 2–6 (2006).

16. Hely, M. A. *et al.* The Sydney multicentre study of Parkinson's disease: progression and mortality at 10 years. *Journal of Neurology, Neurosurgery & Psychiatry* **67,** 300–307 (1999).

17. Parkinson, J. An essay on the shaking palsy. 1817. *The Journal of neuropsychiatry and clinical neurosciences* **14,** 223–36 (2002).

18. Lees, A. J. Unresolved issues relating to the Shaking Palsy on the celebration of James Parkinson's 250th birthday. *Movement Disorders* **22,** 327–334 (2007).

19. Fahn, S. The history of dopamine and levodopa in the treatment of Parkinson's disease. *Movement Disorders* **23,** 497–508 (2008).

20. Schulz-Schaeffer, W. J. The synaptic pathology of alpha-synuclein aggregation in dementia with Lewy bodies, Parkinson's disease and Parkinson's disease dementia. *Acta neuropathologica* **120,** 131–143 (2010).

21. Goedert, M., Jakes, R. & Spillantini, M. G. The Synucleinopathies: Twenty Years On. *Journal of Parkinson's disease* **7,** 51–69 (2017).

22. Cabin, D. E. *et al.* Synaptic Vesicle Depletion Correlates with Attenuated Synaptic Responses to Prolonged Repetitive Stimulation in Mice Lacking α-Synuclein. *The Journal of Neuroscience* **22,** 8797–8807 (2002).

23. Murphy, D. D., Rueter, S. M., Trojanowski, J. Q. & Lee, V. M. Synucleins are developmentally expressed, and alpha-synuclein regulates the size of the presynaptic vesicular pool in primary hippocampal neurons. *The Journal of neuroscience: the official journal of the Society for Neuroscience* **20,** 3214–3220 (2000).

24. Maroteaux, L., Campanelli, J. T. & Scheller, R. H. Synuclein: a neuron-specific protein localized to the nucleus and presynaptic nerve terminal. *The Journal of neuroscience : the official journal of the Society for Neuroscience* **8,** 2804–2815 (1988).

25. Jensen, P. H., Nielsen, M. S., Jakes, R., Dotti, C. G. & Goedert, M. Binding of alpha-synuclein to brain vesicles is abolished by familial Parkinson's disease mutation. *The Journal of biological chemistry* **273,** 26292–26294 (1998).

26. Cheng, F., Vivacqua, G. & Yu, S. The role of α-synuclein in neurotransmission and synaptic plasticity. *Journal of chemical neuroanatomy* **42,** 242–248 (2011).

27. Abeliovich, A. *et al.* Mice lacking alpha-synuclein display functional deficits in the nigrostriatal dopamine system. *Neuron* **25,** 239–252 (2000).

28. Liu, S. *et al.* alpha-Synuclein produces a long-lasting increase in neurotransmitter release. *The EMBO journal* **23,** 4506–4516 (2004).

29. Lou, X., Kim, J., Hawk, B. J. & Shin, Y.-K. α-Synuclein may cross-bridge v-SNARE and acidic phospholipids to facilitate SNARE-dependent vesicle docking. *The Biochemical journal* **474,** 2039–2049 (2017).

30. Burré, J. *et al.* Alpha-synuclein promotes SNARE-complex assembly in vivo and in vitro. *Science (New York, N.Y.)* **329,** 1663–1667 (2010).

31. Lautenschläger, J., Kaminski, C. F. & Kaminski Schierle, G. S. α-Synuclein – Regulator of Exocytosis, Endocytosis, or Both? *Trends in Cell Biology* **27,** 468–479 (2017).

32. Larsen, K. E. *et al.* α-Synuclein Overexpression in PC12 and Chromaffin Cells Impairs Catecholamine Release by Interfering with a Late Step in Exocytosis. *The Journal of Neuroscience* **26,** 11915–11922 (2006).

33. Regan, D., Williams, J., Borri, P. & Langbein, W. Lipid Bilayer Thickness Measured by Quantitative DIC Reveals Phase Transitions and Effects of Substrate Hydrophilicity. *Langmuir* **35,** 13805–13814 (2019).

34. Balgavý, P. *et al.* Bilayer thickness and lipid interface area in unilamellar extruded 1,2-diacylphosphatidylcholine liposomes: a small-angle neutron scattering study. *Biochimica et Biophysica Acta (BBA) - Biomembranes* **1512,** 40–52 (2001).

35. Johnson, S. J. *et al.* Structure of an adsorbed dimyristoylphosphatidylcholine bilayer measured with specular reflection of neutrons. *Biophysical journal* **59,** 289–294 (1991).

36. Devaux, P. & McConnell, H. M. Lateral diffusion in spin-labeled phosphatidylcholine multilayers. *Journal of the American Chemical Society* **94,** 4475–4481 (1972).

37. Alberts, B. *Molecular biology of the cell* 2nd editio (Garland Pub., New York, 1989).

38. Cooper, G. M. *The Cell: A Molecular Approach.* 2nd editio. Chap. 12. Struct (Sinauer Associates, Sunderland (MA), 2000).

39. Van Meer, G., Voelker, D. R. & Feigenson, G. W. Membrane lipids: where they are and how they behave. *Nature Reviews Molecular Cell Biology* **9,** 112–124 (2008).

40. Leventis, P. A. & Grinstein, S. The Distribution and Function of Phosphatidylserine in Cellular Membranes. *Annual Review of Biophysics* **39,** 407–427 (2010).

41. Grassi, S., Chiricozzi, E., Mauri, L., Sonnino, S. & Prinetti, A. Sphingolipids and neuronal degeneration in lysosomal storage disorders. *Journal of Neurochemistry* **148,** 600–611 (2019).

42. Aureli, M. *et al.* Neuronal membrane dynamics as fine regulator of sphingolipid composition. *Glycoconjugate Journal* **35,** 397–402 (2018).

43. Luchini, A. & Vitiello, G. Mimicking the Mammalian Plasma Membrane: An Overview of Lipid Membrane Models for Biophysical Studies. *Biomimetics (Basel, Switzerland)* **6** (2020).

44. Mui, B., Chow, L. & Hope, M. J. B. T. .-. M. i. E. in *Liposomes, Part A* 3–14 (Academic Press, 2003).

45. Olson, F., Hunt, C. A., Szoka, F. C., Vail, W. J. & Papahadjopoulos, D. Preparation of liposomes of defined size distribution by extrusion through polycarbonate membranes. *Biochimica et biophysica acta* **557,** 9–23 (1979).

46. Cho, N.-J., Hwang, L. Y., Solandt, J. J. R. & Frank, C. W. Comparison of Extruded and Sonicated Vesicles for Planar Bilayer Self-Assembly. *Materials (Basel, Switzerland)* **6,** 3294–3308 (2013).

47. Castellana, E. T. & Cremer, P. S. Solid supported lipid bilayers: From biophysical studies to sensor design. *Surface science reports* **61,** 429–444 (2006).

48. Khan, M. S., Dosoky, N. S. & Williams, J. D. Engineering lipid bilayer membranes for protein studies. *International journal of molecular sciences* **14,** 21561–21597 (2013).

49. Kurniawan, J., Ventrici de Souza, J. F., Dang, A. T., Liu, G.-Y. & Kuhl, T. L. Preparation and Characterization of Solid-Supported Lipid Bilayers Formed by Langmuir-Blodgett Deposition: A Tutorial. *Langmuir: the ACS journal of surfaces and colloids* **34,** 15622–15639 (2018).

50. Tamm, L. K. & McConnell, H. M. Supported phospholipid bilayers. *Biophysical journal* **47,** 105–113 (1985).

51. McConnell, H. M., Watts, T. H., Weis, R. M. & Brian, A. A. Supported planar membranes in studies of cell-cell recognition in the immune system. *Biochimica et biophysica acta* **864,** 95–106 (1986).

52. Mennicke, U. & Salditt, T. Preparation of Solid-Supported Lipid Bilayers by Spin-Coating. *Langmuir* **18,** 8172–8177 (2002).

53. Hardy, G. J., Nayak, R. & Zauscher, S. Model cell membranes: Techniques to form complex biomimetic supported lipid bilayers via vesicle fusion. *Current opinion in colloid & interface science* **18,** 448–458 (2013).

54. Lind, T. K. & Cárdenas, M. Understanding the formation of supported lipid bilayers via vesicle fusion-A case that exemplifies the need for the complementary method approach (Review). *Biointerphases* **11,** 20801 (2016).

55. Shepherd, N. E., Hoang, H. N., Abbenante, G. & Fairlie, D. P. Left- and Right-Handed Alpha-Helical Turns in Homo- and Hetero-Chiral Helical Scaffolds. *Journal of the American Chemical Society* **131,** 15877–15886 (2009).

56. Dyson, H. J. Making Sense of Intrinsically Disordered Proteins. *Biophysical journal* **110,** 1013–1016 (2016).

57. Ayyadevara, S., Ganne, A., Balasubramaniam, M. & Shmookler Reis, R. J. Intrinsically disordered proteins identified in the aggregate proteome serve as biomarkers of neurodegeneration. *Metabolic Brain Disease* **37,** 147–152 (2022).

58. Uversky, V. N. Intrinsically disordered proteins and their (disordered) proteomes in neurodegenerative disorders. *Frontiers in Aging Neuroscience* **7** (2015).

59. Tsoi, P. S., Quan, M. D., Ferreon, J. C. & Ferreon, A. C. M. Aggregation of Disordered Proteins Associated with Neurodegeneration. *International Journal of Molecular Sciences* **24** (2023).

60. Angelova, P. R. *et al.* Ca2+ is a key factor in α-synuclein-induced neurotoxicity. *Journal of cell science* **129,** 1792–1801 (2016).

61. Du, X.-Y., Xie, X.-X. & Liu, R.-T. The Role of α-Synuclein Oligomers in Parkinson's Disease. *International journal of molecular sciences* **21** (2020).

62. Ingelsson, M. Alpha-Synuclein Oligomers-Neurotoxic Molecules in Parkinson's Disease and Other Lewy Body Disorders. *Frontiers in neuroscience* **10,** 408 (2016).

63. Burré, J. The Synaptic Function of α-Synuclein. *Journal of Parkinson's disease* **5,** 699–713 (2015).

64. Davidson, W. S., Jonas, A., Clayton, D. F. & George, J. M. Stabilization of alpha-synuclein secondary structure upon binding to synthetic membranes. *The Journal of biological chemistry* **273,** 9443–9449 (1998).

65. Fusco, G., Sanz-Hernandez, M. & De Simone, A. Order and disorder in the physiological membrane binding of α-synuclein. *Current opinion in structural biology* **48,** 49–57 (2018).

66. Shvadchak, V. V., Falomir-Lockhart, L. J., Yushchenko, D. A. & Jovin, T. M. Specificity and kinetics of alpha-synuclein binding to model membranes determined with fluorescent excited state intramolecular proton transfer (ESIPT) probe. *The Journal of biological chemistry* **286,** 13023–13032 (2011).

67. Bodner, C. R., Dobson, C. M. & Bax, A. Multiple tight phospholipid-binding modes of alpha-synuclein revealed by solution NMR spectroscopy. *Journal of molecular biology* **390,** 775–790 (2009).

68. Fusco, G. *et al.* Direct observation of the three regions in α-synuclein that determine its membrane-bound behaviour. *Nature Communications* **5,** 3827 (2014).

69. Makasewicz, K. *α-synuclein interactions with lipid membranes* PhD thesis (Lund University, 2022).

70. Pfefferkorn, C. M., Jiang, Z. & Lee, J. C. Biophysics of α-synuclein membrane interactions. *Biochimica et biophysica acta* **1818,** 162–171 (2012).

71. Eliezer, D., Kutluay, E., Bussell, R. & Browne, G. Conformational properties of α-synuclein in its free and lipid-associated states11Edited by P. E. Wright. *Journal of Molecular Biology* **307,** 1061–1073 (2001).

72. Hellstrand, E. *et al.* Adsorption of α-synuclein to supported lipid bilayers: positioning and role of electrostatics. *ACS chemical neuroscience* **4,** 1339–1351 (2013).

73. Gaspar, R. *et al.* Secondary nucleation of monomers on fibril surface dominates α-synuclein aggregation and provides autocatalytic amyloid amplification. *Quarterly Reviews of Biophysics* **50** (2017).

74. Bohr C, K, H. & A, K. Ueber einen in biologischer Beziehung wichtigen Einfluss, den die Kohlensäurespannung des Blutes auf dessen Sauerstoffbindung übt. Skandinavisches. *Arch. Physiol.* **16,** 402–412 (1904).

75. Nagatomo, S. *et al.* An Origin of Cooperative Oxygen Binding of Human Adult Hemoglobin: Different Roles of the α and β Subunits in the $\alpha 2 \beta 2$ Tetramer. *PloS one* **10,** e0135080 (2015).

76. Allen, D. W., Guthe, K. F. & Wyman, J. J. Further studies on the oxygen equilibrium of hemoglobin. *The Journal of biological chemistry* **187,** 393–410 (1950).

77. Ciaccio, C., Coletta, A., De Sanctis, G., Marini, S. & Coletta, M. Cooperativity and allostery in haemoglobin function. *IUBMB Life* **60,** 112–123 (2008).

78. Stefan, M. I. & Le Novère, N. Cooperative binding. *PLoS computational biology* **9,** e1003106 (2013).

79. Galvagnion, C. *et al.* Chemical properties of lipids strongly affect the kinetics of the membrane-induced aggregation of α-synuclein. *Proceedings of the National Academy of Sciences of the United States of America* **113,** 7065–7070 (2016).

80. Chandra, S., Chen, X., Rizo, J., Jahn, R. & Südhof, T. C. A broken alpha-helix in folded alpha-Synuclein. *The Journal of biological chemistry* **278,** 15313–15318 (2003).

81. Galvagnion, C. *et al.* Lipid vesicles trigger α-synuclein aggregation by stimulating primary nucleation. *Nature Chemical Biology* **11,** 229–234 (2015).

82. Middleton, E. R. & Rhoades, E. Effects of curvature and composition on α-synuclein binding to lipid vesicles. *Biophysical journal* **99,** 2279–2288 (2010).

83. Rhoades, E., Ramlall, T. F., Webb, W. W. & Eliezer, D. Quantification of alpha-synuclein binding to lipid vesicles using fluorescence correlation spectroscopy. *Biophysical journal* **90,** 4692–4700 (2006).

84. Lee, S.-J., Jeon, H. & Kandror, K. V. Alpha-synuclein is localized in a subpopulation of rat brain synaptic vesicles. *Acta neurobiologiae experimentalis* **68,** 509–515 (2008).

85. Burré, J., Sharma, M. & Südhof, T. C. α-Synuclein assembles into higher-order multimers upon membrane binding to promote SNARE complex formation. *Proceedings of the National Academy of Sciences of the United States of America* **111,** 4274–4283 (2014).

86. Nuscher, B. *et al.* Alpha-synuclein has a high affinity for packing defects in a bilayer membrane: a thermodynamics study. *The Journal of biological chemistry* **279,** 21966–21975 (2004).

87. Drescher, M., van Rooijen, B. D., Veldhuis, G., Subramaniam, V. & Huber, M. A stable lipid-induced aggregate of alpha-synuclein. *Journal of the American Chemical Society* **132,** 4080–4082 (2010).

88. Vats, K., Knutson, K., Hinderliter, A. & Sheets, E. D. Peripheral Protein Organization and Its Influence on Lipid Diffusion in Biomimetic Membranes. *ACS Chemical Biology* **5,** 393–403 (2010).

89. Kjaer, L., Giehm, L., Heimburg, T. & Otzen, D. The influence of vesicle size and composition on alpha-synuclein structure and stability. *Biophysical journal* **96,** 2857–2870 (2009).

90. Sanders, H. M., Kostelic, M. M., Zak, C. K. & Marty, M. T. Lipids and EGCG Affect α-Synuclein Association and Disruption of Nanodiscs. *Biochemistry* **61,** 1014–1021 (2022).

91. Jo, E., McLaurin, J. A., Yip, C. M., St. George-Hyslop, P. & Fraser, P. E. α-Synuclein membrane interactions and lipid specificity. *Journal of Biological Chemistry* **275,** 34328–34334 (2000).

92. Pirc, K. & Ulrih, N. P. α-Synuclein interactions with phospholipid model membranes: Key roles for electrostatic interactions and lipid-bilayer structure. *Biochimica et Biophysica Acta (BBA) - Biomembranes* **1848,** 2002–2012 (2015).

93. Dikiy, I. & Eliezer, D. N-terminal acetylation stabilizes N-terminal helicity in lipid- and micelle-bound α-synuclein and increases its affinity for physiological membranes. *The Journal of biological chemistry* **289,** 3652–3665 (2014).

94. Viennet, T. *et al.* Structural insights from lipid-bilayer nanodiscs link α-Synuclein membrane-binding modes to amyloid fibril formation. *Communications Biology* **1** (2018).

95. Das, T. & Eliezer, D. Membrane interactions of intrinsically disordered proteins: The example of alpha-synuclein. *Biochimica et biophysica acta. Proteins and proteomics* **1867,** 879–889 (2019).

96. Pranke, I. M. *et al.* α-Synuclein and ALPS motifs are membrane curvature sensors whose contrasting chemistry mediates selective vesicle binding. *The Journal of cell biology* **194,** 89–103 (2011).

97. Ouberai, M. M. *et al.* α-Synuclein Senses Lipid Packing Defects and Induces Lateral Expansion of Lipids Leading to Membrane Remodeling. *Journal of Biological Chemistry* **288,** 20883–20895 (2013).

98. Braun, A. R., Lacy, M. M., Ducas, V. C., Rhoades, E. & Sachs, J. N. α-Synuclein-Induced Membrane Remodeling Is Driven by Binding Affinity, Partition Depth, and Interleaflet Order Asymmetry. *Journal of the American Chemical Society* **136,** 9962–9972 (2014).

99. Westphal, C. H. & Chandra, S. S. Monomeric synucleins generate membrane curvature. *The Journal of biological chemistry* **288,** 1829–1840 (2013).

100. Braun, A. R., Lacy, M. M., Ducas, V. C., Rhoades, E. & Sachs, J. N. α-Synuclein's Uniquely Long Amphipathic Helix Enhances its Membrane Binding and Remodeling Capacity. *The Journal of membrane biology* **250,** 183–193 (2017).

101. Fusco, G. *et al.* Structural basis of synaptic vesicle assembly promoted by α-synuclein. *Nature communications* **7,** 12563 (2016).

102. Diao, J. *et al.* Native α-synuclein induces clustering of synaptic-vesicle mimics via binding to phospholipids and synaptobrevin-2/VAMP2. *eLife* **2,** 00592–00592 (2013).

103. Makasewicz, K., Wennmalm, S., Linse, S. & Sparr, E. α-synuclein-induced Deformation of Small Unilamellar Vesicles. *QRB Discovery,* 1–51 (2022).

104. Hannestad, J. K. *et al.* Single-vesicle imaging reveals lipid-selective and stepwise membrane disruption by monomeric α-synuclein. *Proceedings of the National Academy of Sciences of the United States of America* **117,** 14178–14186 (2020).

105. Perissinotto, F. *et al.* GM1 Ganglioside role in the interaction of Alpha-synuclein with lipid membranes: Morphology and structure. *Biophysical chemistry* **255,** 106272 (2019).

106. Gaspar, R., Idini, I., Carlström, G., Linse, S. & Sparr, E. Transient Lipid-Protein Structures and Selective Ganglioside Uptake During α-Synuclein-Lipid Co-aggregation. *Frontiers in Cell and Developmental Biology* **9** (2021).

107. Thorn, K. A quick guide to light microscopy in cell biology. *Molecular Biology of the Cell* **27,** 219–222 (2016).

108. Rayleigh, L. On the Theory of Optical Images, with special reference to the Microscope. *Journal of the Royal Microscopical Society* **23,** 474–482 (1903).

109. Abbe, E. Beiträge zur Theorie des Mikroskops und der mikroskopischen Wahrnehmung. *Archiv für Mikroskopische Anatomie* **9,** 413–468 (1873).

110. Peterman, E. *Single molecule analysis: methods and protocols* (Humana Press, Methods Mol Bio, New York, 2018).

111. Ploem, J. S. The use of a vertical illuminator with interchangeable dichroic mirrors for fluorescence microscopy with incidental light. *Zeitschrift fur wissenschaftliche Mikroskopie und mikroskopische Technik* **68,** 129–142 (1967).

112. Masters, B. R. in *Encyclopedia of Life Sciences* (2010).

113. Van Krugten, J. & Peterman, E. J. G. Single-Molecule Fluorescence Microscopy in Living Caenorhabditis elegans. *Methods in molecular biology (Clifton, N.J.)* **1665,** 145–154 (2018).

114. Giepmans, B. N. G., Adams, S. R., Ellisman, M. H. & Tsien, R. Y. The fluorescent toolbox for assessing protein location and function. *Science (New York, N.Y.)* **312,** 217–224 (2006).

115. Gensch, T., Böhmer, M. & Aramendía, P. F. Single molecule blinking and photobleaching separated by wide-field fluorescence microscopy. *The journal of physical chemistry* **109,** 6652–6658 (2005).

116. Ambrose, E. J. A Surface Contact Microscope for the study of Cell Movements. *Nature* **178,** 1194 (1956).

117. Mattheyses, A. L., Simon, S. M. & Rappoport, J. Z. Imaging with total internal reflection fluorescence microscopy for the cell biologist. *Journal of cell science* **123,** 3621–3628 (2010).

118. Axelrod, D. Total internal reflection fluorescence microscopy in cell biology. *Traffic (Copenhagen, Denmark)* **2,** 764–774 (2001).

119. Axelrod, D., Thompson, N. L. & Burghardt, T. P. Total internal reflection fluorescent microscopy. *Journal of Microscopy* **129,** 19–28 (1983).

120. Axelrod, D., Koppel, D. E., Schlessinger, J., Elson, E. & Webb, W. W. Mobility measurement by analysis of fluorescence photobleaching recovery kinetics. *Biophysical journal* **16,** 1055–1069 (1976).

121. Elson, E. L., Schlessinger, J., Koppel, D. E., Axelrod, D. & Webb, W. W. Measurement of lateral transport on cell surfaces. *Progress in clinical and biological research* **9,** 137–147 (1976).

122. Jacobson, K., Derzko, Z., Wu, E. S., Hou, Y. & Poste, G. Measurement of the lateral mobility of cell surface components in single, living cells by fluorescence recovery after photobleaching. *Journal of supramolecular structure* **5,** 565(417)–576(428) (1976).

123. Tolentino, T. P. *et al.* Measuring diffusion and binding kinetics by contact area FRAP. *Biophysical journal* **95,** 920–930 (2008).

124. Jönsson, P., Jonsson, M. P., Tegenfeldt, J. O. & Höök, F. A method improving the accuracy of fluorescence recovery after photobleaching analysis. *Biophysical journal* **95,** 5334–5348 (2008).

125. Mueller, F., Karpova, T. S., Mazza, D. & McNally, J. G. Monitoring dynamic binding of chromatin proteins in vivo by fluorescence recovery after photobleaching. *Methods in molecular biology* **833,** 153–176 (2012).

126. Université de Genève. *SOP FRAP* Accessed: 2023-07-19. `https://www.unige.ch/sciences/chifi/wiki/lib/exe/fetch.php?media=sugi:sop_frap.pdf`.

127. Wright, G. & Sibarita, J.-B. in *Practical manual for fluorescence microscopy techniques* chap. 6 (PicoQuant).

128. Firmino, J., Tinevez, J.-Y. & Knust, E. Crumbs Affects Protein Dynamics In Anterior Regions Of The Developing Drosophila Embryo. *PloS one* **8,** e58839 (2013).

129. Soumpasis, D. M. Theoretical analysis of fluorescence photobleaching recovery experiments. *Biophysical journal* **41,** 95–97 (1983).

130. Chiu, S.-W. & Leake, M. C. Functioning nanomachines seen in real-time in living bacteria using single-molecule and super-resolution fluorescence imaging. *International journal of molecular sciences* **12,** 2518–2542 (2011).

131. Penczek, P. A. Resolution measures in molecular electron microscopy. *Methods in enzymology* **482,** 73–100 (2010).

132. Rust, M. J., Bates, M. & Zhuang, X. Sub-diffraction-limit imaging by stochastic optical reconstruction microscopy (STORM). *Nature Methods* **3,** 793–796 (2006).

133. Betzig, E. *et al.* Imaging Intracellular Fluorescent Proteins at Nanometer Resolution. *Science* **313,** 1642–1645 (2006).

134. Hell, S. W. & Wichmann, J. Breaking the diffraction resolution limit by stimulated emission: stimulated-emission-depletion fluorescence microscopy. *Optics letters* **19,** 780–782 (1994).

135. Hirschfeld, T. Optical microscopic observation of single small molecules. *Applied Optics* **15,** 2965–2966 (1976).

136. Moerner, W. E. & Fromm, D. P. Methods of single-molecule fluorescence spectroscopy and microscopy. *Review of Scientific Instruments* **74,** 3597–3619 (2003).

137. Yildiz, A. *et al.* Myosin V Walks Hand-Over-Hand: Single Fluorophore Imaging with 1.5-nm Localization. *Science* **300,** 2061–2065 (2003).

138. Thompson, R. E., Larson, D. R. & Webb, W. W. Precise nanometer localization analysis for individual fluorescent probes. *Biophysical journal* **82,** 2775–2783 (2002).

139. Manzo, C. & Garcia-Parajo, M. F. A review of progress in single particle tracking: from methods to biophysical insights. *Reports on progress in physics. Physical Society (Great Britain)* **78,** 124601 (2015).

140. Liu, C., Liu, Y.-L., Perillo, E. P., Dunn, A. K. & Yeh, H.-C. Single-Molecule Tracking and Its Application in Biomolecular Binding Detection. *IEEE journal of selected topics in quantum electronics: a publication of the IEEE Lasers and Electro-optics Society* **22** (2016).

141. Shashkova, S. & Leake, M. C. Single-molecule fluorescence microscopy review: shedding new light on old problems. *Bioscience reports* **37** (2017).

142. Bally, M. *et al.* Interaction of Single Viruslike Particles with Vesicles Containing Glycosphingolipids. *Physical Review Letters* **107,** 188103 (2011).

143. Horrocks, M. H. *et al.* Single-Molecule Imaging of Individual Amyloid Protein Aggregates in Human Biofluids. *ACS Chemical Neuroscience* **7,** 399–406 (2016).

144. Ferreon, A. C. M., Gambin, Y., Lemke, E. A. & Deniz, A. A. Interplay of α-synuclein binding and conformational switching probed by single-molecule fluorescence. *Proceedings of the National Academy of Sciences* **106,** 5645–5650 (2009).

145. Weber, T. *et al.* SNAREpins: Minimal Machinery for Membrane Fusion. *Cell* **92,** 759–772 (1998).

146. Diao, J. *et al.* A single vesicle-vesicle fusion assay for in vitro studies of snares and accessory proteins. *Nature Protocols* **7,** 921–934 (2012).

147. Cha, M. *et al.* Quantitative imaging of vesicle–protein interactions reveals close cooperation among proteins. *Journal of Extracellular Vesicles* **12,** 12322 (2023).

148. Cai, B., Yu, L., Sharum, S. R., Zhang, K. & Diao, J. Single-vesicle measurement of protein-induced membrane tethering. *Colloids and surfaces. B, Biointerfaces* **177,** 267–273 (2019).

149. Olsson, T., Zhdanov, V. P. & Höök, F. Total internal reflection fluorescence microscopy for determination of size of individual immobilized vesicles: Theory and experiment. *Journal of Applied Physics* **118,** 64702 (2015).

150. Kunding, A. H., Mortensen, M. W., Christensen, S. M. & Stamou, D. A fluorescence-based technique to construct size distributions from single-object measurements: application to the extrusion of lipid vesicles. *Biophysical journal* **95,** 1176–1188 (2008).

151. Hatzakis, N. S. *et al.* How curved membranes recruit amphipathic helices and protein anchoring motifs. *Nature Chemical Biology* **5,** 835–841 (2009).

152. Bhatia, V. K. *et al.* Amphipathic motifs in BAR domains are essential for membrane curvature sensing. *The EMBO Journal* **28,** 3303–3314 (2009).

153. Tabaei, S. R., Rabe, M., Zhdanov, V. P., Cho, N.-J. & Höök, F. Single vesicle analysis reveals nanoscale membrane curvature selective pore formation in lipid membranes by an antiviral α-helical peptide. *Nano letters* **12,** 5719–5725 (2012).

154. Junghans, V. *et al.* Hydrodynamic trapping measures the interaction between membrane-associated molecules. *Scientific reports* **8,** 12479 (2018).

155. Lohse, B., Bolinger, P.-Y. & Stamou, D. Encapsulation Efficiency Measured on Single Small Unilamellar Vesicles. *Journal of the American Chemical Society* **130,** 14372–14373 (2008).

156. Gaspar, R. *α-Synuclein Fibril Formation and the Effects of Lipid Membranes* PhD thesis (Lund University, 2018).

157. Chivers, C. E., Koner, A. L., Lowe, E. D. & Howarth, M. How the biotin-streptavidin interaction was made even stronger: investigation via crystallography and a chimaeric tetramer. *The Biochemical journal* **435,** 55–63 (2011).

158. Shi, L. *et al.* Effects of polyethylene glycol on the surface of nanoparticles for targeted drug delivery. *Nanoscale* **13,** 10748–10764 (2021).

159. Hill, A. V. The Combinations of Haemoglobin with Oxygen and with Carbon Monoxide. I. *The Biochemical journal* **7,** 471–480 (1913).

160. Hill, V. The possible effects of the aggregation of the molecules of haemoglobin on its dissociation curves. *Journal of Physiology* **40.** 4–12.

161. Forsén, S. & Linse, S. Cooperativity: over the Hill. *Trends in biochemical sciences* **20,** 495–497 (1995).

162. Adair, G. S., Bock, A. V. & Field, H. The hemoglobin system: VI. The oxygen dissociation curve of hemoglobin. *Journal of Biological Chemistry* **63,** 529–545 (1925).

163. Heimburg, T., Angerstein, B. & Marsh, D. Binding of Peripheral Proteins to Mixed Lipid Membranes: Effect of Lipid Demixing upon Binding. *Biophysical Journal* **76,** 2575–2586 (1999).

164. Simunovic, M., Srivastava, A. & Voth, G. A. Linear aggregation of proteins on the membrane as a prelude to membrane remodeling. *Proceedings of the National Academy of Sciences* **110,** 20396–20401 (2013).

165. Goose, J. E. & Sansom, M. S. P. Reduced Lateral Mobility of Lipids and Proteins in Crowded Membranes. *PLOS Computational Biology* **9,** e1003033 (2013).

166. Alenghat, F. J. & Golan, D. E. Membrane protein dynamics and functional implications in mammalian cells. *Current topics in membranes* **72,** 89–120 (2013).

167. Ma, X. *et al.* Phosphatidylserine, inflammation, and central nervous system diseases. *Frontiers in aging neuroscience* **14,** 975176 (2022).

168. Mouritsen, O. G. & Bagatolli, L. A. Lipid domains in model membranes: a brief historical perspective. *Essays in biochemistry* **57,** 1–19 (2015).

169. Nagy, A., Baker, R. R., Morris, S. J. & Whittaker, V. P. The preparation and characterization of synaptic vesicles of high purity. *Brain Research* **109,** 285–309 (1976).

170. Binotti, B., Jahn, R. & Pérez-Lara, Á. An overview of the synaptic vesicle lipid composition. *Archives of Biochemistry and Biophysics* **709,** 108966 (2021).

171. Deutsch, J. W. & Kelly, R. B. Lipids of synaptic vesicles: relevance to the mechanism of membrane fusion. *Biochemistry* **20,** 378–385 (1981).

172. Takamori, S. *et al.* Molecular Anatomy of a Trafficking Organelle. *Cell* **127,** 831–846 (2006).

173. Kay, J. G., Koivusalo, M., Ma, X., Wohland, T. & Grinstein, S. Phosphatidylserine dynamics in cellular membranes. *Molecular Biology of the Cell,* 2198–2212 (2012).

174. Kelly, S. M., Jess, T. J. & Price, N. C. How to study proteins by circular dichroism. *Biochimica et Biophysica Acta (BBA) - Proteins and Proteomics* **1751,** 119–139 (2005).

175. Barrow, C. J., Yasuda, A., Kenny, P. T. M. & Zagorski, M. G. Solution conformations and aggregational properties of synthetic amyloid β-peptides of Alzheimer's disease: Analysis of circular dichroism spectra. *Journal of Molecular Biology* **225,** 1075–1093 (1992).

176. Adler, A. J., Greenfield, N. J. & Fasman, G. D. B. T. .-. M. i. E. in *Part D: Enzyme Structure* 675–735 (Academic Press, 1973).

177. Sreerama, N. & Woody, R. Computation and Analysis of Protein Circular Dichroism Spectra. *Numerical Computer Methods, Part D* **383,** 318–351 (2004).

178. Greenfield, N. J. Using circular dichroism spectra to estimate protein secondary structure. *Nature protocols* **1,** 2876–2890 (2006).

179. Matsuo, K., Sakurada, Y., Yonehara, R., Kataoka, M. & Gekko, K. Secondary-structure analysis of denatured proteins by vacuum-ultraviolet circular dichroism spectroscopy. *Biophysical journal* **92,** 4088–4096 (2007).

180. Pallbo, J., Sparr, E. & Olsson, U. Aggregation behavior of the amyloid model peptide NACore. *Quarterly Reviews of Biophysics* **52,** e4 (2019).

181. Pallbo, J. *et al.* NACore Amyloid Formation in the Presence of Phospholipids. *Frontiers in physiology* **11,** 592117 (2020).

182. Petrache, H. I. *et al.* Structure and Fluctuations of Charged Phosphatidylserine Bilayers in the Absence of Salt. *Biophysical Journal* **86,** 1574–1586 (2004).

183. Sajadi, F. & Rowley, C. Simulations of lipid bilayers using the CHARMM36 force field with the TIP3P-FB and TIP4P-FB water models. *PeerJ* **6,** e5472 (2018).

184. Boes, D. M., Godoy-Hernandez, A. & McMillan, D. G. G. Peripheral Membrane Proteins: Promising Therapeutic Targets across Domains of Life. *Membranes* **11** (2021).

185. Johnson, J. E. & Cornell, R. B. Amphitropic proteins: regulation by reversible membrane interactions (review). *Molecular membrane biology* **16,** 217–235 (1999).

186. Sternberg, S. R. Biomedical image processing. *Computer* **16,** 22–34 (1983).

187. Stridfeldt, F. *et al.* Analyses of single extracellular vesicles from non-small lung cancer cells to reveal effects of epidermal growth factor receptor inhibitor treatments. *Talanta* **259,** 124553 (2023).

188. Kohze, R., Dieteren, C. E. J., Koopman, W. J. H., Brock, R. & Schmidt, S. Frapbot: An open-source application for FRAP data. *Cytometry Part A* **91,** 810–814 (2017).

189. Koulouras, G. *et al.* EasyFRAP-web: a web-based tool for the analysis of fluorescence recovery after photobleaching data. *Nucleic acids research* **46,** 467–472 (2018).

190. Kuhn, T., Hettich, J., Davtyan, R. & Gebhardt, J. C. M. Single molecule tracking and analysis framework including theory-predicted parameter settings. *Scientific Reports* **11,** 9465 (2021).

191. Oviedo-Bocanegra, L. M., Hinrichs, R., Rotter, D. A. O., Dersch, S. & Graumann, P. L. Single molecule/particle tracking analysis program SMTracker 2.0 reveals different dynamics of proteins within the RNA degradosome complex in Bacillus subtilis. *Nucleic Acids Research* **49,** e112–e112 (2021).

192. Reina, F. *et al.* TRAIT2D: a Software for Quantitative Analysis of Single Particle Diffusion Data [version 2; peer review: 2 approved]. *F1000Research* **10** (2022).

193. Hansen, A. S. *et al.* Robust model-based analysis of single-particle tracking experiments with Spot-On. *eLife* **7** (ed Sherratt, D.) e33125 (2018).

194. Wilhelm, B. G. *et al.* Composition of isolated synaptic boutons reveals the amounts of vesicle trafficking proteins. *Science (New York, N.Y.)* **344,** 1023–1028 (2014).

Scientific publications

The struggle itself toward the heights, is enough to fill a man's heart.

— Albert Camus

Mot nya djärva misslyckanden, framåt

Printed by Media-Tryck, Lund 2023 NORDIC SWAN ECOLABEL 3041 0903

ISBN 978-91-7422-972-1

Department of Chemistry
Faculty of Science
Lund University